Experimental Modal Survey of a Horizontal Cylindrical Shell Partly Filled with Water

F. Eberle, J. Kadlec, G. Hailfinger, R. Scharnowell

Institut für Reaktorentwicklung
Projekt Nukleare Sicherheit

Kernforschungszentrum Karlsruhe

Experimental modal survey of a horizontal cylindrical shell
partly filled with water

by

F. Eberle, J. Kadlec, G. Hailfinger and R. Scharnowell

Theoretical and Experimental Modal Survey of a Horizontal Cylindrical Shell Partly Filled with Water

Abstract

The report deals with theoretical and experimental modal surveys of a horizontally located cylindrical shell, requested for experimental verification of the SING-S coupled fluid/structure-interaction computer program. The eigenfrequencies, the mode shapes and the critical damping ratios of the test cylinder used (ϕ 1000 x 3 x 1600 mm, empty or partly filled with water, water level 680 mm) were extracted from the set of simultaneously measured relaxation response signals. The transient response was achieved via a snapback-process or an impulse excitation of the test cylinder shell. The EVA computer program was used to extract the modal characteristics from the acceleration response signals. A total number of 57 eigenmodes were identified experimentally - 33 eigenmodes of the test cylinder partly filled with water and 24 eigenmodes of the empty test cylinder. It has been found that the horizontal arrangement of the shell destroys the regular cosine patterns of its eigenmodes. The eigenmodes of the empty test cylinder are composed of significant contributions by several cosine patterns with a distinct main contribution by one of them. The natural frequencies f of the empty test cylinder can be plotted over the circumferential order v of the "predominant" cosine pattern (v-f-plot) and reveal trends similar to those of the vertical shell. The presence of the water charge in the test cylinder causes additional distortions of the eigenmode patterns. The contribution to the individual mode shapes of the particular "predominant" cosine pattern is less significant, and tracing the v-f-plots is not meaningful. The calculated and the extracted mode shapes are nearly congruent; the deviations observable in individual sections are in most cases caused by different spatial orientations of these modes which in turn are caused by structural imperfections of the test cylinder. The calculated and extracted natural frequencies are well intercomparable and the mutual deviations generally do not exceed several per cent. The extracted values of the critical damping ratio ξ are of the order of several per mill and do not attain 0.5 %.

Theoretische und experimentelle Modalanalyse einer horizontalen, z.T.
mit Wasser gefüllten Zylinderschale

Zusammenfassung

Der Bericht befaßt sich mit theoretischer und experimenteller Modalana-
lyse einer horizontal positionierten, leeren oder z.T. mit Wasser
gefüllten Zylinderschale ϕ 1000 x 3 x 1600 mm. Zweck dieser Untersuchung
war die experimentelle Verifizierung des gekoppelten, fluid/strukturdy-
namischen Rechenprogrammes SING-S. Die Eigenfrequenzen, die Eigenschwin-
gungsformen und die entsprechenden modalen Dämpfungsquotienten des un-
tersuchten Testbehälters wurden bei verschiedenen Experimenten jeweils
aus einem Satz von simultan gemessenen transienten Antwortsignalen mit
dem Rechenprogramm EVA extrahiert. Die dafür benötigte transiente Ant-
wort der Zylinderschale wurde mit einer Snapback-Vorrichtung oder mit
einem Impulshammer angeregt. Insgesamt wurden 57 Eigenschwingungsmodes
des Testzylinders identifiziert; davon entfallen 24 Eigenmodes auf den
leeren und 33 auf den wassergefüllten (Wasserspiegelhöhe 680 mm) Testzy-
linder. Es hat sich herausgestellt, daß die horizontale Positionierung
des Testzylinders die Eigenschwingungsmodes wesentlich beeinträchtigt.
Die Eigenschwingungsformen des leeren Testzylinders bestehen jeweils aus
mehreren regulären Kosinuskomponenten mit einer ausgeprägten Hauptkompo-
nente. Die entsprechenden Eigenfrequenzen f, geplottet über die Umfangs-
ordnung v der Hauptkomponente weisen einen ähnlichen Verlauf auf wie im
f-v-Diagramm des vertikalen Zylinders. Durch die Wirkung der Wasservor-
lage entstehen weitere Verzerrungen der Eigenschwingungsformen. Der
Beitrag der Hauptkomponente ist weniger signifikant und das Zeichnen des
f-v-Diagramms ist nicht mehr sinnvoll. Die vorausberechneten und die
extrahierten Eigenschwingungsformen sind weitgehend kongruent; die indi-
viduellen Abweichungen sind in der Regel durch unterschiedliche Orien-
tierungen im Raum verursacht, die wiederum auf die Wirkung von struktu-
rellen Imperfektionen des Testzylinders zurückzuführen sind. Die voraus-
berechneten und die extrahierten Eigenfrequenzen stimmen miteinander gut
überein; die eventuellen Abweichungen sind in der Regel nicht größer als
einige Prozent. Die extrahierten Dämpfungsquotienten ξ betragen einige
Promille und erreichen nicht den Wert von 0,5 %.

Contents

1. Introduction

The submitted report deals with theoretical and experimental modal surveys of a horizontal test cylinder, which is either empty or partly filled with water. It constitutes second case in a test series carried out to check the SING-S fluid-structure interaction code /1-3/. The first, simpler case in this test series was the modal survey of the same shell positioned vertically, which constituted a quasi-axisymmetric problem /4-7/. Compared to this simpler case, the horizontal cylinder investigated here constitutes a three-dimensional problem. Some preliminary results obtained by an experimental modal analysis of the horizontal test cylinder are summarized in paper /8/.

A schematic sketch of the stainless-steel test cylinder used in our investigations and its principal dimensions are given in the upper part of fig. 1. A bird's eye view of the experimental setup is shown in fig. 2. The test cylinder shell, dia. 1000 mm x 3 mm x 1600 mm, is welded on both ends to quadratic stainless-steel plates (1250 x 1250 x 30 mm) which are in turn screwed to a heavy fastening plate of approx. 3300 kg weight. The test cylinder was empty or, in some experiments, partly filled with water up to the level of 680 mm. The theoretical modal analysis of the test cylinder was performed with the STRUDL /9/ and SING-S /1-3/ computer codes. The technique applied in the experimental modal survey of the test cylinder involves transient step or impulse excitation of the shell, simultaneous measurement and recording of the resulting acceleration responses of the shell, and subsequent evaluation of these response signals with the EVA computer code /10/. This yields a set of natural frequencies, mode shapes and critical damping ratios of the test cylinder. The calculations performed are specified in section 2. The experimental setup and the procedure of evaluation used are explained in section 3. The calculated eigenfrequencies and the associated mode shapes of the test cylinder are presented and compared with the corresponding experimental data in section 4, where also the extracted values of the critical damping ratio are presented. The conclusions are drawn in section 5.

2. Computer programmes used in the theoretical modal analysis

The natural frequencies and the corresponding mode shapes of the empty

test cylinder were calculated with the STRUDL finite-element programme
/9/ implemented on an IBM 3033 computer. As plane symmetry had been
postulated for the test cylinder, only one half of it was incorporated
into the theoretical model; the corresponding discretization is il-
lustrated in fig. 3. The defined half-structure was represented by 570
SSHQ-elements and 294 SBCT-elements with a total of 734 nodal points and
549 dynamic degrees of freedom. The calculations performed yielded 549
eigenmodes with the eigenfrequency values located in the frequency
interval of 115.77 - 4466.8 Hz. The stiffness and mass matrices created
here were used as an input data set in the modal calculations of the
test cylinder partly filled with water. These calculations were perfor-
med with the SING-S fluid-structure-interaction-code /1-3/. The corres-
ponding discretization is illustrated in fig. 4. It uses 495 elements
with 447 unknowns and constitutes 323 coupling degrees of freedom. The
calculations performed yielded 549 eigenmodes with the eigenfrequency
values in the frequency range 54.98 - 4465.2 Hz. Several typical low-
frequency modes obtained in both calculations are presented and compared
with the corresponding experimental quantities in section 4.

The mechanical properties of the structural material of the test cylinder were
described in all calculations by the Young's modulus value $E = 1.991 \times 10^{11} N/m^2$,
the steel density $\varrho = 7.8 \times 10^3$ kg/m^3, and the Poisson's ratio $\mu = 0.3$. The
density of water was estimated at the value $\varrho_F = 1000$ kg/m^3.

3. Experimental setup and modal evaluation procedures

The experimental setup used is illustrated in figs. 1 and 2. Two single
excitation means, e.g. a snapback device acting on the lower generatrix
or an impact hammer (provided with a soft rubber stick) applied on the
upper generatrix of the test cylinder, were alternatively used to generate
the relaxation response of the shell which is needed to derive its modal
characteristics. The resulting response of the shell was simultaneously
measured with 32 piezoresistive accelerometers, type 2264-200 (Endevco)
or GY-155-200 (Kulite), installed stepwise in 157 measuring positions on
the shell (see the shell development presented in the lower part of fig. 1).
Four fixed reference positions were used in all experiments; the corres-
ponding coordinates are z = 800 mm, $\varphi = 0°$; z = 800 mm, $\varphi = 180°$;

z = 1000 mm, $\varphi = 0^O$ and z = 1000 mm, $\varphi = 180^O$. The remaining 28 accelerometers were located somewhere on two cylinder perimeters (30 equidistantly spaced positions at z = 800 or z = 1000 mm) and seven generatrices (17 equidistantly spaced positions at $\varphi = 0^O$, 45°, 126°, 150°, 162°, 180° and 270°, respectively). The accelerometers were fed from 5 kHz-carrier amplifiers, type VD6 (Elan), connected to a computerized data acquisition system /11/. All 32 simultaneously measured response signals of each individual experiment were recorded on magnetic tape, which was subsequentely used as an input for the IBM 3033-computer. The modal characteristics of the test cylinder were extracted from the signals recorded using the EVA computer code. The mathematical background and the most important subroutines of this code are described in detail in /10/. The output of this code is a system of natural frequencies f_n, critical damping ratios ζ_n and initial values C_{rn}; the latter relating to R accelerometer positions denoted by r = 1, 2, ..., R.

A new subroutine, MODAP, has been developed to make visible the mode shapes extracted. It approximates the set of R C_{rn}-values (for each n fixed) through one three-dimensional modal surface C_n (z, ϕ). This approximation is based on the assumption

$$C_n (z, \phi) = \sum_{m=1}^{M} Z_m (z) \phi_m (\phi). \qquad (1)$$

Each of the two separated functions $Z_m(z)$ and $\phi_m(\phi)$ is represented by one Fourier series according to the equations

$$Z_m(z) = \sum_{l=L_1}^{L_1+L-1} \left(a_{l,m}\, e^{i2\pi lz/z_p} + b_{l,m}\, e^{-i2\pi lz/z_p} \right) \qquad (2)$$

and

$$\phi_m(\phi) = \sum_{k=K_1}^{K_1+K-1} \left(\alpha_{k,m}\, e^{ik\phi} + \beta_{k,m}\, e^{-ik\phi} \right) \qquad (3)$$

where $0 \le z \le z_{max}$, $0 \le \phi \le 2\pi$, $1 \le L_1 \le 8$ and $1 \le K_1 \le 4$; M, L. K, z_p and z_{max} are variable input parameters (in both examples presented further below the

following input parameter values were used: M=2, L=3, K=7, z_p=3200 and z_{max}=1600). The coefficients $a_{l,m}$, $b_{l,m}$, $\alpha_{k,m}$ and $\beta_{k,m}$ as well as the integers L_1 and K_1 are determined automatically by the subroutine.

A total of 18 modal experiments were performed on the empty shell; their evaluation yielded 24 eigenmodes identified in the frequency range 0 - 320 Hz. In case of the test cylinder partly filled with water, execution of 60 modal experiments utilising all 157 accelerometer positions was necessary to identify the rather complicated modes. Their evaluation yielded 17 modes identified in the frequency range 0 - 200 Hz.

4. Comparison of theoretical and experimental results

To compare the theoretical and experimental mode shapes and the corresponding eigenfrequencies, two sets of plots are presented and discussed in this section. In each figure of each set at least two longitudinal sections and two developed circumferential sections through the particular three-dimensional mode shape are plotted. A solid line in each plot denotes the theoretical mode shape calculated with the STRUDL or SING-S computer code. A set of discrete points (e.g. ● , O or □) denotes the experimental mode shape extracted from the response signals by the EVA computer code. The corresponding calculated and experimental eigenfrequencies f_n as well as the extracted critical damping ratio ζ_n are summarized at the bottom of each figure.

4.1 Empty test cylinder

The results of theoretical and experimental modal analyses of the empty test cylinder are illustrated in figs. 5 through 33. Figures 5 through 15 show the mode shapes with one half-wave in the axial direction and 2 to 10 full waves on the perimeter of the test cylinder. Figure 5 shows the calculated and extracted modes with two full waves in the circumferential direction. The experimental points exhibit remarkable scatter, indicating a poor signal/noise ratio of the contribution in the original response signal used for the extraction of the mode. This is due to a low capability of excitation of the given mode. However, the agreement between the calculated and the extracted mode shapes is acceptable. The calculated natural frequency (280.38Hz) is approx. 7.5 % higher than the

extracted value (260.56 Hz). This is presumably due to an overestimation by the STRUDL computer code of the rigidity of the welded connection between cylindrical shell and test cylinder flanges. A similar result was obtained in case of the vertical test cylinder /7/. Figure 6 illustrates the mode shape with three full waves in the circumferential direction. This mode, similar to the preceding one, also reveals considerable scatter of experimental points as well as an overestimation of the calculated natural frequency value. Moreover, an impressed orientation of the extracted mode with the maximum at approx. 150° can be observed. It is supposed that this mode orientation is due to the influence of the weld seam, which constitutes an imperfection in the second quadrant (see fig. 1). Figure 7 shows the mode shape with four full waves in the circumferential direction. An interesting feature of this mode is a distinct deterioration approx. at 200° of an ideal wave form, indicating a superposition of two mode shapes. Also the calculations did not yield a "clear" mode shape with four full waves on the perimeter; the "mixed mode" obtained will be discussed further below in this section. Figures 8 and 9 illustrate the extracted doublet with five full waves in the circumferential direction. There is only a slight difference of approx. 3 % between both natural frequencies extracted (111.61 and 113.23 Hz, respectively), but a distinct difference of approx. 10° in the orientation. The calculated natural frequency of 115.77 Hz is slightly higher, namely 3.7 and 2.2 %, respectively, than the extracted values. Only one mode with five full waves in the circumferential direction was calculated, in accordance with the suppositon of a plane symmetrical shell used in the corresponding mathematical model. The occurence of the doublet is presumably caused by the structural imperfections mentioned above; a similar observation was made also for the vertical test cylinder /7/. Figures 10 and 11 illustrate a doublet with six full waves in the circumferential direction. Also here only a slight difference between the natural frequencies extracted (125.80 and 126.45 Hz) can be observed. It indicates the presence of minor structural imperfections giving rise to the doublet. The calculations did not yield a clear mode with six full waves in the circumferential direction; the "mixed modes" obtained will be presented further below. Figures 12 through 15 illustrate the mode shapes with 7, 8, 9 and 10 full waves, respectively, on the perimeter. The calculated and the extracted natural frequencies of these modes are very similar and reveal differences smaller than 1 %.

This indicates that mathematical modelling of the test cylinder shell by the STRUDL computer code is adequate.

The calculated and the extracted natural frequencies of the modes discussed above are plotted in fig. 16 over the parameter v, denoting the number of full waves in the circumferential direction. The theoretical values are denoted by the symbol ● , the experimental ones by ○. The plot is very similar to that of the vertical cylinder traced in fig. 41 of the report /7/ and reproduced here as fig. 17. To elimi- nate possible misunderstandings resulting from the intercomparison of figs. 16 and 17, it should be mentioned here that an equivalent of the fundamental beam mode (mode with a natural frequency of approx. 32 Hz) cannot be expected in case of the horizontal test cylinder. Moreover, the natural frequency of the mode with one half-wave in the axial direc- tion and one full wave in the circumferential direction will presumably be located near 400 Hz which is well above the upper frequency limit of 320 Hz used in our experiments. The same is true in case of the modes with more than 10 full waves on the test cylinder perimeter.

Figures 18 through 25 illustrate the mode shapes with one full wave in the axial direction and 5 to 10 full waves on the perimeter of the test cylinder. For the calculated mode shape with 10 full waves on the peri- meter (f = 312.31 Hz, fig. 25) no experimental counterpart was extracted from the response signals. On the other hand, three doublets with slightly different natural frequencies were identified (modes with five, eight and nine full waves on the perimeter, figs. 18, 19, 22, 23 and 24). The natural frequencies of all these modes are plotted over the parameter v in fig. 16 (symbol △ denotes the experimental and symbol ● the calculated values). It follows from this plot that the calculated eigenfrequencies of the modes with a small number of waves on the test cylinder perimeter are slightly overestimated; the corresponding devia- tion (max. value 3.6 %) decreases with v and practically vanishes at v = 8 and 9. A similar trend was observed in case of the vertical test cylinder (see fig. 17).

Figures 26 through 29 demonstrate the mode shapes with three half-waves in the axial direction and seven, eight or nine waves, respectively, on the perimeter of the test cylinder. The wave forms are considerably

distorted. For instance, the seven distinct full waves noticed in the
upper right plot in fig. 26 cannot be identified on another perimeter
(lower plot). Moreover, a remarkable mutual phase shift in the axial
direction can be seen on the plots on the left side of fig. 26. Figures
27 and 28 illustrate the doublet with eight full waves on the perimeter;
fig. 29 illustrates an extracted single mode with nine full waves. The
corresponding natural frequencies are plotted over the parameter v in fig.
16; symbol ● denotes the calculated and symbol ◇ the experimental va-
lues. They seem to follow a trend similar to that plotted in fig. 17.

Figures 30 through 33 illustrate the "mixed modes" announced above.
Figure 30 shows the mode shape with one half-wave in the axial direction
and six distorted full waves in the circumferential direction. This indicates
the superposition of forms with five and seven full waves, respectively,
on the perimeter. The measured eigenfrequency of 120.63 Hz fits very well
the lower curve in fig. 16 at v = 5 (symbol +). Figure 31 illustrates a
superposition of modes with four and six full waves, respectively, in
the circumferential direction. The calculated eigenfrequency of 128.19
Hz fits very well the lower curve in fig. 16 at v = 4 and 6, respective-
ly (symbol X). It should be recalled here that the calculations did not
furnish any "clear" mode with one half-wave in the axial and four or six
waves, respectively, in the circumferential directions. This circumstan-
ce has already been mentioned above in the discussion of fig.s 7, 10 and
11. Figures 32 and 33 present the calculated, strongly distorted mode
shapes for which no experimental counterpart was extracted.

Some additional insight into the complicated structure of mode shapes of
the horizontal test cylinder is offered by use of the MODAP subroutine
of the EVA computer code. As already mentioned in section 3, the objec-
tive of this subroutine was to visualize the mode shapes extracted.
However, the decomposition of each mode into components according to
eqs. (1) through (3) quantifies the measure of contributions of "ideal"
cosine modes and offers more information on the mode structure than pure
intuitive considerations. Several typical relief plots generated by the
MODAP subroutine are displayed as examples in fig. 34. The corresponding
original extracted mode shapes are presented in figs. 9,30 and 10. For
instance, the lower mode in fig. 34 (f = 125.85 Hz) was identified in fig.
10 as a mode with one half-wave in the axial direction and six full waves

in the circumferential direction. However, application of the MODAP sub-
routine reveals a rather more complicated structure. This reality is
illustrated in table I. In this table the complex coefficients $a_{1,m}$ and
$b_{1,m}$ of eq. (2) are summarized for m = 1 and 2 and l = 1, 2 and 3 as well
as the complex coefficients $\alpha_{k,m}$ and $\beta_{k,m}$ of eq. (3) for m = 1 and 2 and
k = 3, 4, 5, 6 and 7. It immediately follows from this table that the
regular cosine pattern with one half-wave in the axial direction and six
full waves in the circumferential direction constitutes the biggest con-
tribution to the given eigenmode. However, it is also evident that the
contributions not to be neglected of other patterns (mainly the fourth and
fifth circumferential orders) are also included. Similar additional infor-
mation was provided by the analysis with the subroutine MODAP of all
remaining extracted eigenmodes.

The critical damping ratios ζ of all modes extracted enter beside the
corresponding natural frequency value at the bottom of each figure. The
majority of them is comparable to critical damping ratios of the verti-
cal cylinder /7/. Several exceptions are the critical damping ratios of
the modes with one half-wave in the axial direction and a small number
of waves in the circumferential direction v ≤ 7; which are in general
substantially smaller than those of the vertical cylinder. It is assumed
that this phenomenon is caused by a lower energy dissipation rate in
test cylinder flanges. The energy dissipation in the test cylinder shell
is presumably the same in both cases.

4.2 Test cylinder partly filled with water

The presence of the water charge in the test cylinder causes a further
modification of the eigenmode patterns. The mode shapes are only of the
"mixed type" with strong participation of several regular cosine pat-
terns and they do not reveal any distinct predominance of one of these
patterns. Therefore, plotting the natural frequencies f over the circum-
ferential order v of the "predominant" cosine mode contribution is not
meaningful and does not furnish smooth f-v-curves as in the case of the
empty test cylinder.

Figures 35 through 44a illustrate the mode shapes with one half-wave in
the axial direction and 4 to 9 distorted waves on the perimeter of the
test cylinder. Figures 35 and 35a show the mode shape with four distorted

waves. This mode is similar to the "mixed mode" shown in fig. 30 which
comprises the components with 4 and 6 full waves on the perimeter of the
test cylinder. The calculated and the extracted mode shapes are well
comparable, and the calculated natural frequency is approx. 2.5 % smaller
than the corresponding experimental value. Figures 36 and 36a illustrate
the mode with 5 distorted waves on the perimeter. The circumferential wave
form is similar to that of the preceding case. The attenuated amplitudes
at the top of the test cylinder indicate the predominant influence on this
mode of the water charge. Figures 37 through 39 illustrate the mode with 6
distorted waves on the perimeter. The modes presented in figs. 38, 38a, 39
and 39a are symmetric with respect to the 0 - 180° plane. In contrast, the
mode shown in fig. 37 is skew-symmetric and cannot be predicted theoreti-
cally by postulating the plane symmetry mentioned in section 2. However, it
is not clear to which extent the existence of this mode might be caused by
the structural imperfections discused in the preceding paragraph. Figures
40 and 40a illustrate the mode with seven distorted waves on the perimeter.
It is plane symmetric and fits very well the calculated mode. Figures 41
and 41a illustrate the mode with 8 distorted waves on the perimeter. The
structure of this mode was analysed with the subroutine MODAP; the corres-
ponding results are summarized in table II and the reconstructed mode shape
is presented as a relief plot at the bottom of fig. 42 (the analysis
relates to the results of modal experiment other than that illustrated in
fig. 41, and the extracted eigenfrequency is approx. 0.8 % higher). It
follows from table II that the total contribution of the regular cosine
patterns with 4, 5 and 9 waves on the perimeter even exceeds the contribu-
tion of the "predominant pattern" with 8 cosine waves. A similar struc-
ture is revealed also by the modes with 9 distorted waves on the perime-
ter, illustrated in figs. 43 through 44a. The extracted modes constitute a
doublet with one symmetric (fig. 44) and one skew-symmetric (fig. 43)
mode. The mode shape of the symmetric mode fits very well the mode shape
of the calculated mode, but the corresponding natural frequency is approx.
5 % lower.

Figures 45 through 51 show 7 extremely distorted modes with partly one and
partly two half-waves in the axial direction and 7 to 9 waves on the
perimeter of the cylinder. Figures 45 and 45a illustrate the mode with
seven distorted waves on the perimeter, one full wave at $\varphi = 0^{o}$, one half-
wave in the first and second quadrants ($\varphi = 45^{o}$, 126°, 150° and 162°) and
quasi-nodes at 180° and 270°. This mode is skew-symmetric with respect to

the 0-180°-plane and has no calculated counterpart. The calculated mode
with seven distorted waves on the perimeter, presented in fig. 46, reveals
one distorted half-wave at $\varphi = 0°$ and one distorted full-wave at 180° and
270°. Figures 47 through 50 illustrate the modes with 8 waves on the
perimeter. They are characterized by two distorted half-waves at $\varphi = 0°$
and one distorted half-wave at $\varphi = 180°$. The calculated mode shape presen-
ted in fig. 48 is tentatively compared with two experimental mode shapes,
yielding (apart from opposite polarities) partial agreement in indivi-
dual sections. It should be noted here that the modes illustrated in
figs. 47 to 48a have maximum amplitudes at $\varphi = 180°$, indicating that
their dynamics is governed primarily by the test cylinder shell. This
makes them susceptible to the influence of the structural imperfections.
The modes governed by the water charge and presented further below in
this paragraph do not have the same susceptibility and reveal better
congruence between calculated and extracted mode shapes. For calculated
mode shapes presented in figs. 49 to 51 no experimental counterparts
were found, presumably due to the presence of quasi-nodes in the loca-
tion of the snapback devices ($\varphi = 0°$ and z = 800 and 1000 mm).

Figures 52 through 54a illustrate the mode shapes with one full-wave in
the axial direction and 6 to 9 distorted waves on the perimeter of the
test cylinder. The presence of the nodes in the middle of the test cylin-
der (z = 800 mm) makes these modes less sensitive to excitation acting on
this plane. This is presumably the reason why no experimental counterparts
to the calculated modes presented in figs. 52 and 53 were found. An
adequate experimental counterpart was found only in case of the mode with
nine waves on the perimeter, illustrated in figs. 54 and 54a. The axial
sections of this mode reveal good agreement between the calculations and
the experiment. However, only a rough agreement can be observed to exist
for both radial sections presented.

Figures 55 through 57a illustrate the mode shapes with three half-waves in
the axial direction and 7 or 9 full waves on the perimeter of the test
cylinder. The wave forms are considerably distorted and reveal very small
amplitudes at the top of the test cylinder ($\varphi = 180°$), indicating a tight
coupling of the corresponding modes with the water charge of the test
cylinder. The experiments yielded two slightly different modes with seven
not clearly modelled waves on the perimeter, illustrated in figs. 55, 55a
and 55b. They have opposite polarities at $\varphi = 270°$ and slightly different

natural frequency values of 166.73 and 168.35 Hz, respectively. They are both tentatively compared with the corresponding calculated mode in fig. 55. There is a good global congruence of all three modes presented; the deviations observable in individual sections are obviously caused by different orientations in space of these modes. Figures 56 and 57 show two calculated mode shapes with nine distorted waves on the perimeter. The first of them has maximum amplitudes near $\varphi = 60^{\circ}$ and 300° and quasi-nodes at the locations of the exciting devices. Thanks to this circumstance no experimental counterpart of the calculated mode was found. The calculated and the extracted mode shapes plotted in fig. 57 reveal good mutual accordance, especially in sections with the distinct amplitudes ($\varphi = 0^{\circ}$ and 270°).

The critical damping ratios ζ of the modes extracted are of the order of several per mill and generally do not exceed the critical damping ratios of the empty test cylinder. However, due to the non-congruence of the extracted mode shapes of the both test objects (test cylinder empty or partly filled with water) it is not possible to intercompare the corresponding critical damping ratios and to assess quantitatively the contribution of the viscous damping to the total damping.

Conclusions

Unlike in the vertical case, the horizontal arrangement of the shell destroys the regular cosine pattern of its eigenmodes. The eigenmodes of the empty test cylinder have been found to be composed of significant contributions by several cosine patterns with a distinct main contribution by one of them. The natural frequencies of the empty test cylinder can be plotted over the circumferential order of the predominant cosine pattern (v-f-plot) and reveal trends similar to those of the vertical shell.

The presence of the water charge in the test cylinder causes additional distortions of the eigenmode patterns. The contribution to the individual mode shapes of the particular "predominant" cosine patterns is less significant, and tracing the v-f-plots is not meaningful. The calculated and the extracted mode shapes are nearly congruent; the deviations observable in individual sections are in most cases caused by different spatial orientations of these modes which in turn are caused by structural imperfections

of the test cylinder. The calculated and extracted natural frequencies are well intercomparable and the mutual deviations generally do not exceed several per cent. The extracted values of the critical damping ratio ζ are of the order of several per mill and do not attain 0.5%.

References

/1/ Krieg, R.: Coupled Problems in Transient Fluid and Structural
Dynamics in Nuclear Engineering. Appl. Math. Modelling, June 1978,
Vol. 2, S. 81-89

/2/ Krieg, R., Hailfinger, G.: Transient, Three-dimensional Potential
Flow Problems and Dynamic Response of the Surrounding Structures.
Part I: Description of the Fluid Dynamics by a Singularity Method.
Journal of Computational Physics, 34, No. 2, p. 139 - 163, (1980)

/3/ Krieg, R., Göller, B., Hailfinger, G.: Transient, Three-dimensional
Potential Flow Problems and Dynamics Response of the Surrounding
Structures.
Part II: Simultaneous Coupling between Fluid and Structural
Dynamics. Journal of Computational Physics, 34, No. 2, p. 164 - 183,
(1980)

/4/ Eberle, F., Göller, B., Hailfinger, G., Kadlec, J.: Eigenoscillations
of a fluid filled cylindrical shell - comparison between theoretical
and experimental results. Transactions Sixth Int. Conf. on Structural
Mechanics in Reactor Technology, Paris 17 - 21 Aug. 1981, Vol. B,
Paper B5/4, p. 1 - 8

/5/ Eberle, F., Kadlec, J., Scharnowell, R.: Vergleich vier verschiede-
ner Methoden der experimentellen Modalanalyse. VDI-Berichte Nr. 456,
195 - 200, 1982

/6/ Eberle, F., Kadlec, J.: Optimization of Procedures for the Experi-
mental Modal Analysis of Fluid/Structure-Interaction Systems. Trans-
actions Seventh Int. Conf. on Structural Mechanics in Reactor Tech-
nology, Chicago, USA, 22 - 26 Aug. 1983, Vol. B, Paper B7/11,
p. 425 - 434

/7/ Eberle, F., Kadlec, J., Hailfinger, G., Scharnowell, R.: Experimental
Modal Survey of a Vertical Cylindrical Shell Partly Filled with
Water. KfK 4004, Kernforschungszentrum Karlsruhe, Jan. 1986.

/8/ Eberle, F., Hailfinger, G., Kadlec, J.: Eigenoscillations of a Horizontal Cylindrical Shell Partly Filled with Water. Transactions Seventh Int. Conf. on Structural Mechanics in Reactor Technology, Chicago, USA, 22 - 26 Aug. 1983, Paper B8/5, p. 483 - 490

/9/ Handbuch für ICES-STRUDL, Version MAN-MBB, Band 1 und 2, MAN, Nürnberg

/10/ Eberle, F., Kadlec, J.: Extraction of Eigenfrequencies, Mode Shapes and Critical Damping Ratios of HDR Core Barrel Mockup from Step Relaxation Response Signals Measured in the Snapback Test Series V59, KfK 3408, Kernforschungszentrum Karlsruhe, Oct. 1982

/11/ Rittirsch, G.: Dezentrales gekoppeltes Mehrrechnersystem zur breitbandigen Meßdatenerfassung und Auswertung. KfK-Nachrichten 1-2, p. 91 - 95, Kernforschungszentrum Karlsruhe, 1980.

List of tables

List of figures

Fig. 48a: Mode shape of the 136.06 Hz-eigenmode (test cylinder partly filled with water)

Fig. 49: Mode shape of the 141.30 Hz-eigenmode (test cylinder partly filled with water)

Fig. 50: Mode shape of the 148.53 Hz-eigenmode (test cylinder partly filled with water)

Fig. 51: Mode shape of the 204.24 Hz-eigenmode (test cylinder partly filled with water)

Fig. 52: Mode shape of the 107.87 Hz-eigenmode (test cylinder partly filled with water)

Fig. 53: Mode shape of the 115.18 Hz-eigenmode (test cylinder partly filled with water)

Fig. 54: Mode shape of the 185.40 Hz-eigenmode (test cylinder partly filled with water)

Fig. 54a: Mode shape of the 185.40 Hz-eigenmode (test cylinder partly filled with water)

Fig. 55: Mode shape of the 166.73 and 168.35 Hz-eigenmodes (test cylinder partly filled with water)

Fig. 55a: Mode shape of the 166.73 Hz-eigenmode (test cylinder partly filled with water)

Fig. 55b: Mode shape of the 168.35 Hz-eigenmode (test cylinder partly filled with water)

Fig. 56: Mode shape of the 173.52 Hz-eigenmode (test cylinder partly filled with water)

Fig. 57: Mode shape of the 195.42 Hz-eigenmode (test cylinder partly filled with water)

Fig. 57a: Mode shape of the 195.42 Hz-eigenmode (test cylinder partly filled with water)

Table I: Coefficients $a_{l,m}$, $b_{l,m}$, $\alpha_{k,m}$ and $\beta_{k,m}$, calculated by the subroutine MODAP for one typical mode ($f = 125{,}85\,Hz$) of the empty test cylinder

$Z_m(z)$

m	l	$Re\{a_{l,m}\}$	$Im\{a_{l,m}\}$	$Re\{b_{l,m}\}$	$Im\{b_{l,m}\}$
1	1	0.246	0.68	- 0.226	- 0.644
	2	0.006	0.016	0.055	0.005
	3	0.02	0.038	0.014	0.009
2	1	- 0.393	- 0.264	- 0.321	- 0.097
	2	- 0.244	0.429	0.135	- 0.412
	3	0.178	0.105	0.364	0.109

$\Phi_m(\phi)$

m	k	$Re\{\alpha_{k,m}\}$	$Im\{\alpha_{k,m}\}$	$Re\{\beta_{k,m}\}$	$Im\{\beta_{k,m}\}$
1	3	- 1.72	1.06	- 2.09	0.72
	4	7.48	2.59	8.72	2.51
	5	3.60	1.33	4.19	1.40
	6	21.42	12.94	23.10	-12.62
	7	- 0.29	- 0.47	- 0.75	0.54
2	3	0.96	2.64	1.38	0.63
	4	0.87	- 6.55	- 2.25	3.57
	5	1.57	- 2.32	- 1.57	0.88
	6	2.91	- 7.73	- 0.53	10.68
	7	1.60	- 0.53	0.11	- 1.19

Table II: Coefficients $a_{l,m}$, $b_{l,m}$, $\alpha_{k,m}$ and $\beta_{k,m}$, calculated by the subroutine MODAP for one typical mode ($f = 136.06\,Hz$) of the test cylinder, partly filled with water

$Z_m(z)$

m	l	$Re\{a_{l,m}\}$	$Im\{a_{l,m}\}$	$Re\{b_{l,m}\}$	$Im\{b_{l,m}\}$
1	1	- 0.114	0.161	- 0.157	-0.105
	2	0.060	- 0.645	0.079	0.648
	3	0.161	- 0.131	0.176	0.068
2	1	- 0.297	-0.647	- 0.022	0.684
	2	- 0.016	-0.057	0.021	0.0514
	3	0.091	0.017	0.0819	-0.05

$\Phi_m(\phi)$

m	k	$Re\{\alpha_{k,m}\}$	$Im\{\alpha_{k,m}\}$	$Re\{\beta_{k,m}\}$	$Im\{\beta_{k,m}\}$
1	3	- 0.183	0.064	- 0.165	- 0.144
	4	1.83	0.597	1.96	- 0.481
	5	1.22	0.940	1.06	- 1.00
	6	- 0.552	-0.200	- 0.537	0.208
	7	- 0.166	- 0.360	- 0.157	0.365
	8	2.74	1.94	2.93	2.05
	9	1.95	0.375	1.95	-0.260
2	3	0.28	0.48	0.429	-0.416
	4	0.06	- 0.468	- 0.219	0.477
	5	0.902	0.686	1.057	0.574
	6	- 1.078	- 0.367	- 1.224	0.179
	7	0.680	0.447	0.902	- 0.388
	8	0.634	0.015	- 0.744	-0.158
	9	- 0.039	0.332	- 0.194	0.378
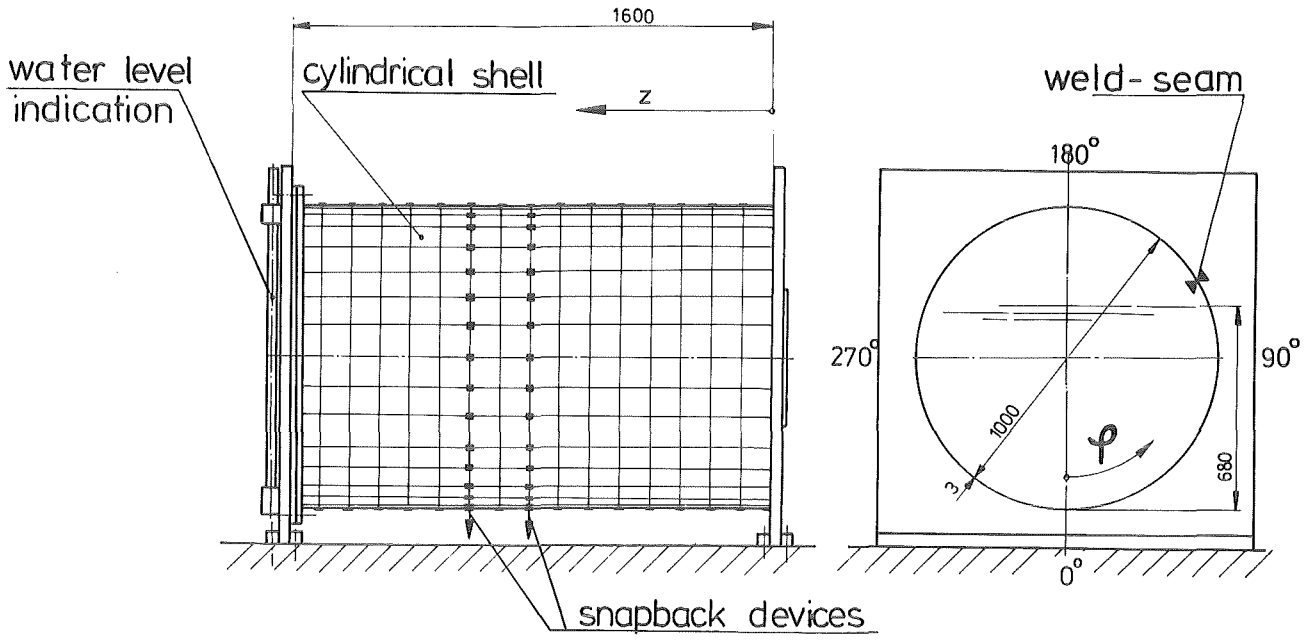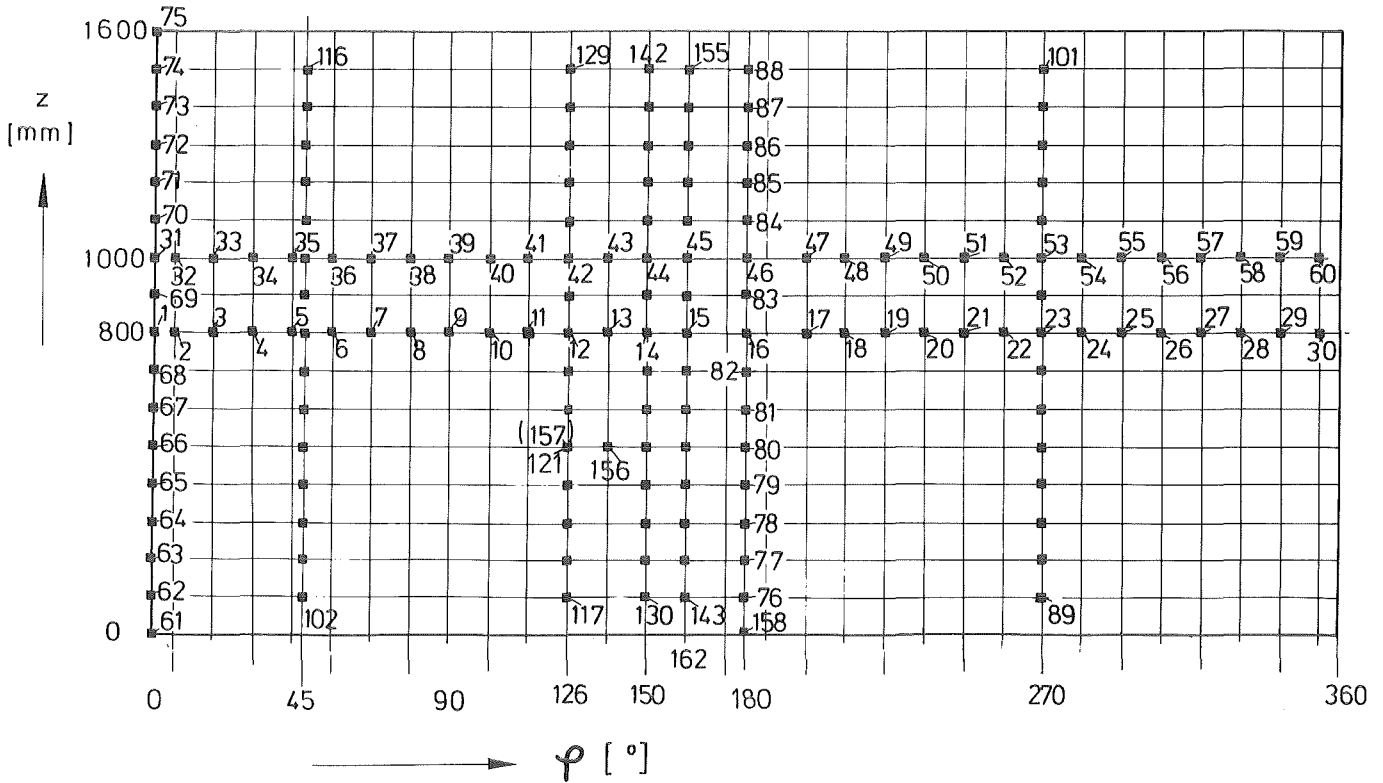
Fig. 1: Test cylinder and instrumentation
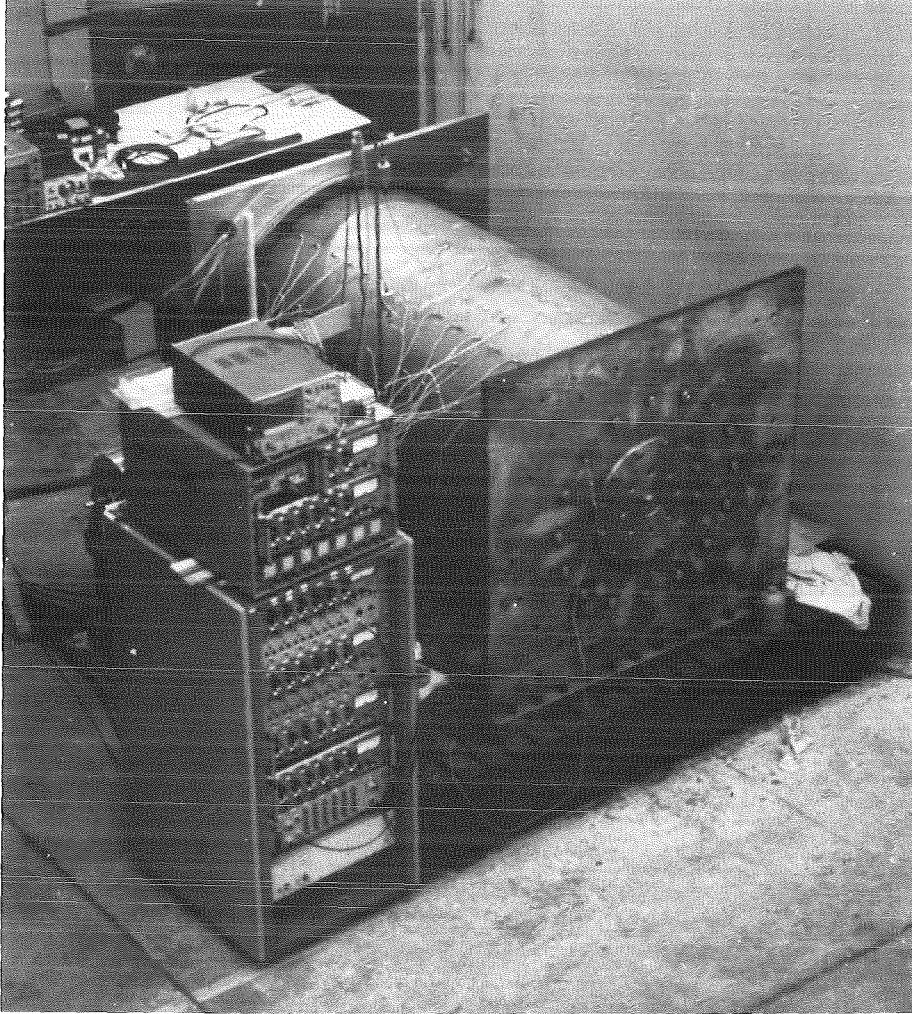
Fig. 2 : Experimental setup
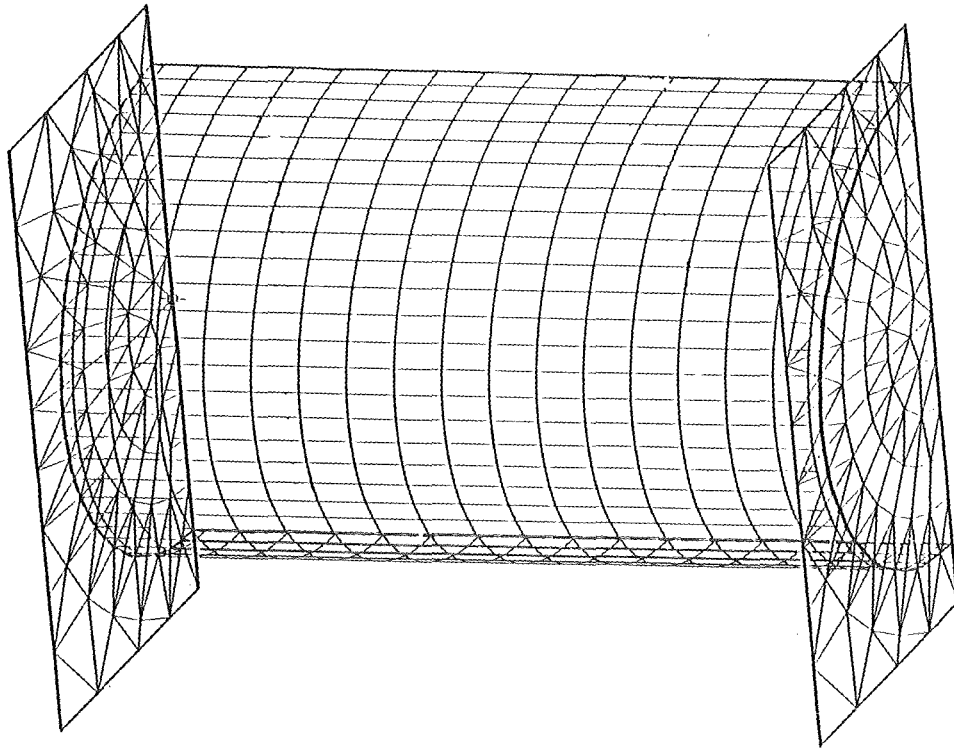
Fig. 3 : Discretization of the empty test cylinder
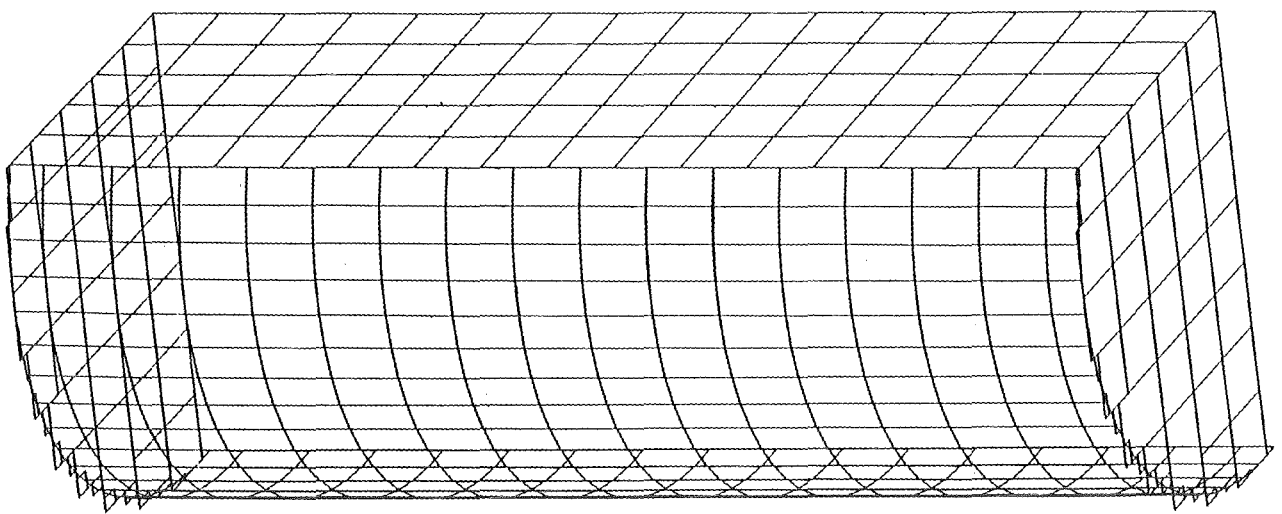
Fig. 4 : Discretization of the water charge boundaries
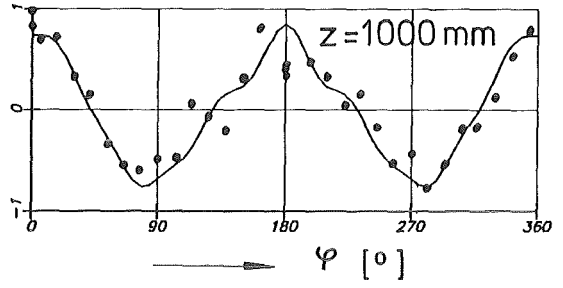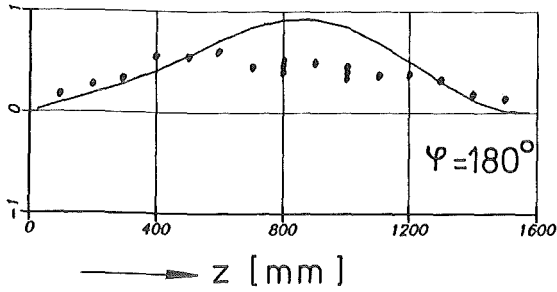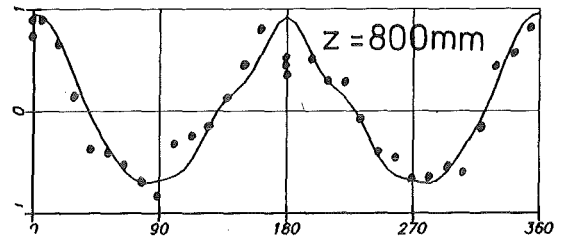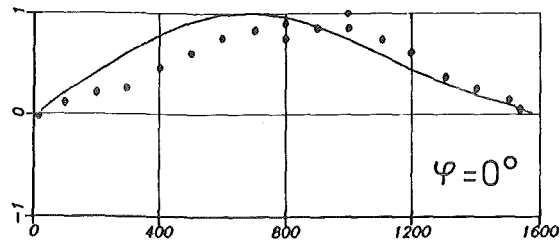
Fig. 5 : Mode shape of the 260.56 Hz-eigenmode (test cylinder empty)
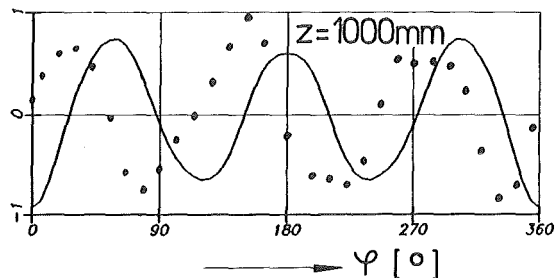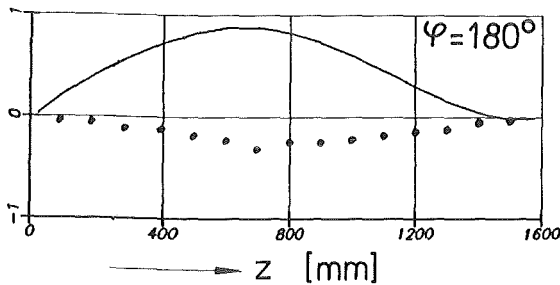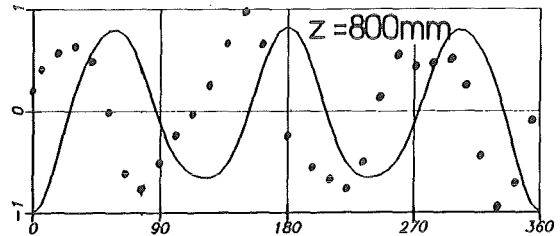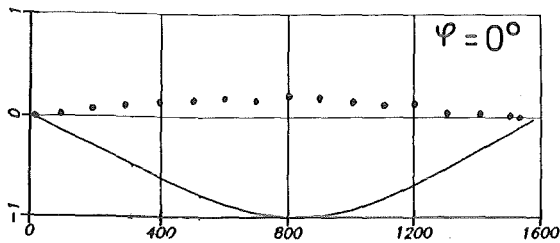
Fig. 6 : Mode shape of the 156.47 Hz-eigenmode (test cylinder empty)
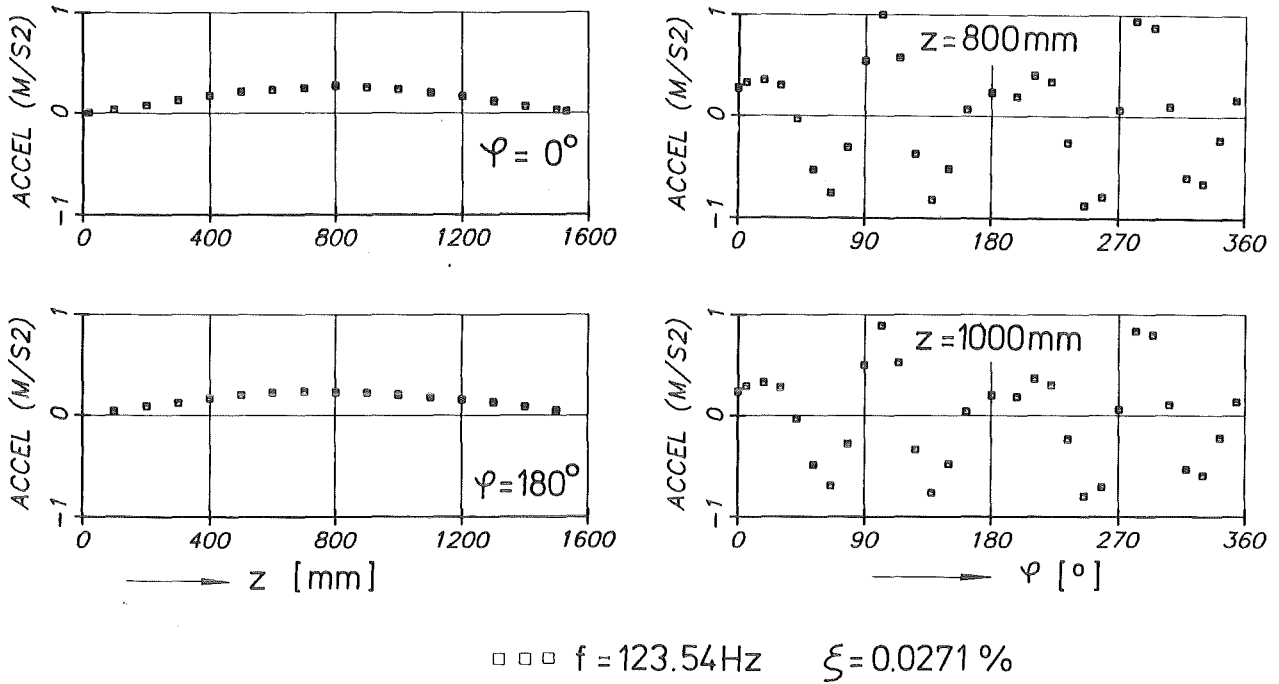
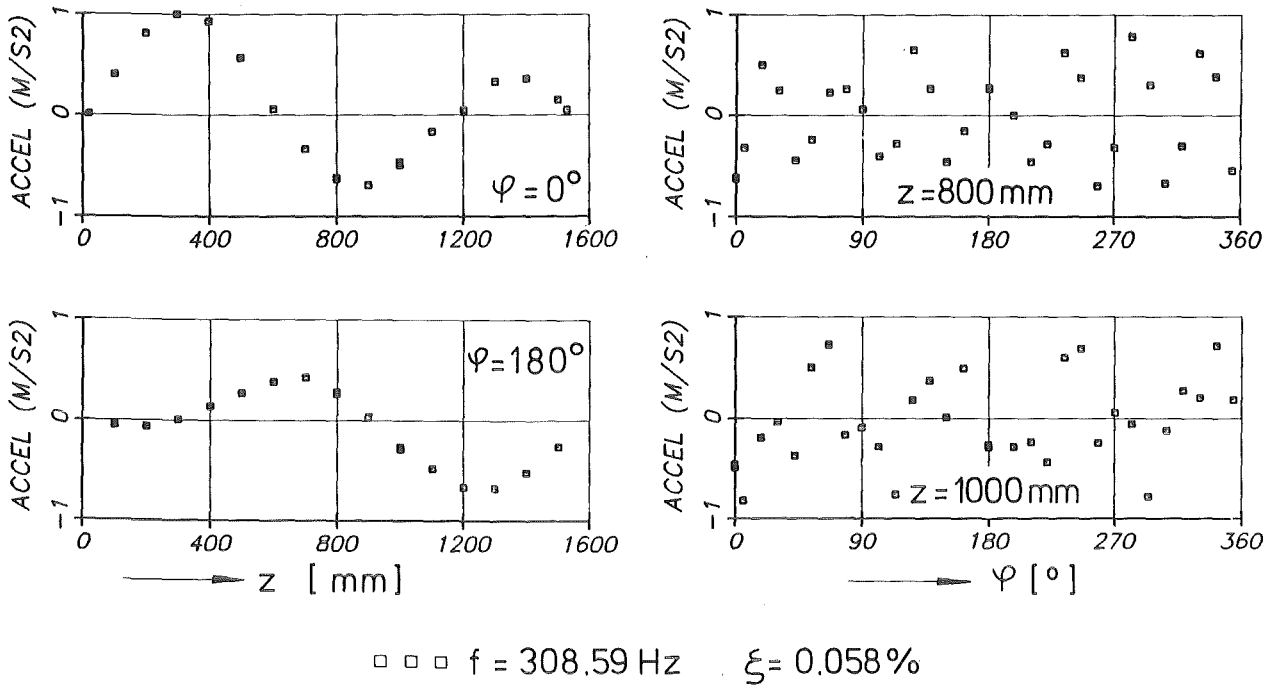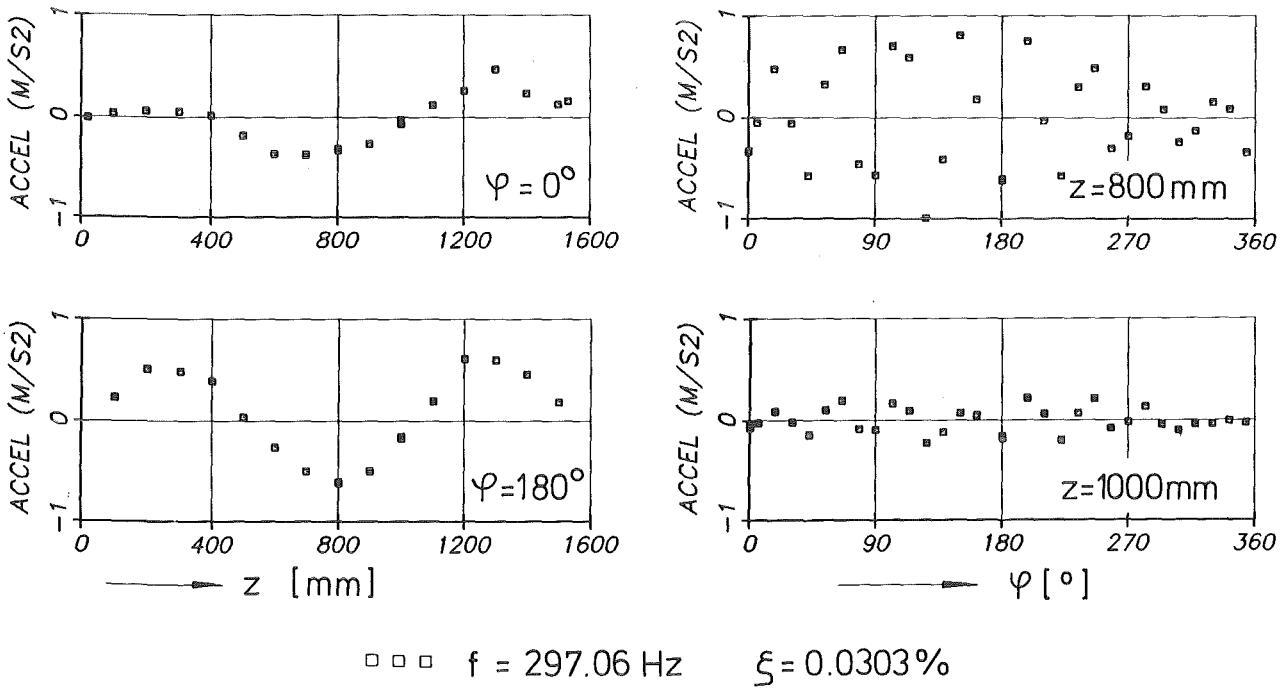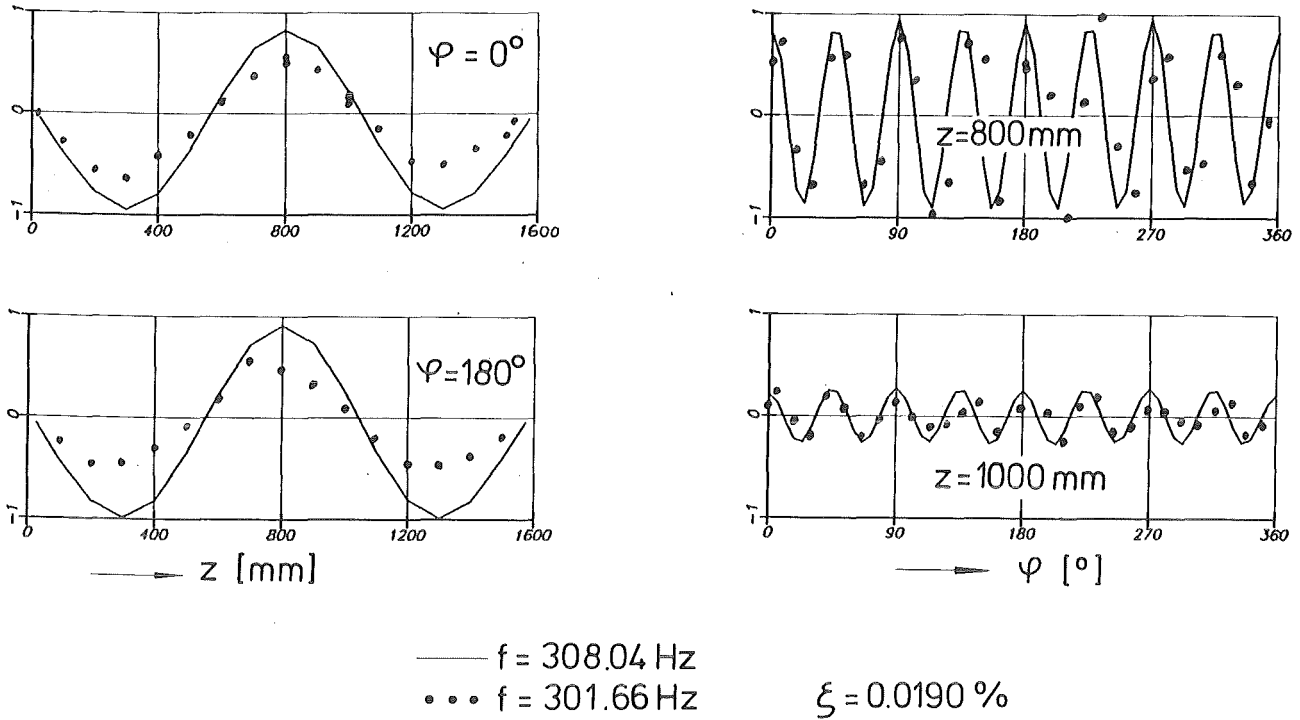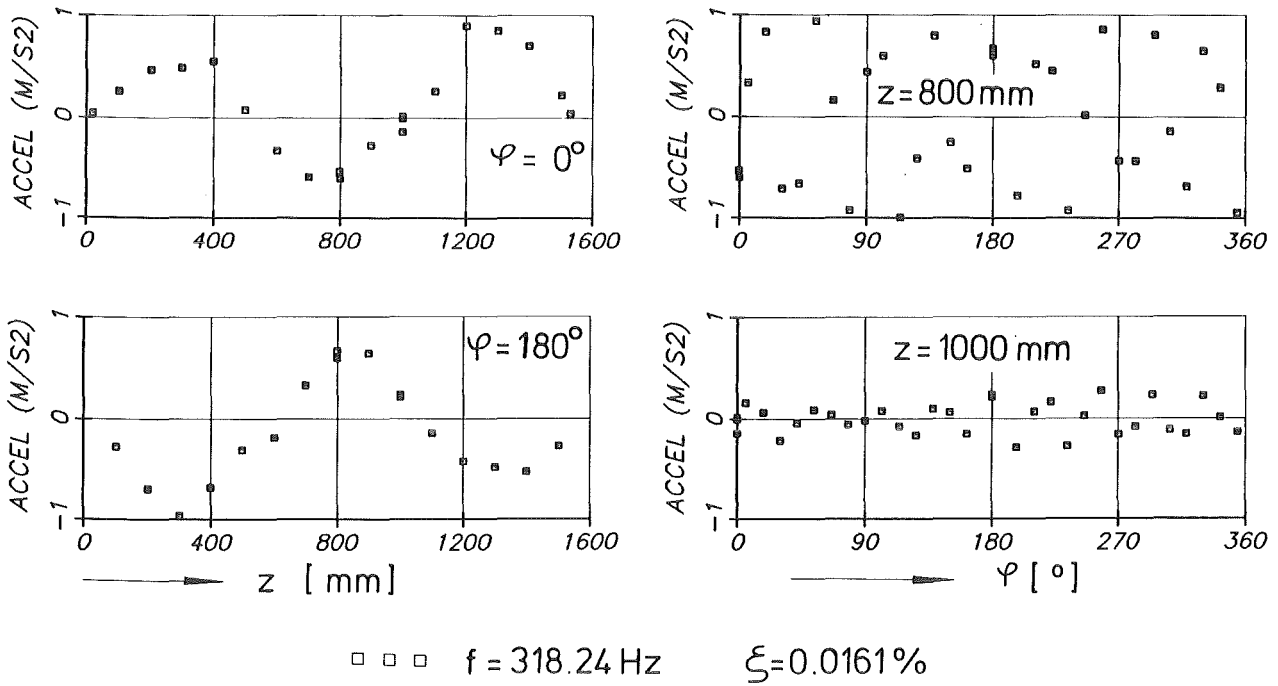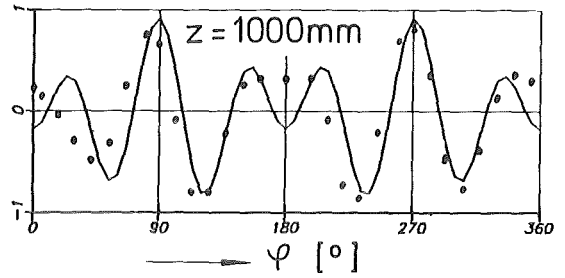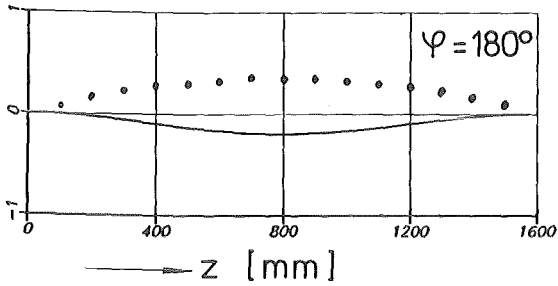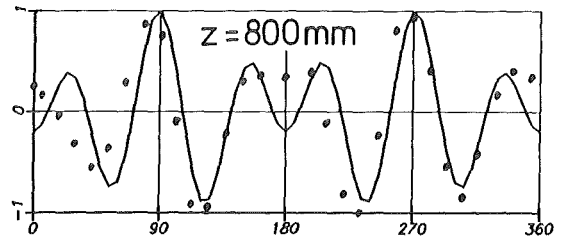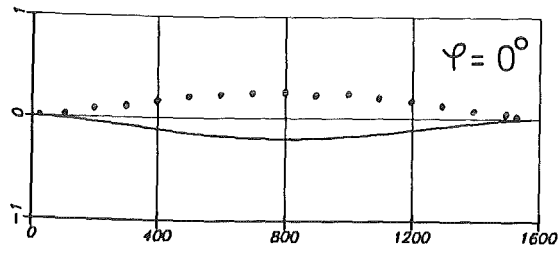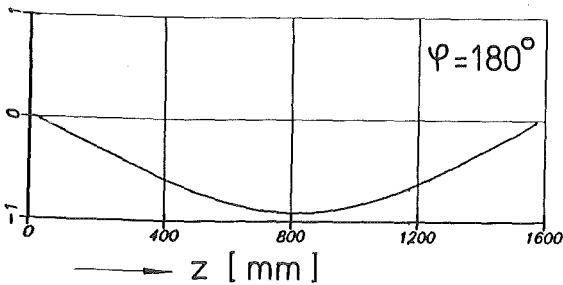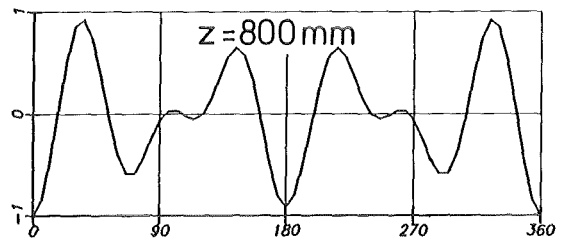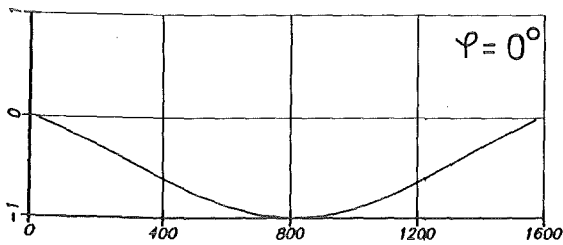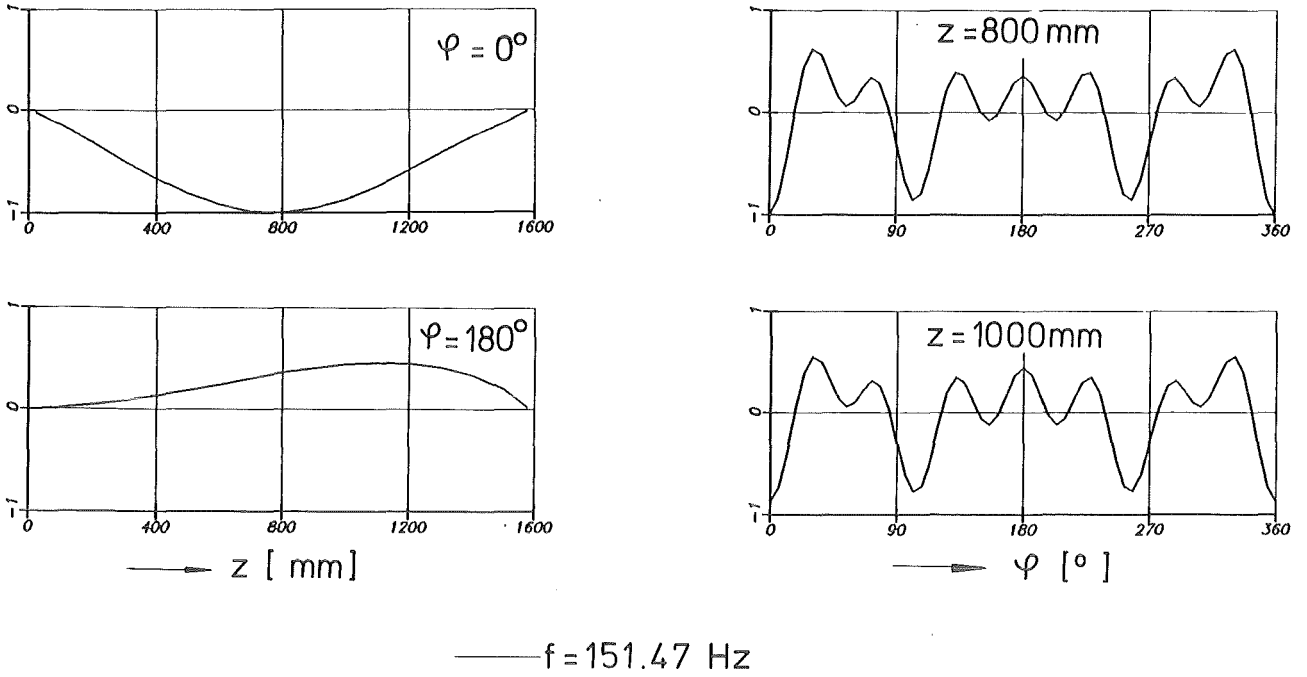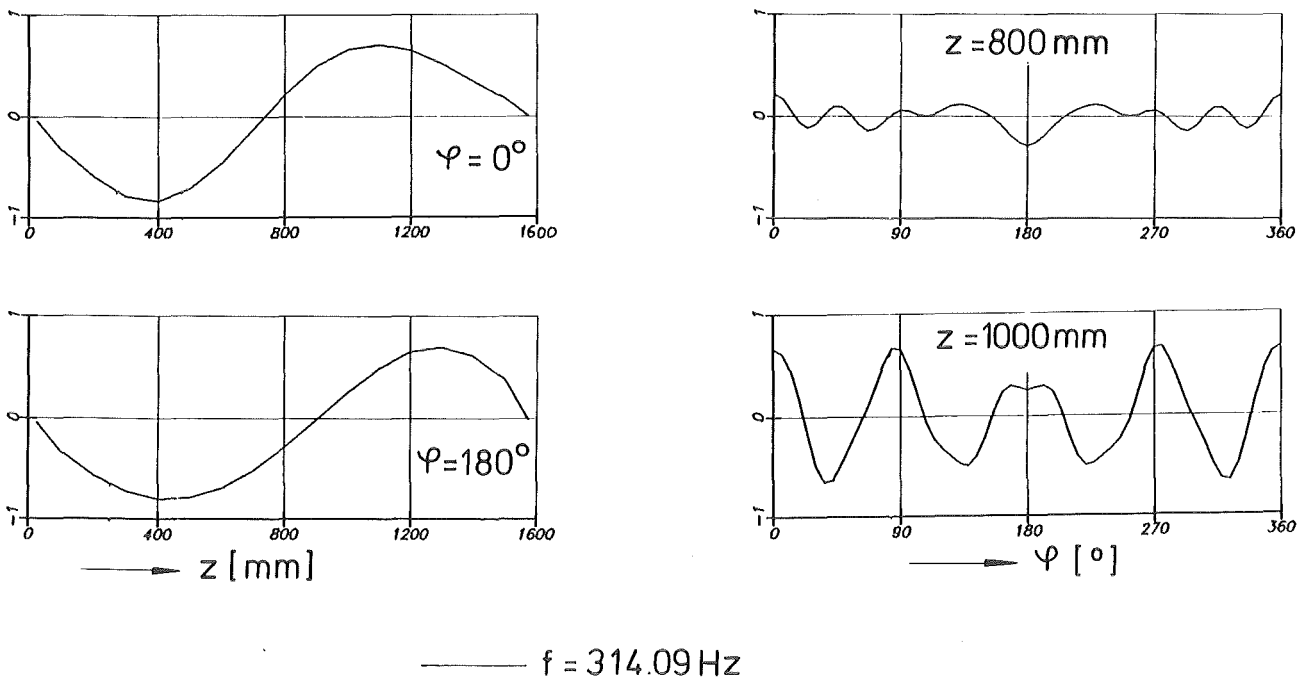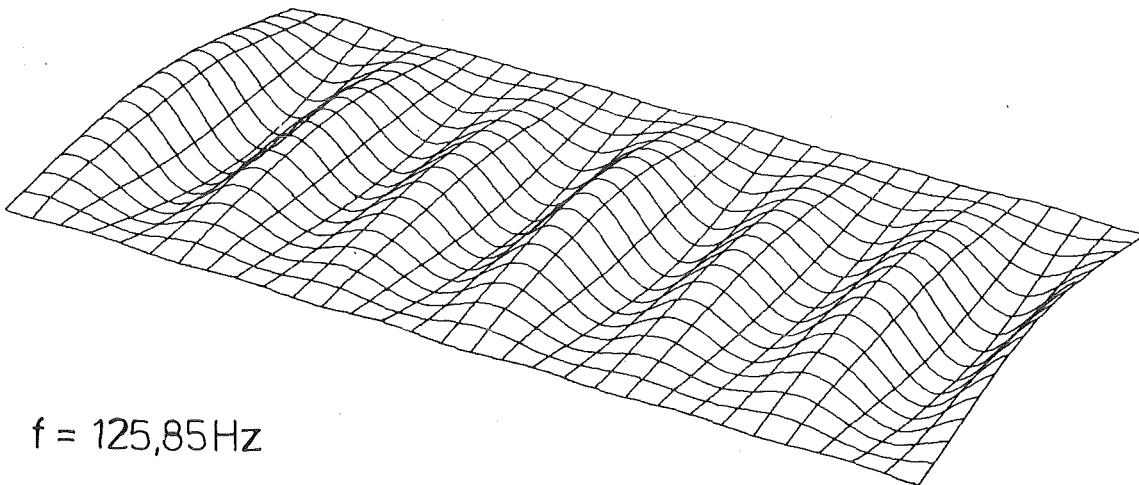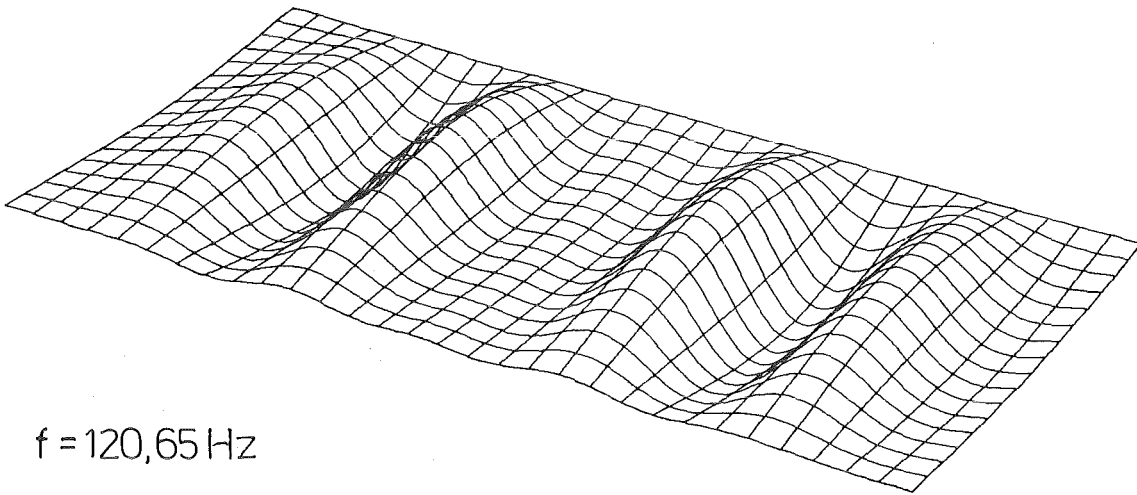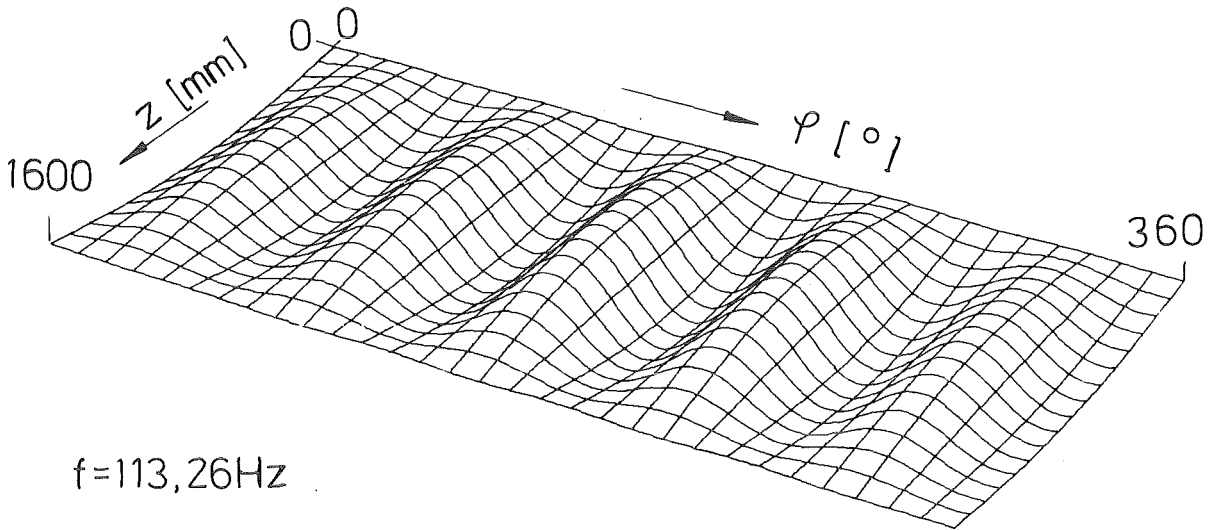Fig. 7 : Mode shape of the 123.54 Hz – eigenmode (test cylinder empty)
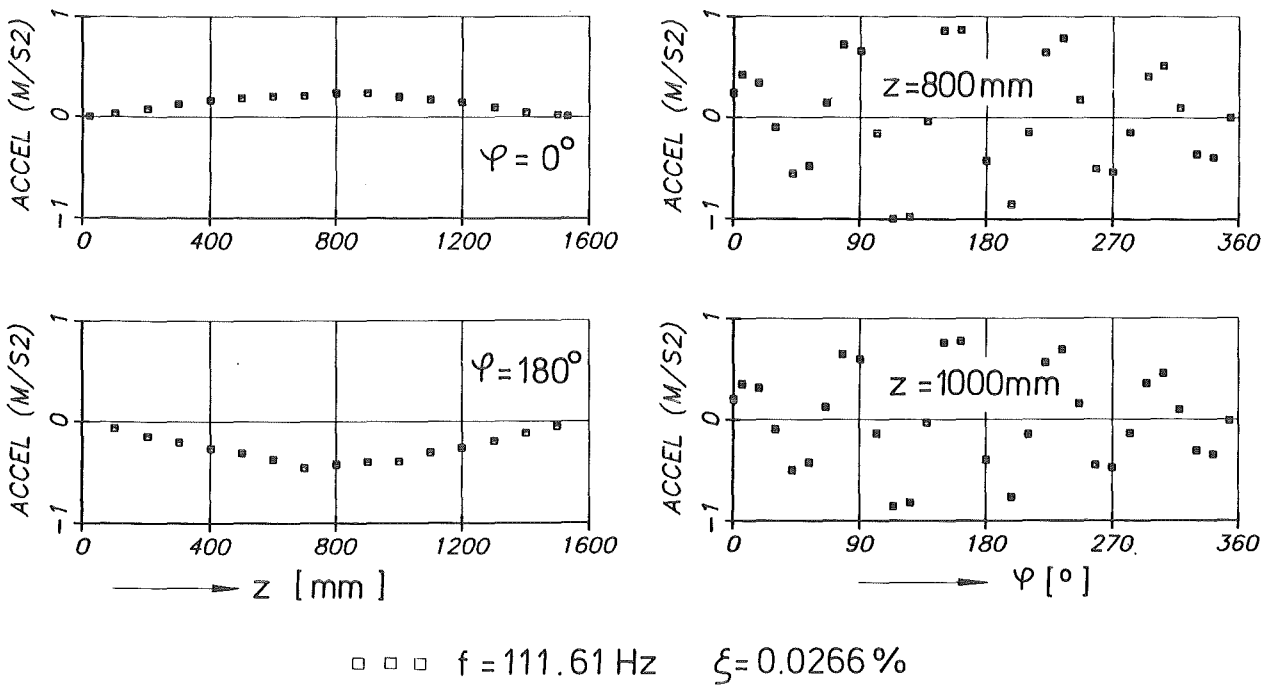
Fig. 8 : Mode shape of the 111.61 Hz – eigenmode (test cylinder empty)
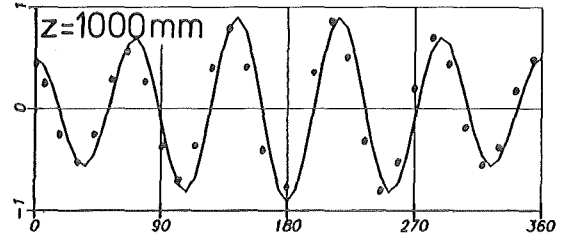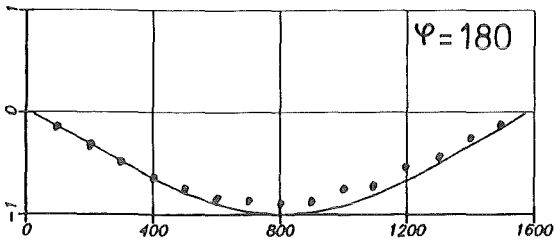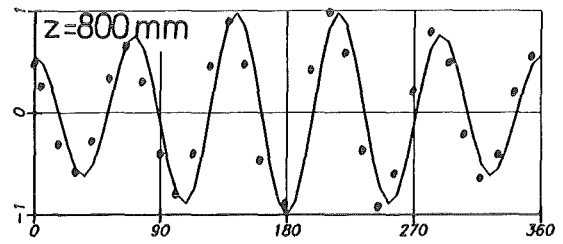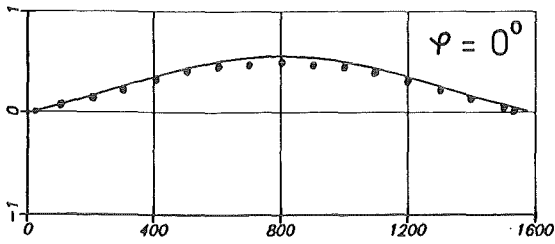
—— f = 115.77 Hz
••• f = 113.23 Hz   ξ = 0.0341%

Fig. 9 : Mode shape of the 113.23 Hz - eigenmode (test cylinder empty)
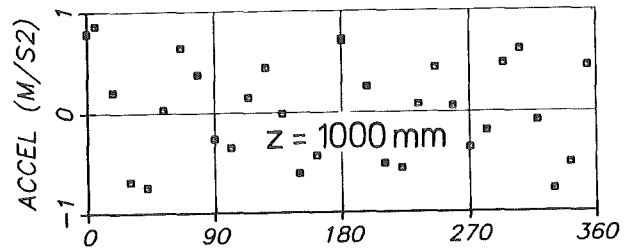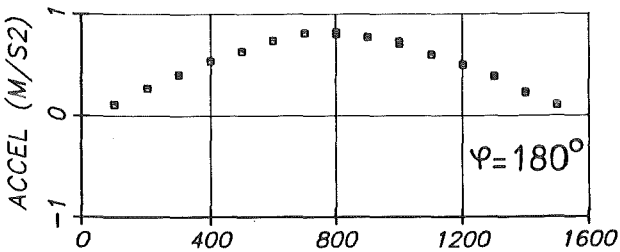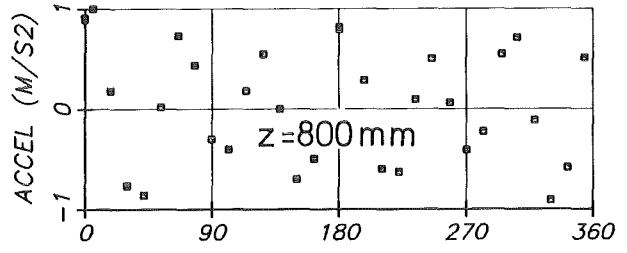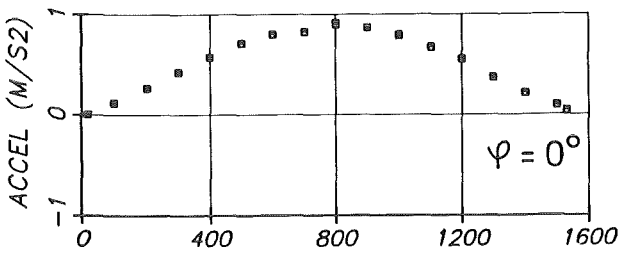
▫ ▫ ▫ f = 125.80 Hz   ξ = 0.0399%

Fig. 10 : Mode shape of the 125.80 Hz - eigenmode (test cylinder empty)
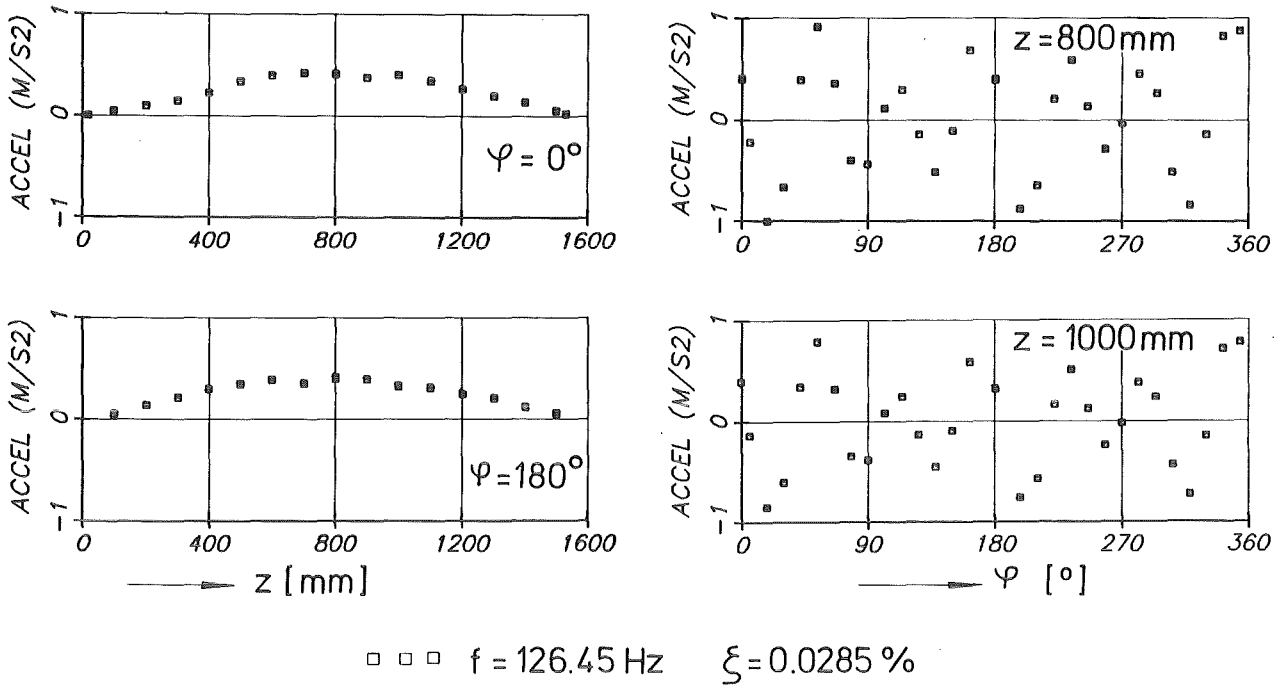
Fig. 11 : Mode shape of the 126.45 Hz - eigenmode (test cylinder empty)
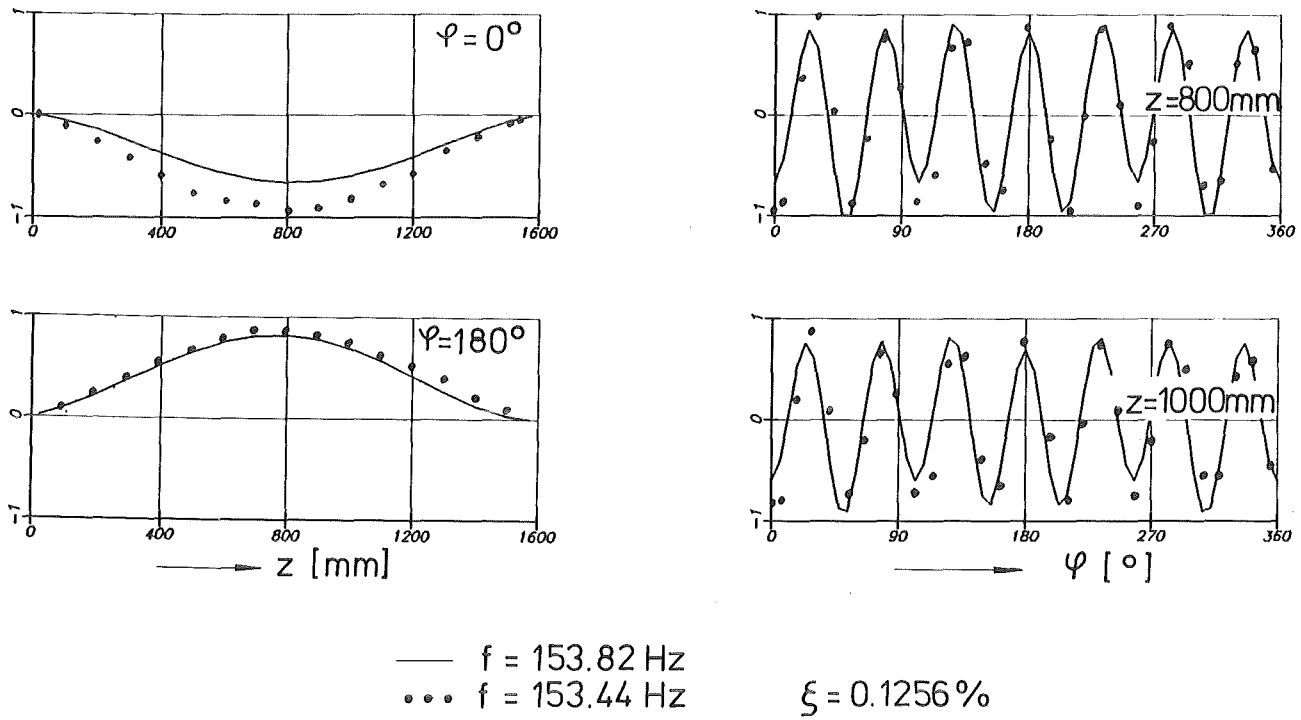
Fig. 12 : Mode shape of the 153.44 Hz - eigenmode (test cylinder empty)

— f = 191.89 Hz
••• f = 192.91 Hz   ξ = 0.0342%
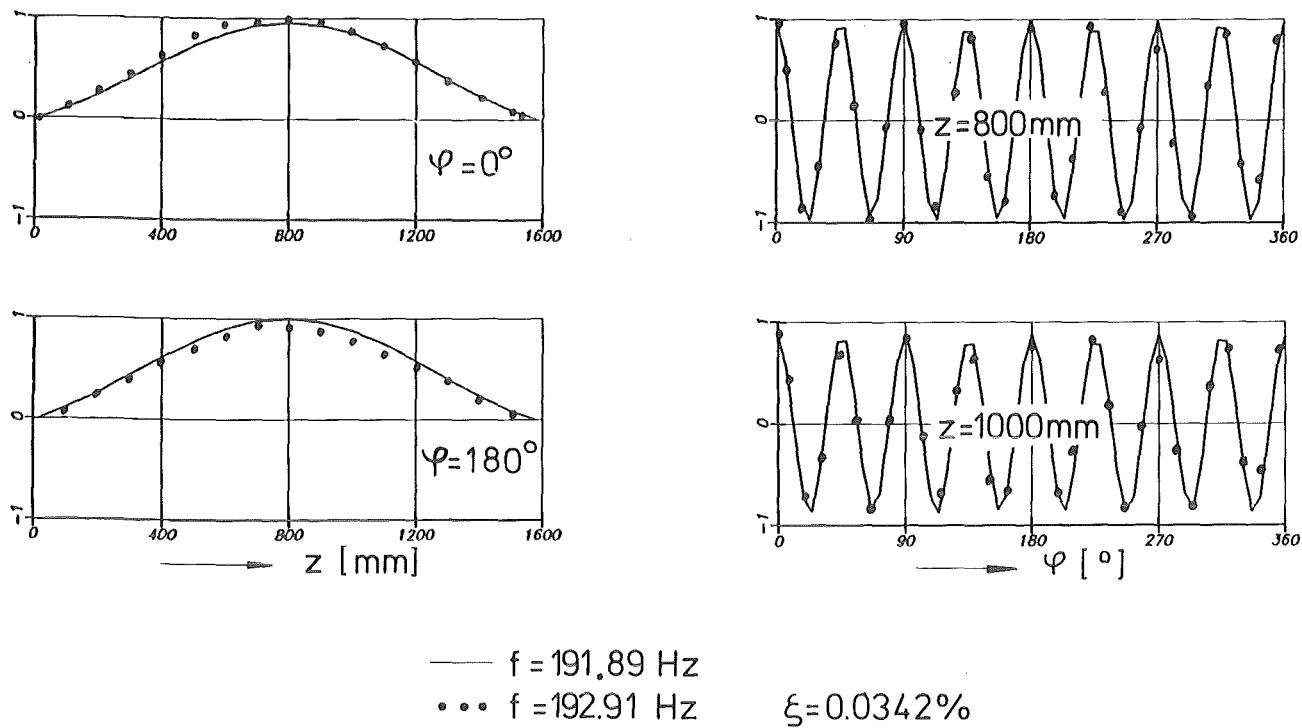
Fig. 13 : Mode shape of the 192.91 Hz – eigenmode (test cylinder empty)

— f = 238.82 Hz
••• f = 240.40 Hz   ξ = 0.022%
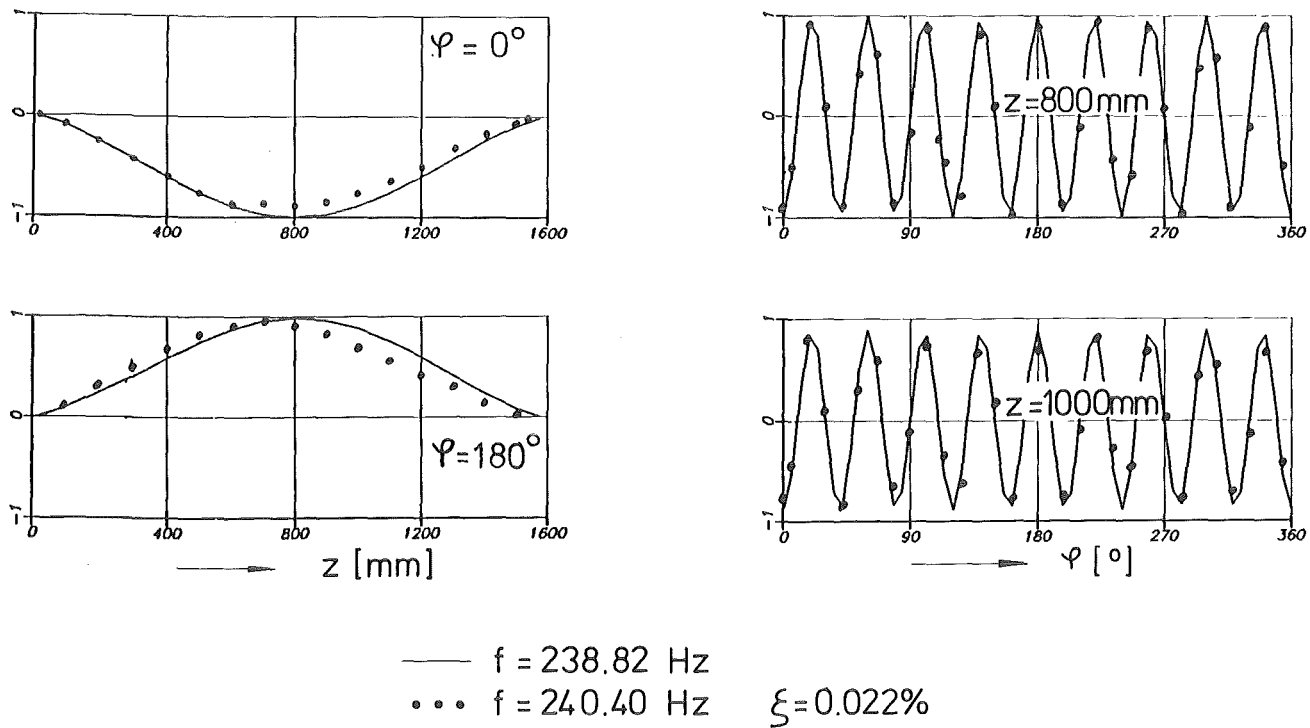
Fig. 14 : Mode shape of the 240.40 Hz – eigenmode (test cylinder empty)
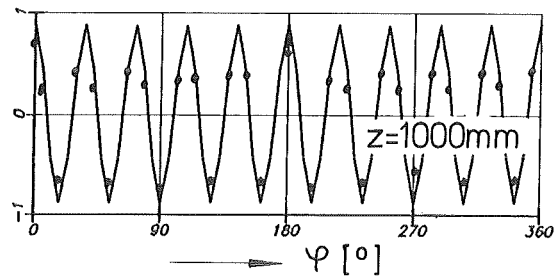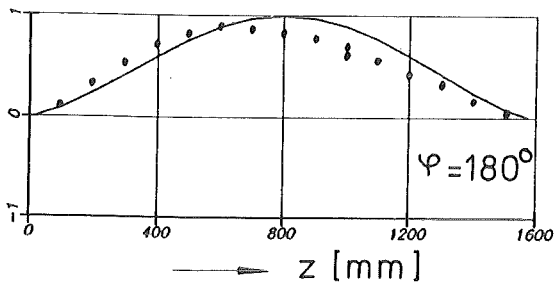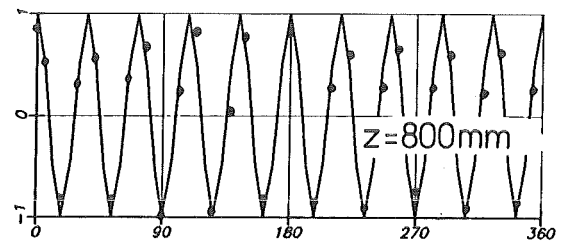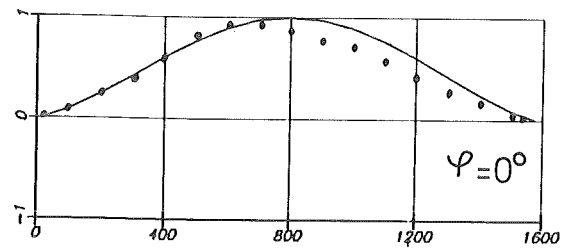
Fig. 15 : Mode shape of the 295.14 Hz-eigenmode (test cylinder empty)
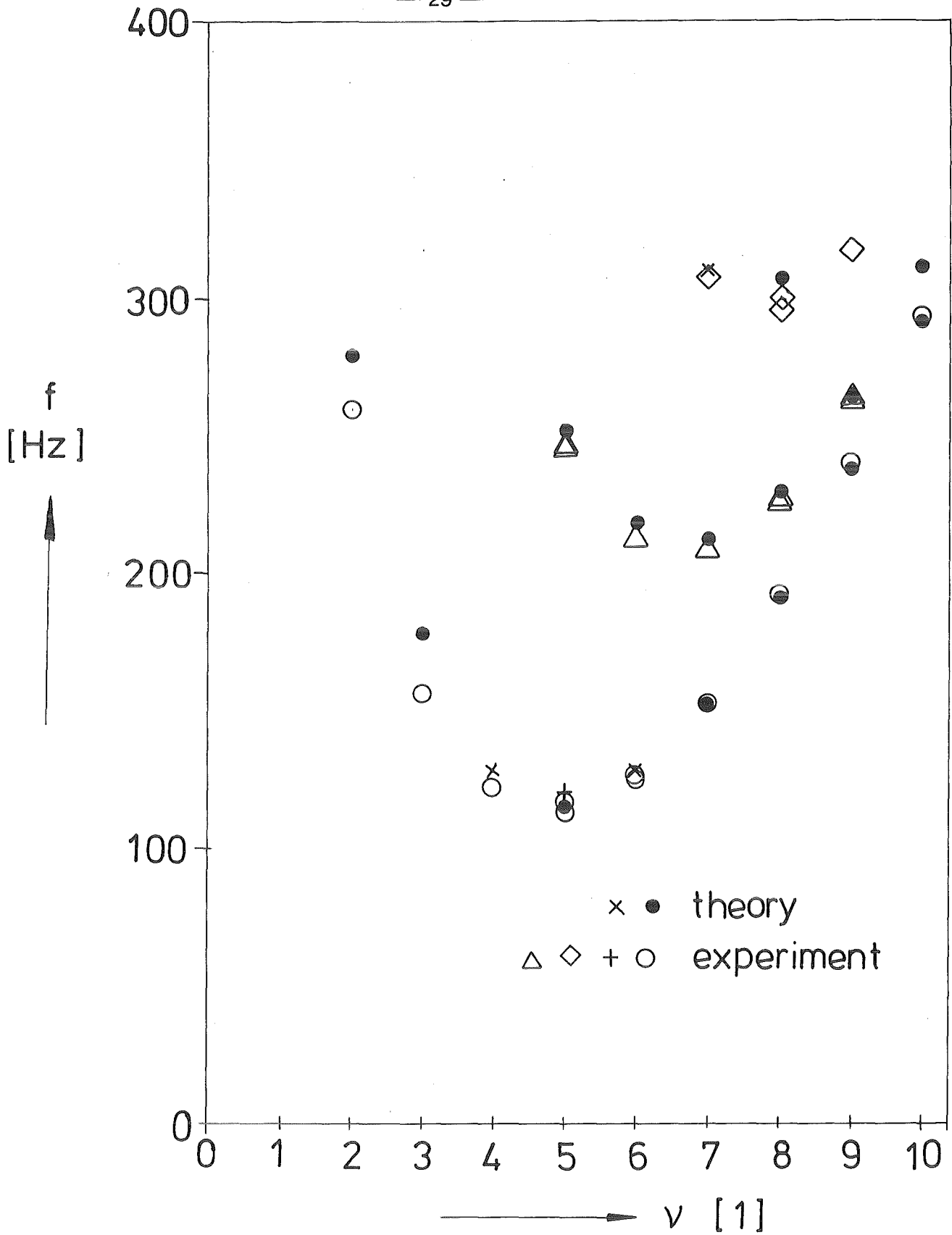
Fig. 16: Comparison of the calculated and measured natural frequencies of the empty horizontal test cylinder
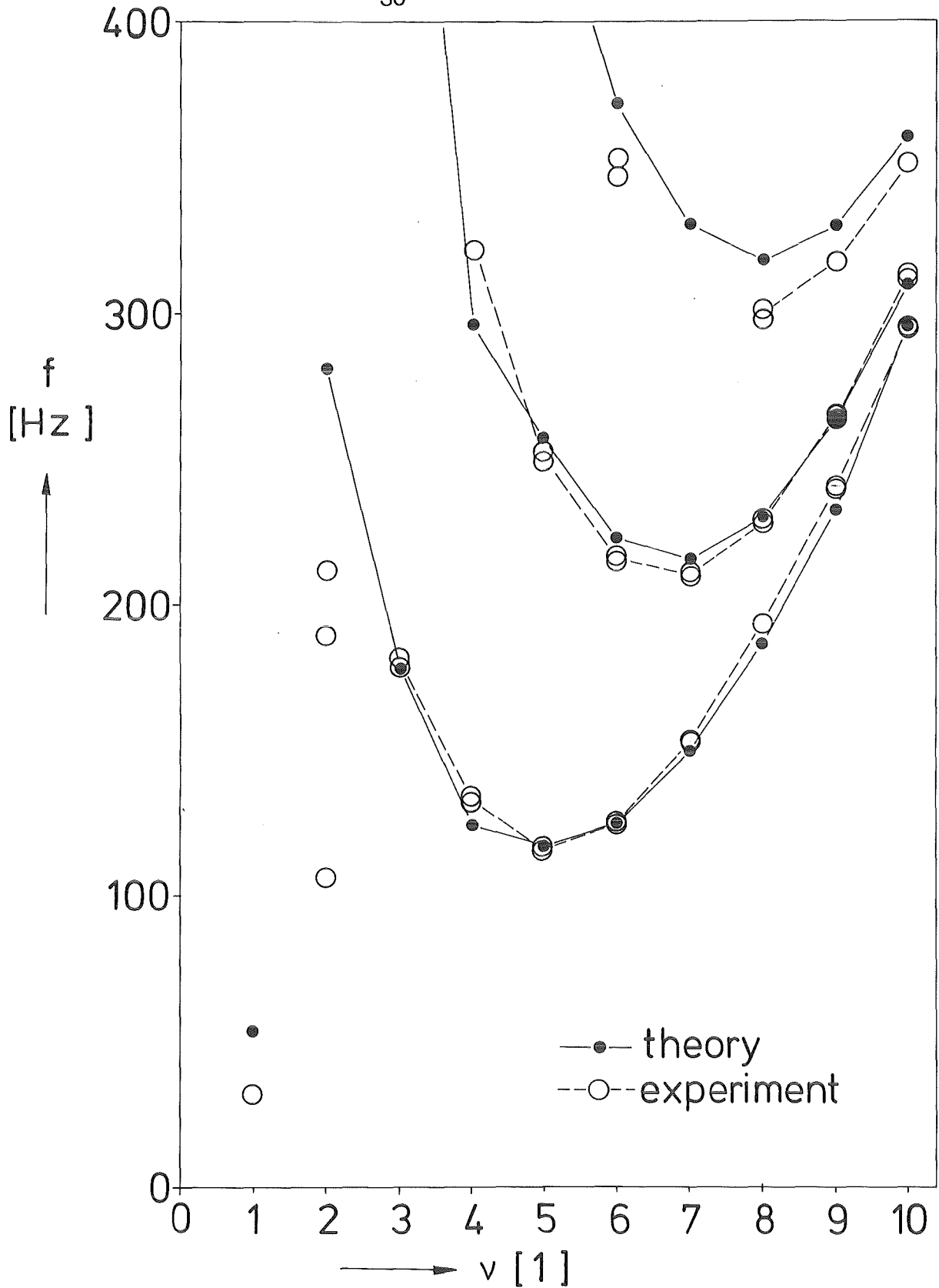
Fig. 17 : Comparison of the calculated and measured natural frequencies of the empty vertical test cylinder (figure reproduced from [7])
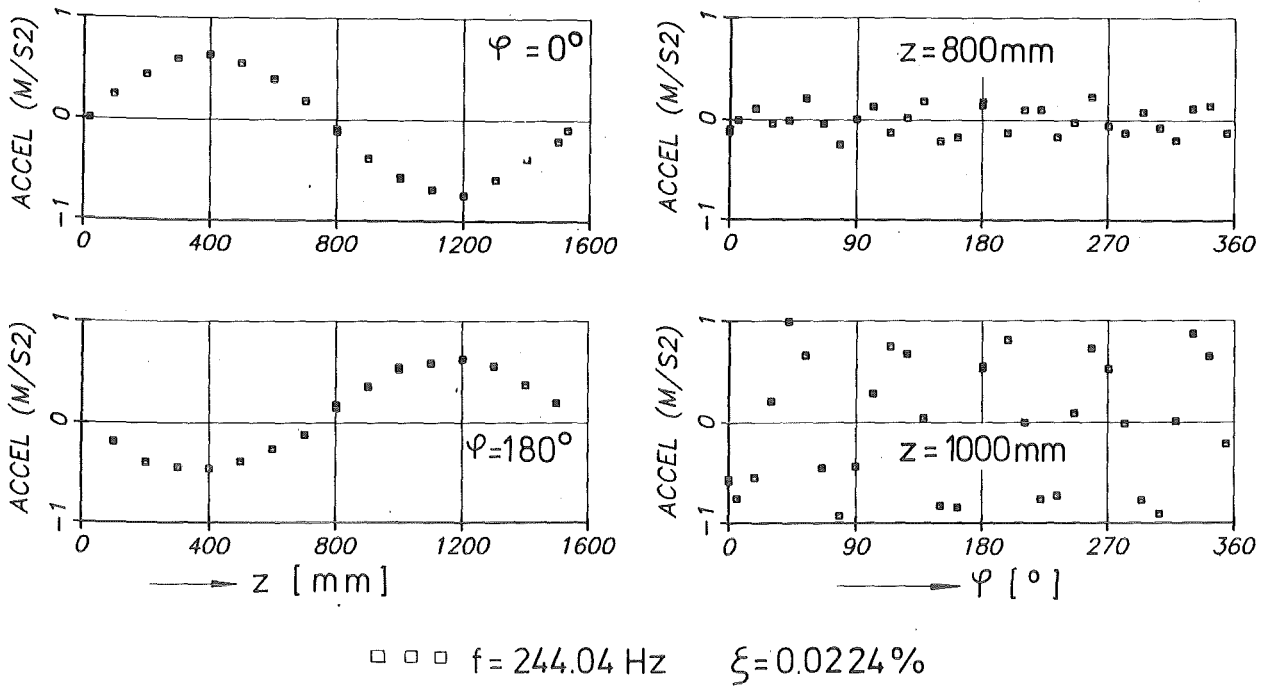
Fig. 18 : Mode shape of the 244.04 Hz-eigenmode (test cylinder empty)
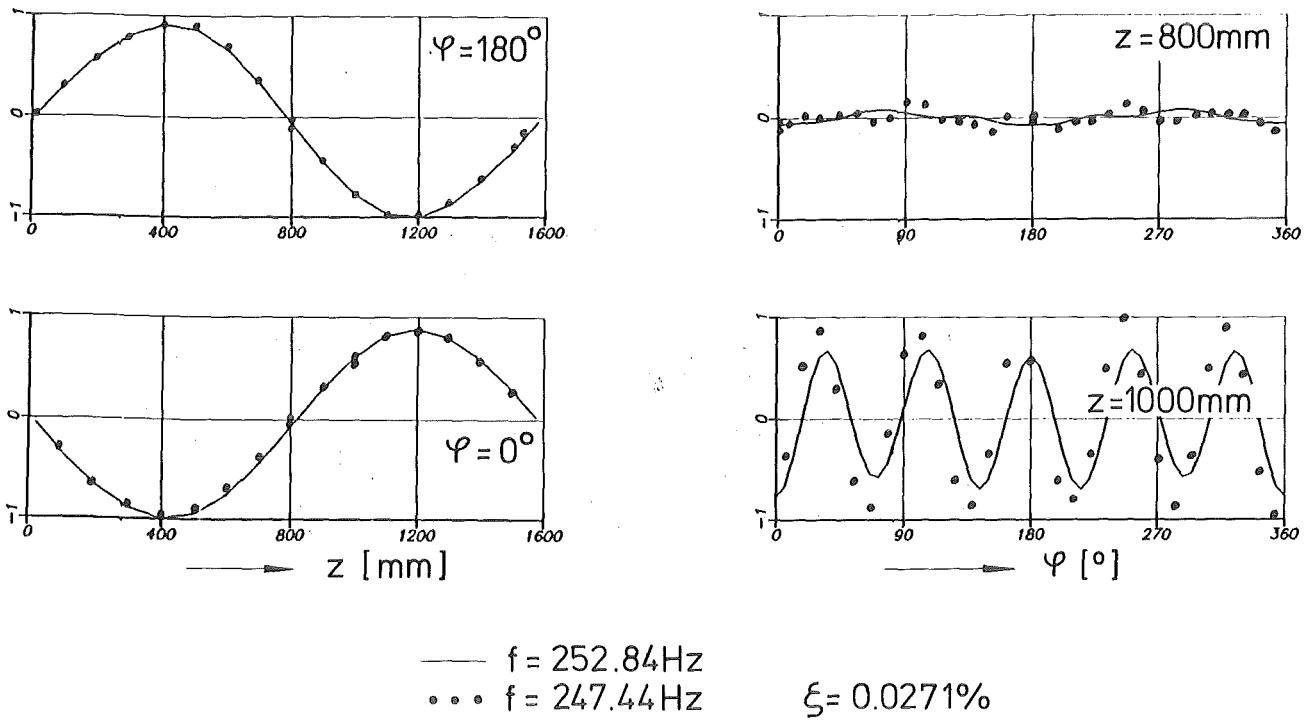
Fig. 19 : Mode shape of the 247.44 Hz-eigenmode (test cylinder empty)

$$\text{——— } f = 219.29 \, \text{Hz}$$
$$\bullet \bullet \bullet \; f = 213.38 \, \text{Hz} \qquad \xi = 0.0241\%$$
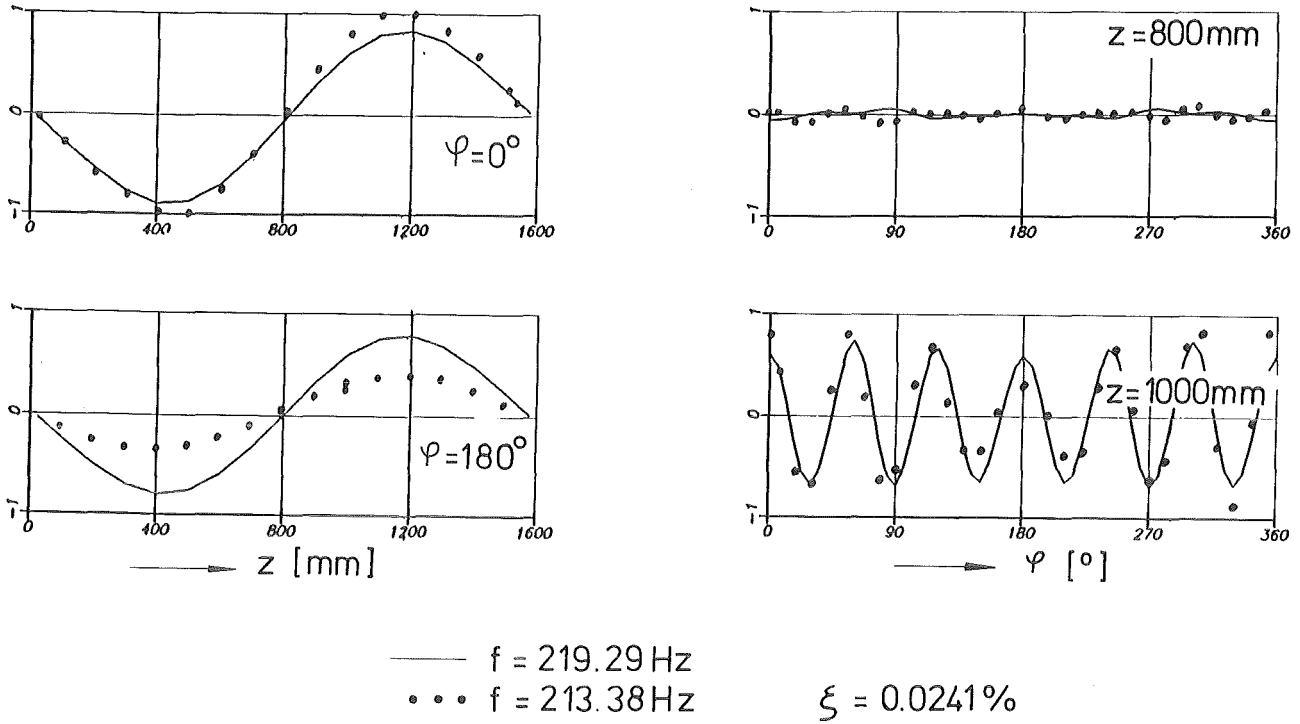
Fig. 20 : Mode shape of the 213.38 Hz – eigenmode (test cylinder empty)

$$\text{——— } f = 213.35 \, \text{Hz}$$
$$\bullet \bullet \bullet \; f = 208.80 \, \text{Hz} \qquad \xi = 0.0263\%$$
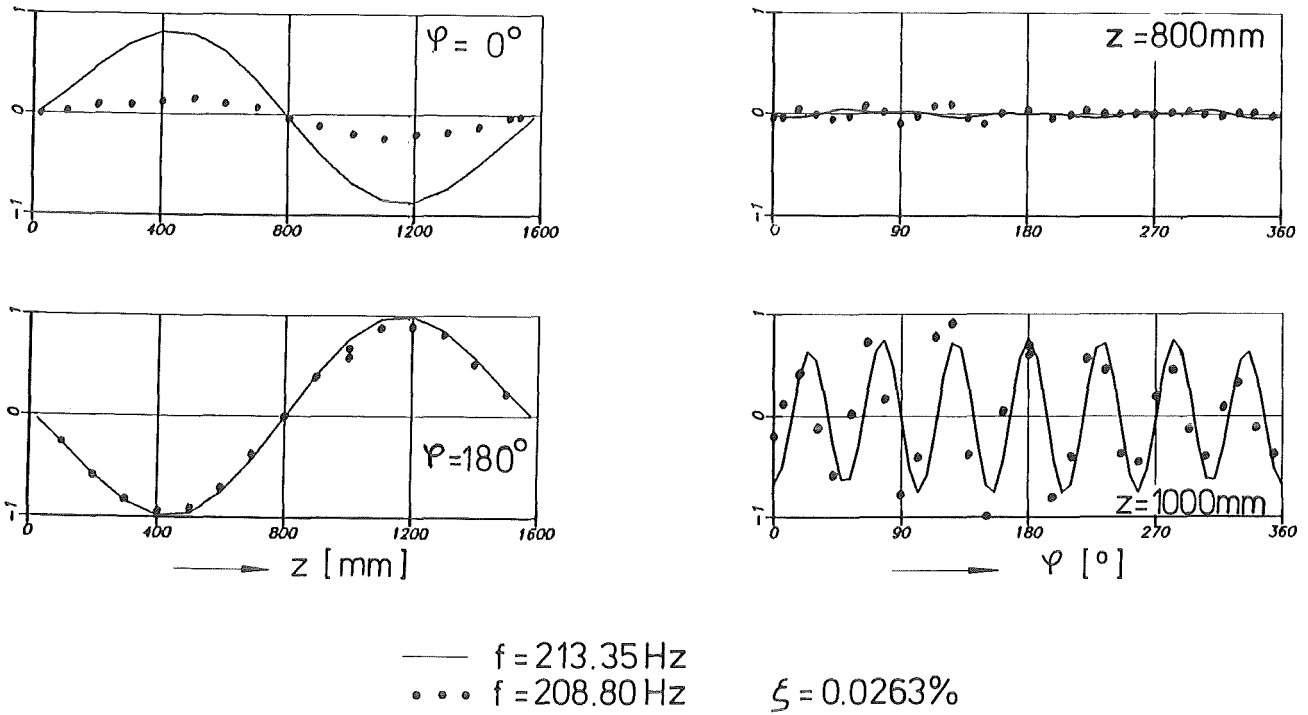
Fig. 21: Mode shape of the 208.80 Hz – eigenmode (test cylinder empty)

$$\varphi = 0°$$

$$z = 800\,mm$$

$$\varphi = 180°$$

$$z = 1000\,mm$$

$$\longrightarrow \ z\,[mm]$$

$$\longrightarrow \ \varphi\,[°]$$

——— f = 230.69 Hz

• • • f = 229.74 Hz   ξ = 0.0208 %

+ + + f = 228.57 Hz   ξ = 0.0777 %
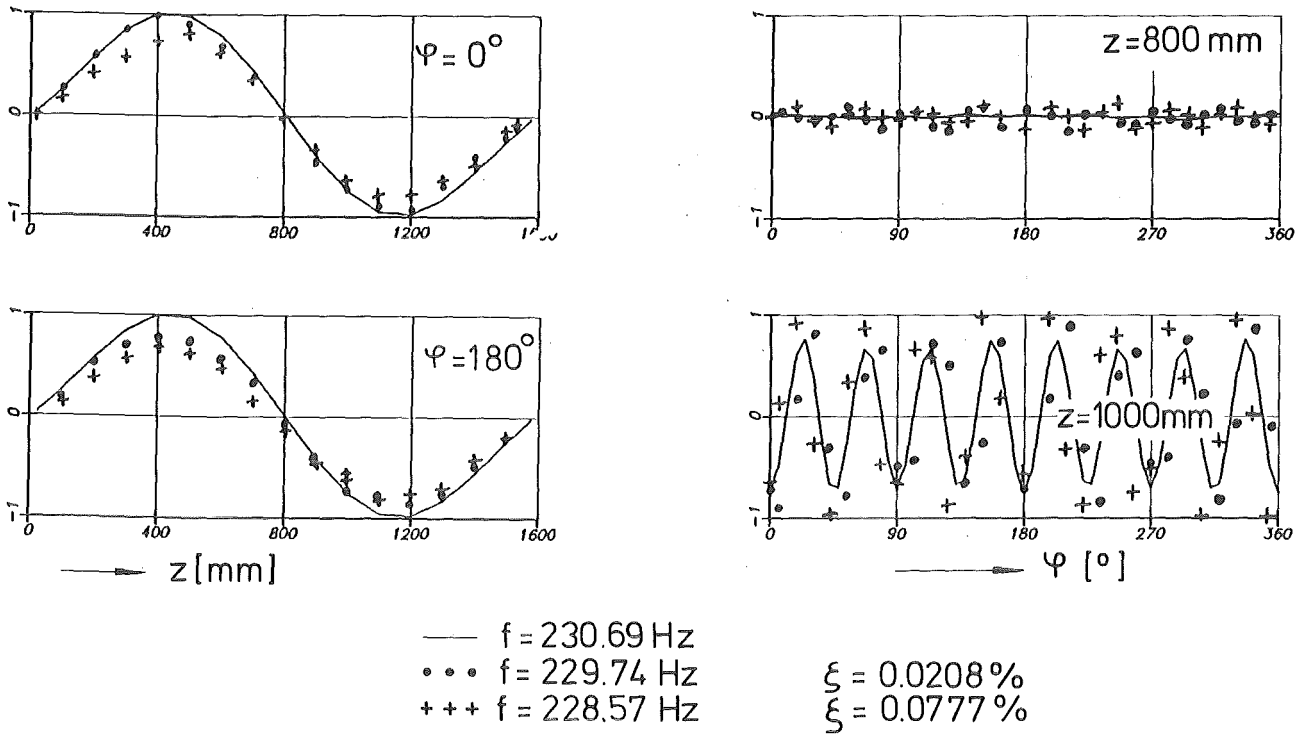
Fig. 22 : Mode shape of 229.74 Hz and 228.57 Hz-eigenmodes (test cylinder empty)

$$\varphi = 0°$$

$$z = 800\,mm$$

$$\varphi = 180°$$

$$z = 1000\,mm$$

$$\longrightarrow \ z\,[mm]$$

$$\longrightarrow \ \varphi\,[°]$$

□ □ □   f = 264.57 Hz   ξ = 0.0150 %
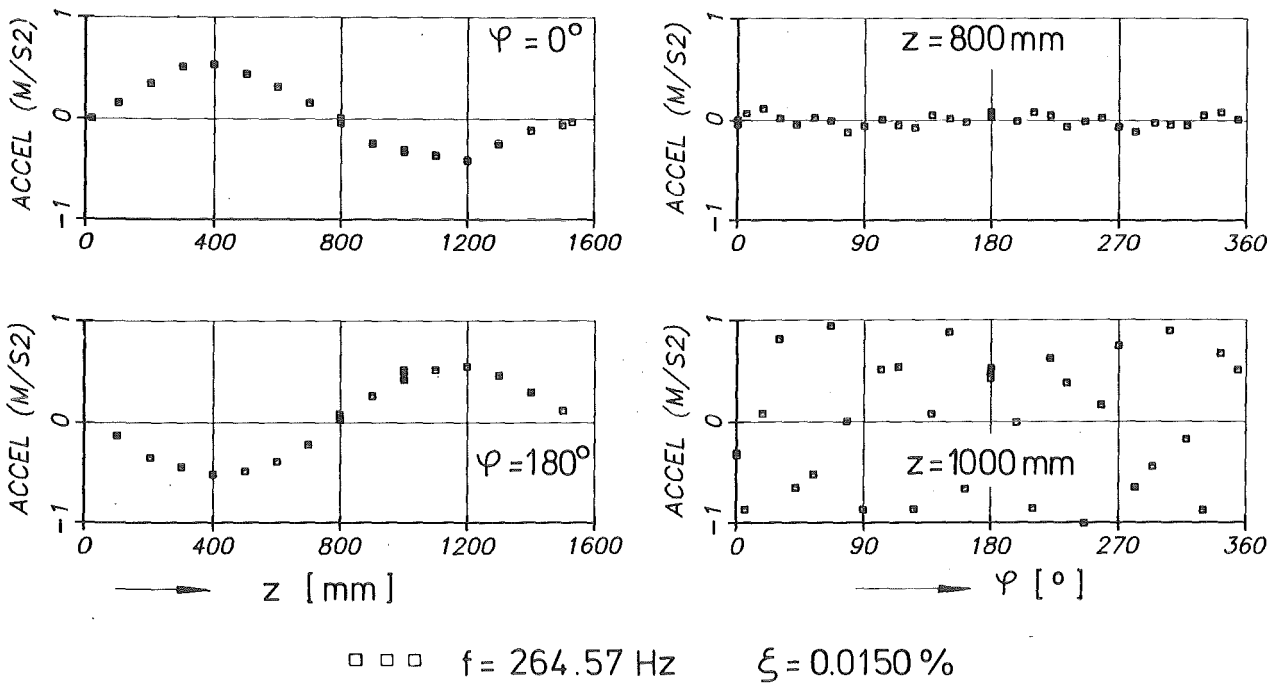
Fig. 23 : Mode shape of the 264.57 Hz-eigenmode (test cylinder empty)

—— f = 265.23 Hz
••• f = 265.70 Hz   ξ = 0.0306%
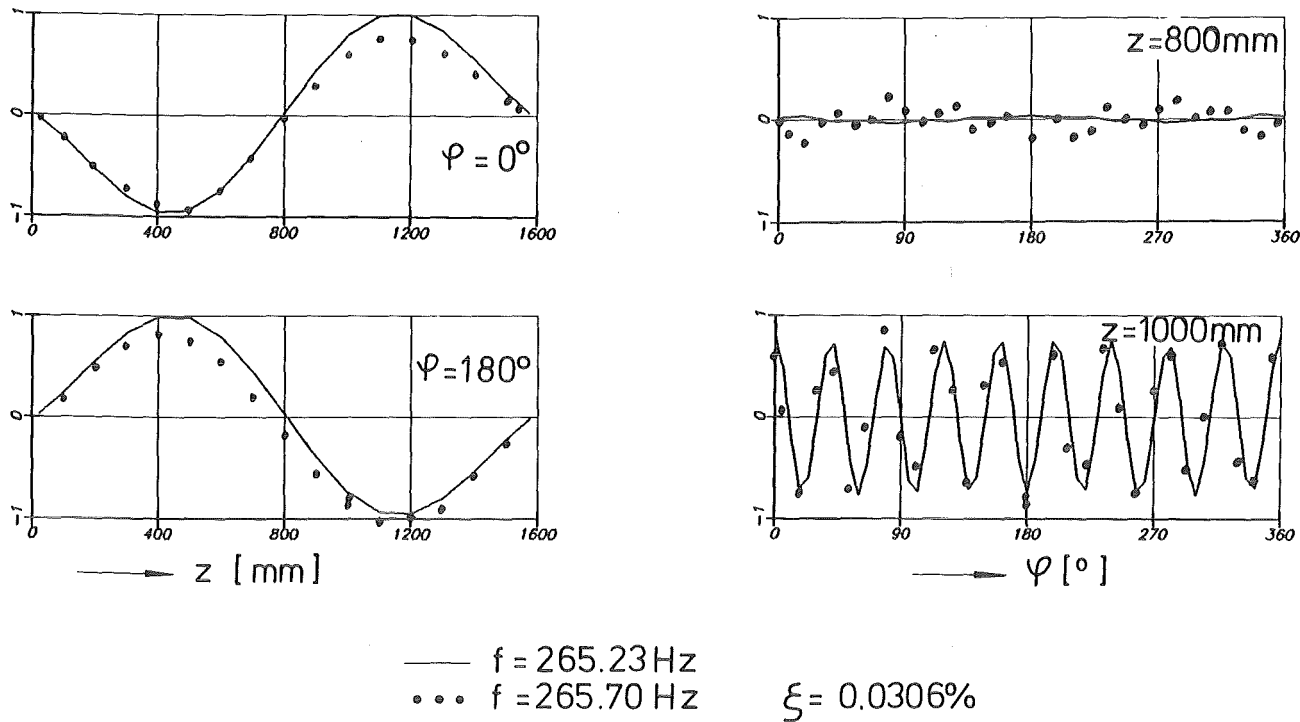
Fig. 24 : Mode shape of the 265.70 Hz - eigenmode (test cylinder empty)
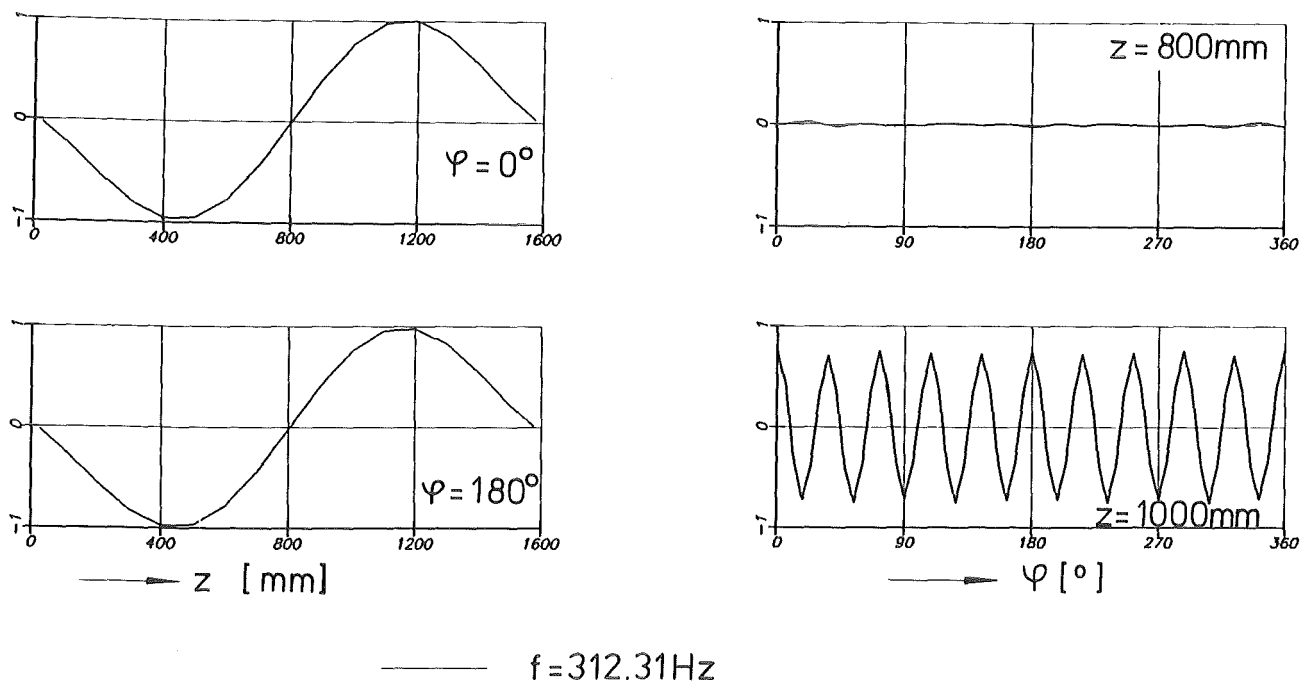
—— f = 312.31 Hz

Fig. 25 : Mode shape of the 312.31 Hz - eigenmode (test cylinder empty)

Fig. 26: Mode shape of the 308.59 Hz-eigenmode (test cylinder empty)

Fig. 27 : Mode shape of the 297.06 Hz - eigenmode (test   cylinder empty)

$\varphi = 0°$

z = 800 mm

$\varphi = 180°$

z = 1000 mm

z [mm]

φ [°]

——— f = 308.04 Hz

• • • f = 301.66 Hz $\xi = 0.0190$ %

Fig. 28 : Mode shape of the 301.66 Hz-eigenmode (test cylinder empty)

ACCEL (M/S2)

$\varphi = 0°$

z = 800 mm

ACCEL (M/S2)

$\varphi = 180°$

z = 1000 mm

ACCEL (M/S2)

ACCEL (M/S2)

z [mm]

φ [°]

□ □ □   f = 318.24 Hz $\xi = 0.0161$ %

Fig. 29 : Mode shape of the 318.24 Hz-eigenmode (test cylinder empty)

$\varphi = 0°$

$\varphi = 180°$

$z = 800\,mm$

$z = 1000\,mm$

$\longrightarrow z\ [mm]$

$\longrightarrow \varphi\ [°]$

—— f = 125.84 Hz
••• f = 120.63 Hz $\xi = 0.0295\%$

Fig.30 : Mode shape of the 120.63 Hz-eigenmode (test cylinder empty)

$\varphi = 0°$

$\varphi = 180°$

$z = 800\,mm$

$z = 1000\,mm$

$\longrightarrow z\ [mm]$

$\longrightarrow \varphi\ [°]$
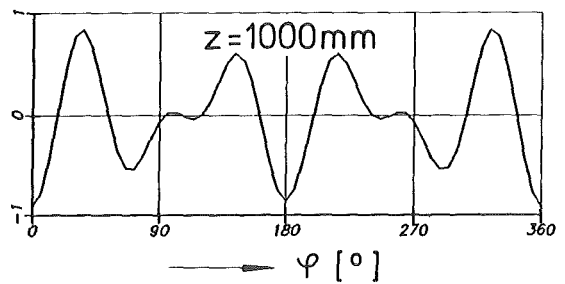
—— f = 128.19 Hz

Fig.31 : Mode shape of the 128.19 Hz-eigenmode (test cylinder empty)

Fig.32 : Mode shape of the 151.47 Hz - eigenmode (test cylinder empty)

Fig. 33 : Mode shape of the 314.09 Hz - eigenmode (test cylinder empty)

f = 113,26 Hz

f = 120,65 Hz

f = 125,85 Hz

Fig.34: Relief plots of typical mode shapes extracted
(test cylinder empty)
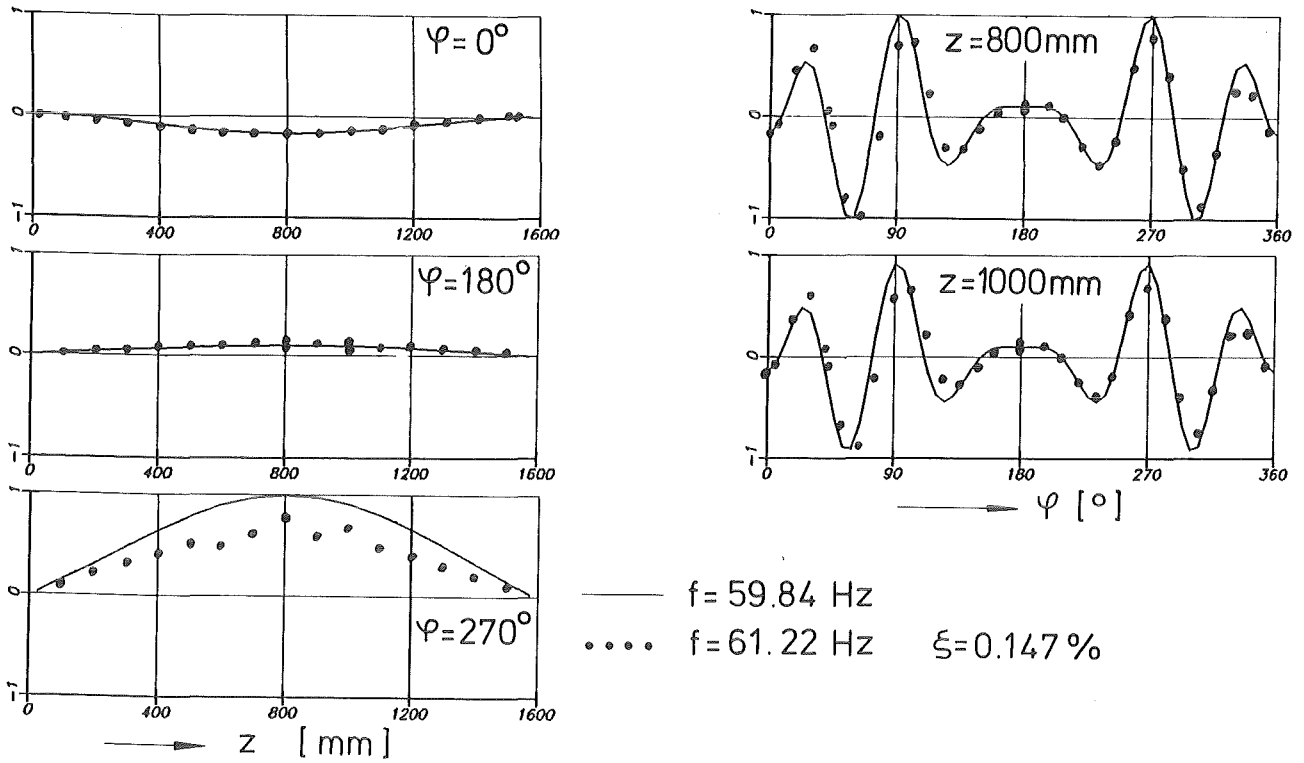
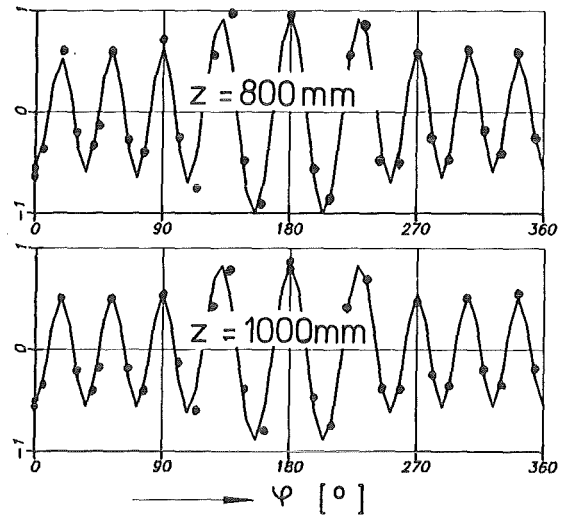Fig. 35 : Mode shape of the 61.22 Hz-eigenmode (test cylinder partly filled with water)
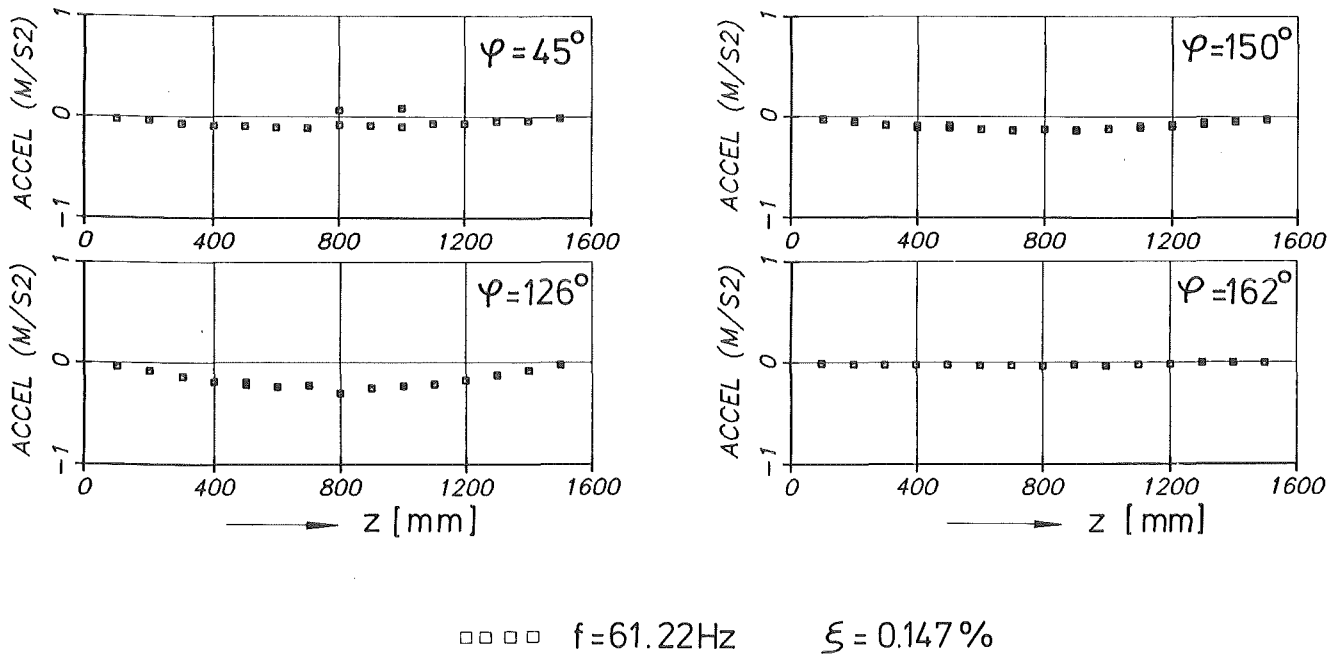
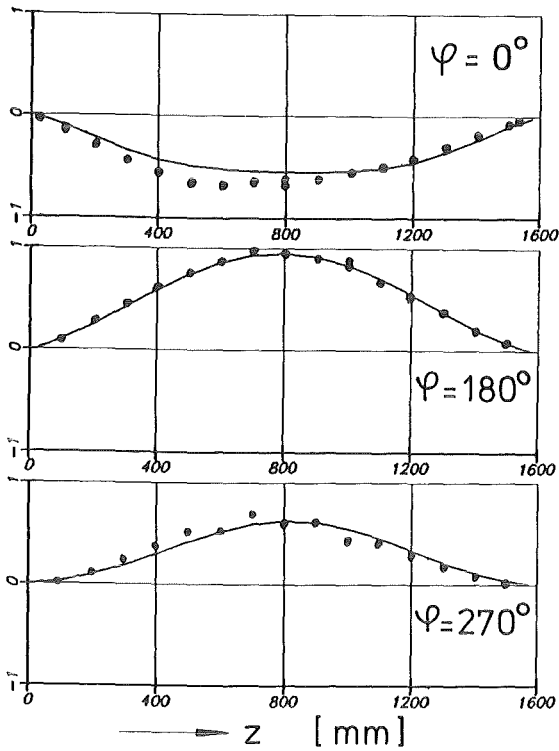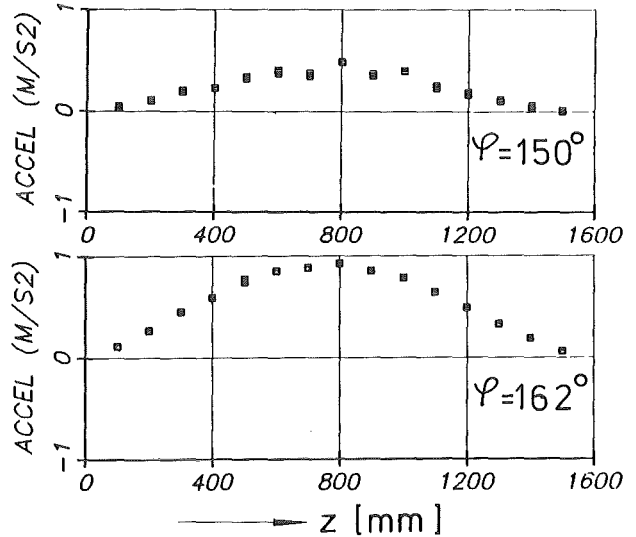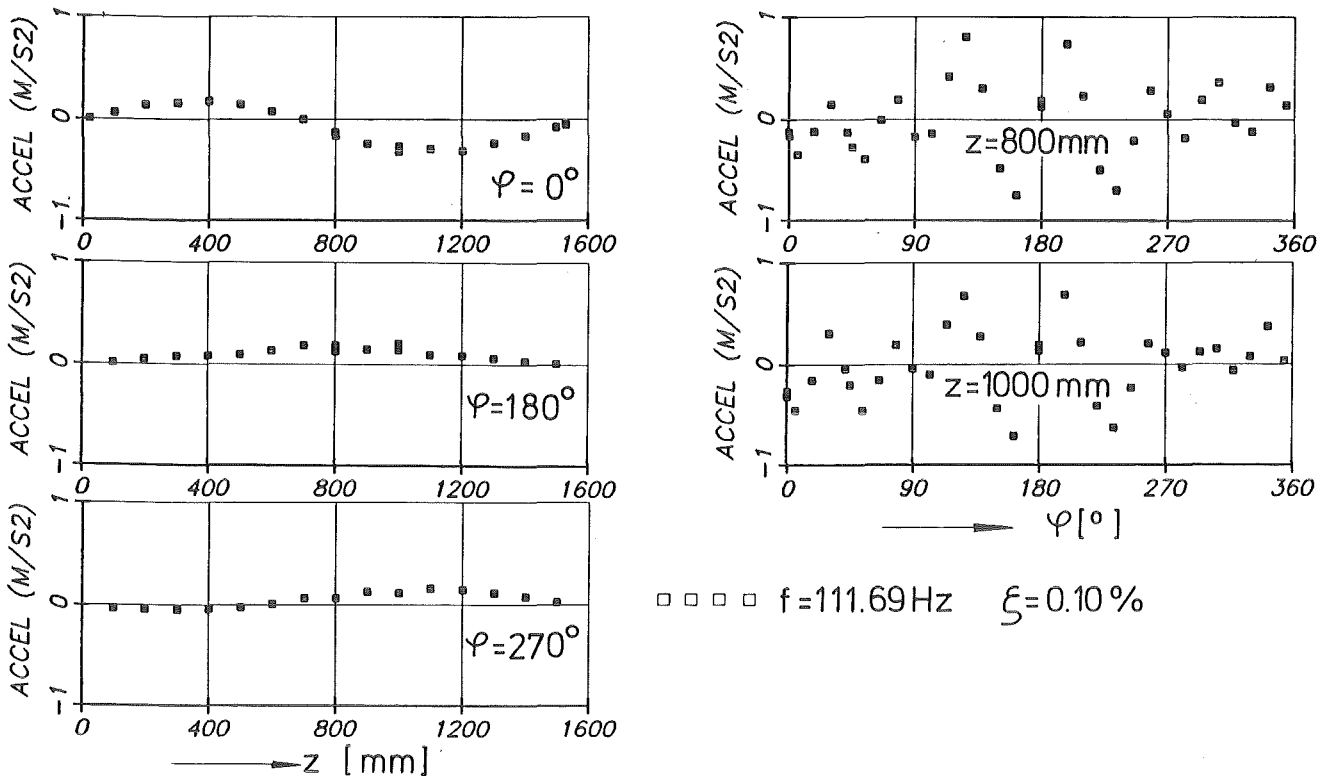Fig. 35a: Mode shape of the 61.22 Hz-eigenmode (test cylinder partly filled with water)
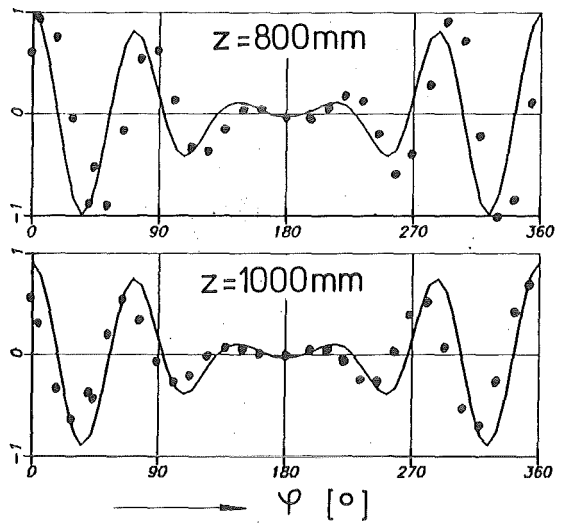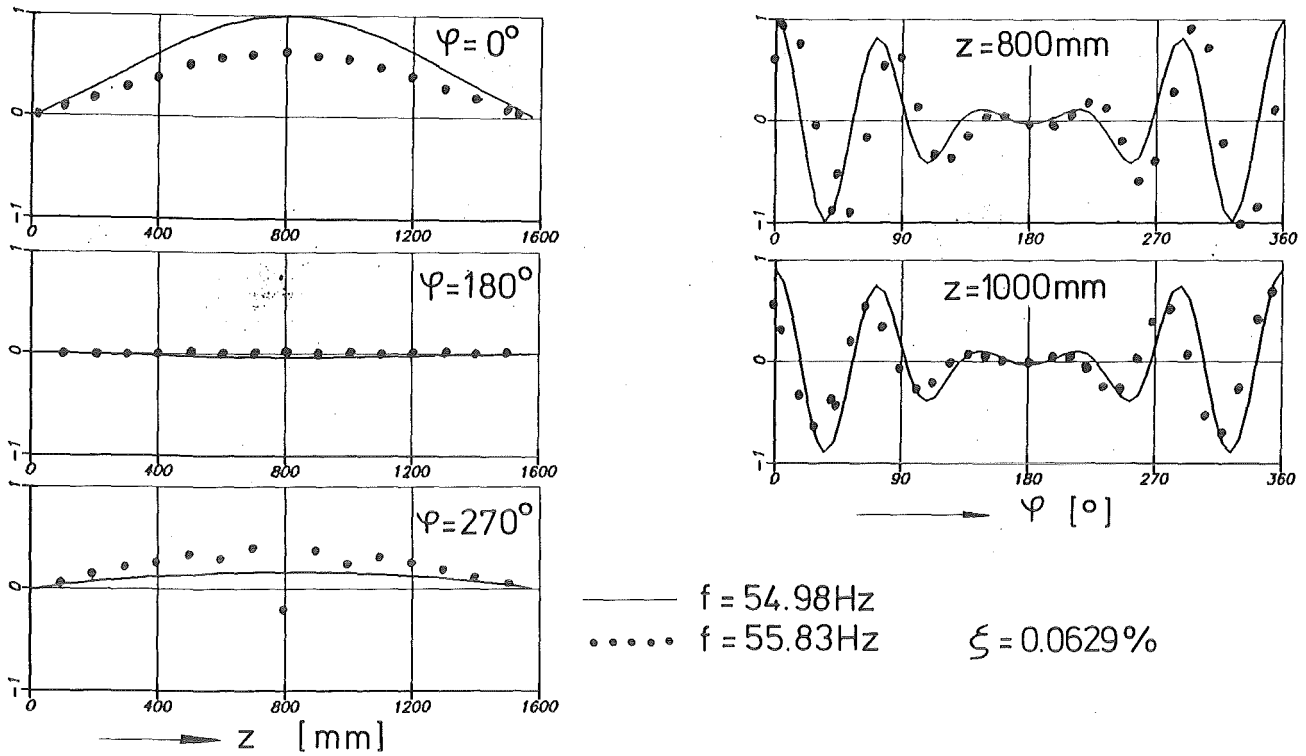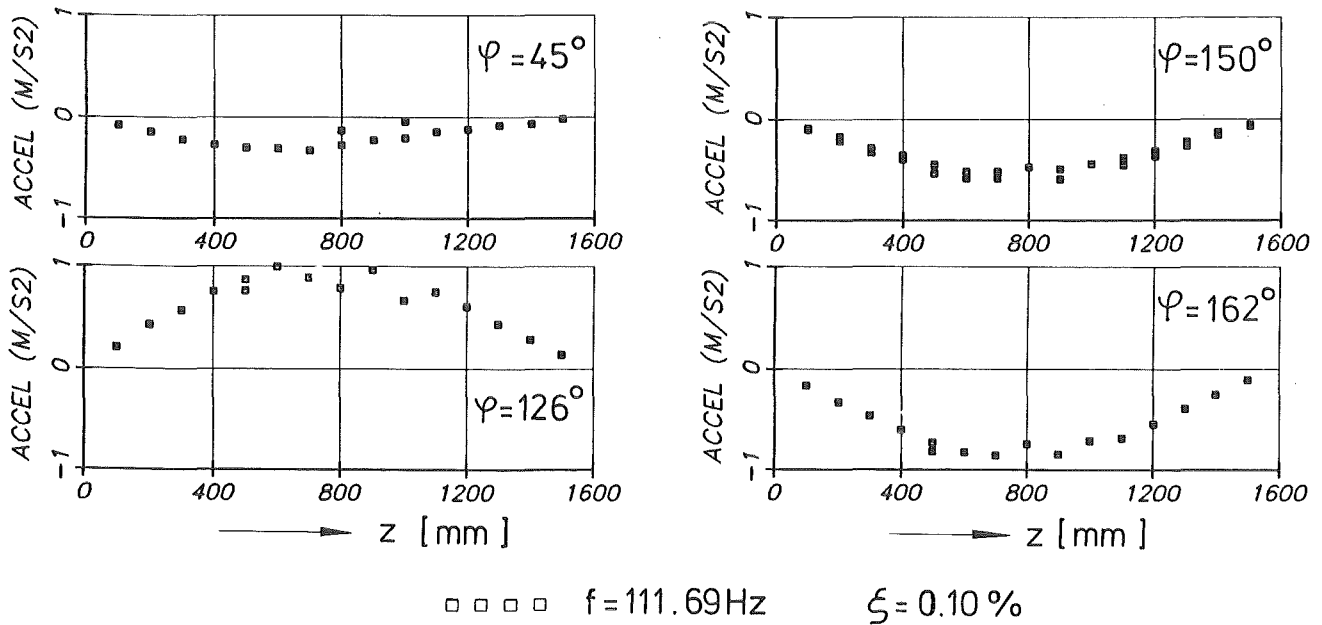
Fig. 36: Mode shape of the 55.83 Hz-eigenmode (test cylinder partly filled with water)
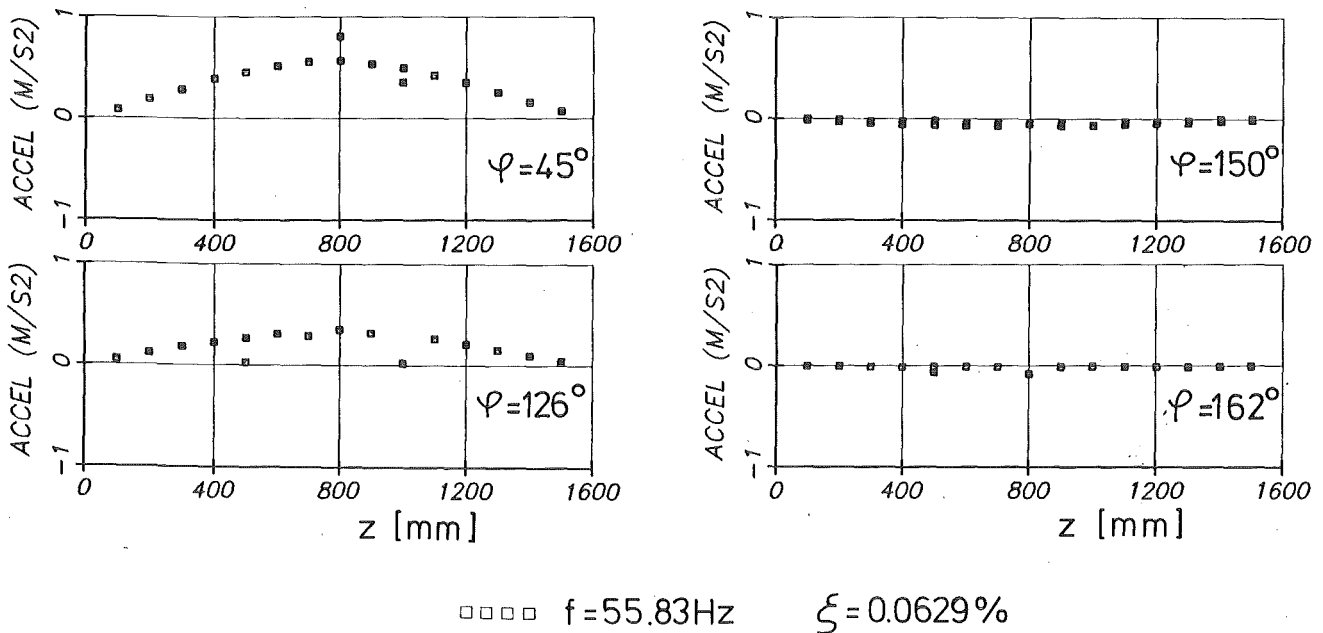
Fig.36a: Mode shape of the 55.83 Hz-eigenmode (test cylinder partly filled with water)
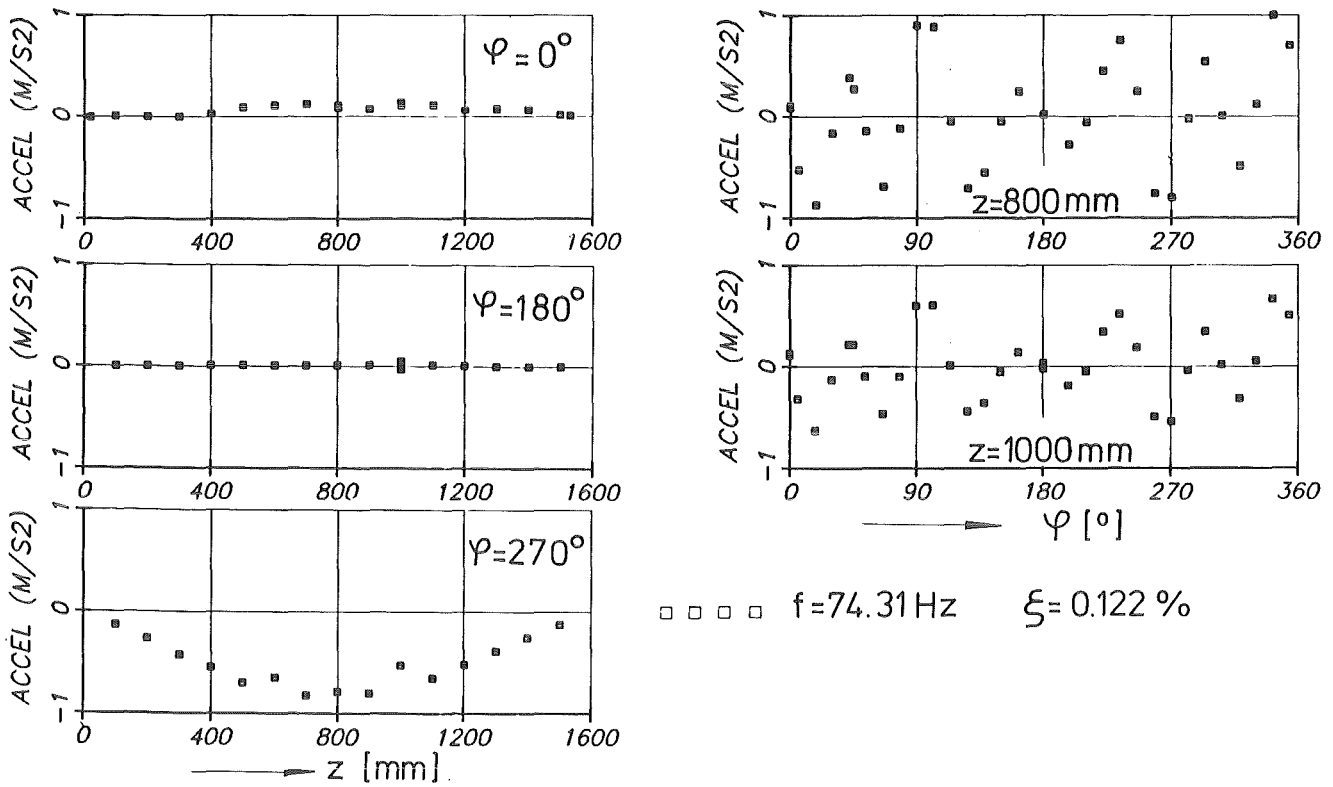
Fig.37 : Mode shape of the 74.31Hz-eigenmode (test cylinder partly filled with water
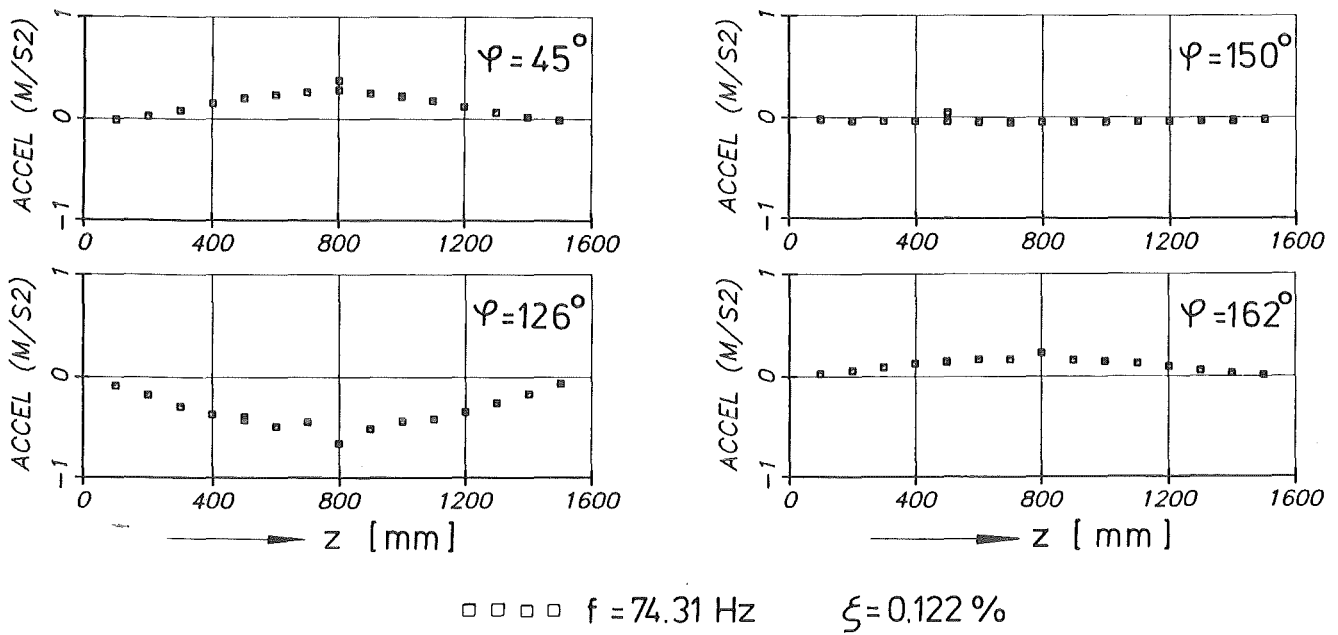
Fig.37a: Mode shape of the 74.31Hz-eigenmode (test cylinder partly filled with water)
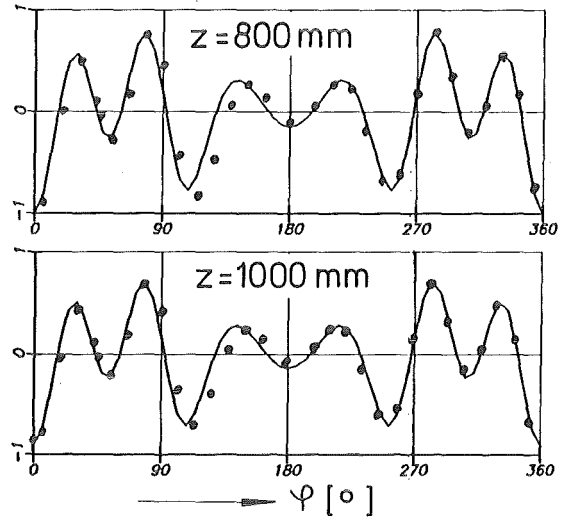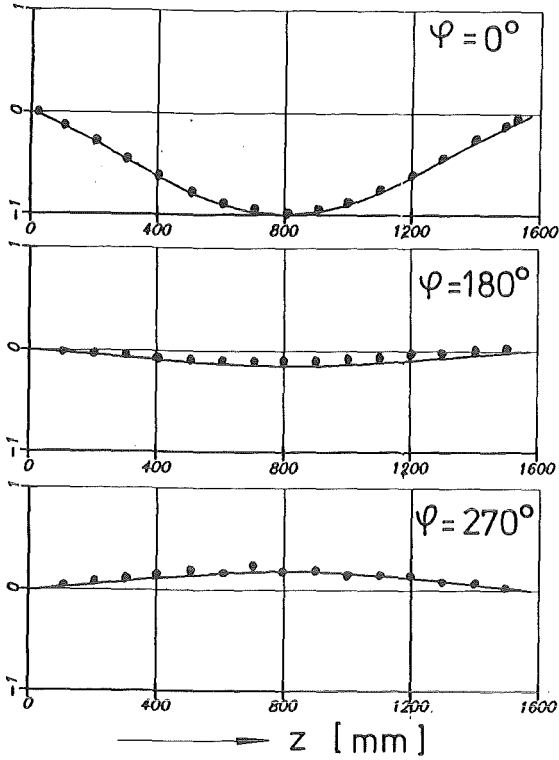
Fig. 38:Mode shape of the 75.92 Hz-eigenmode (test cylinder partly filled with water)
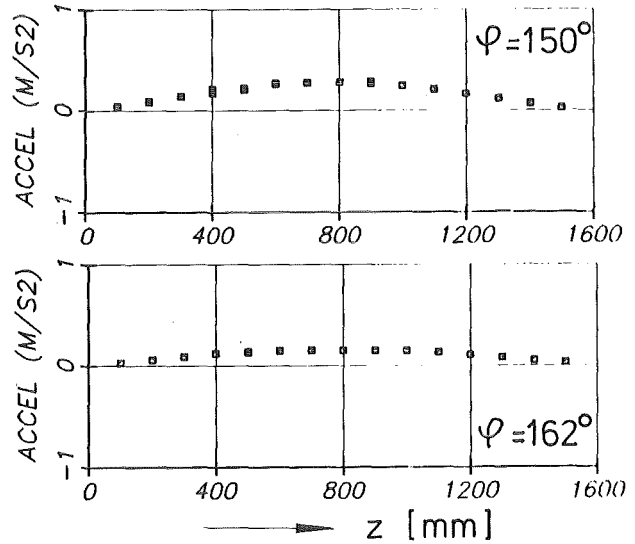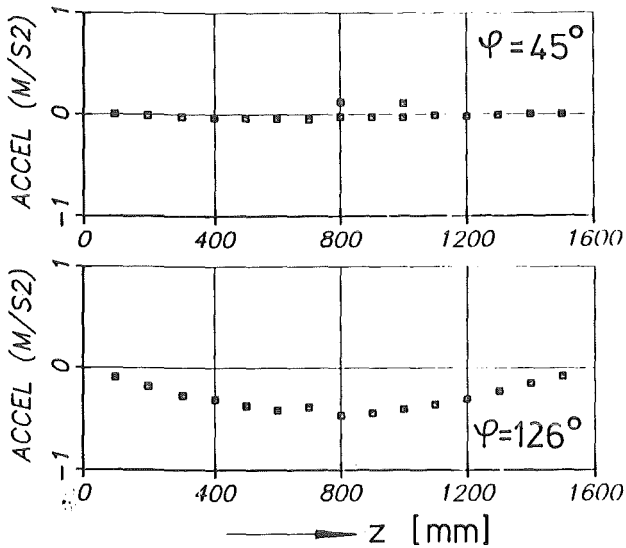
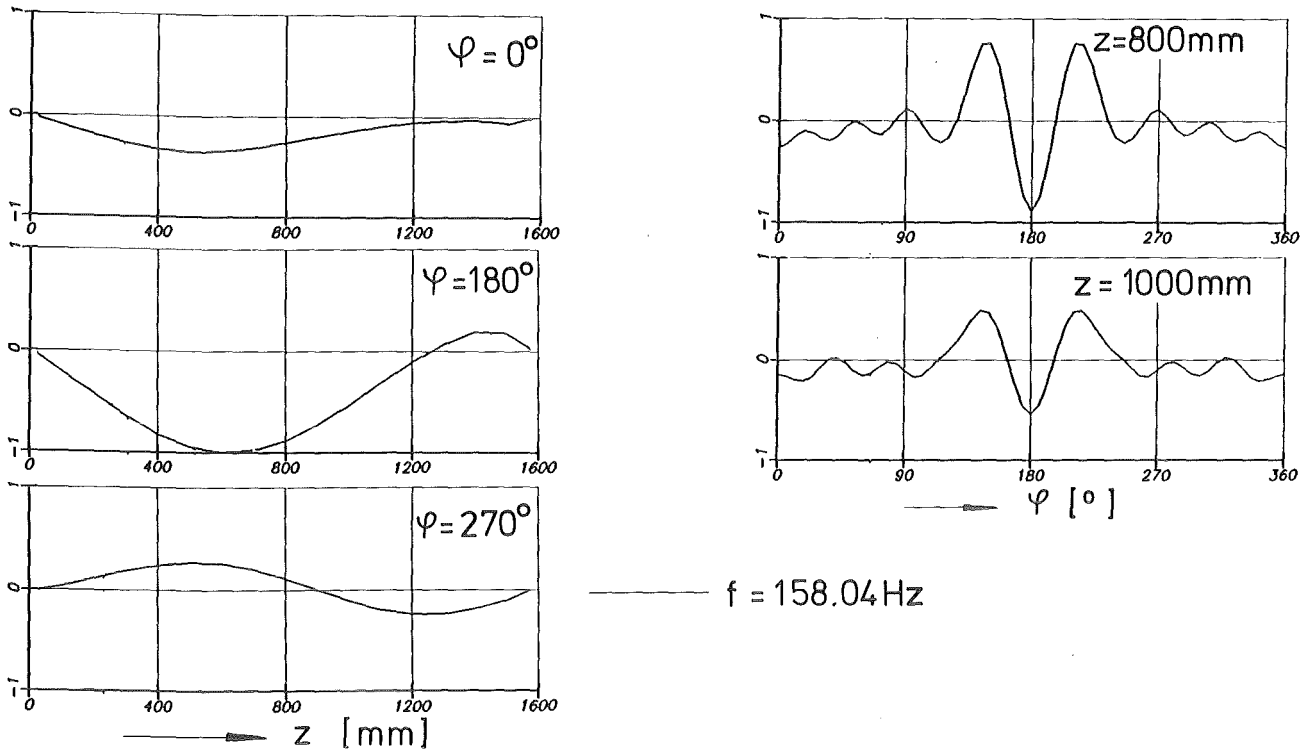Fig.38a:Mode shape of the 75.92 Hz-eigenmode (test cylinder partly filled with water)
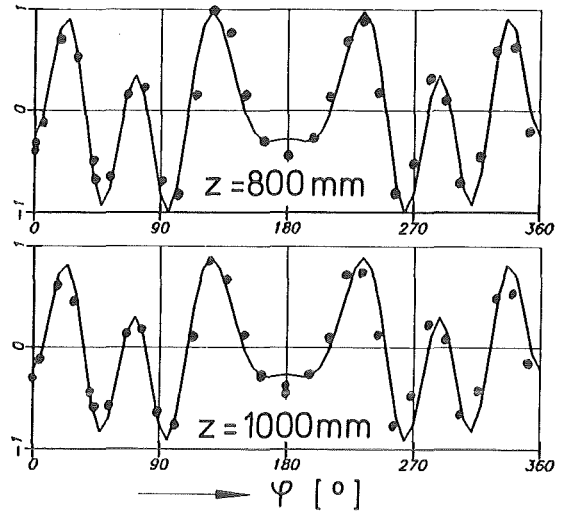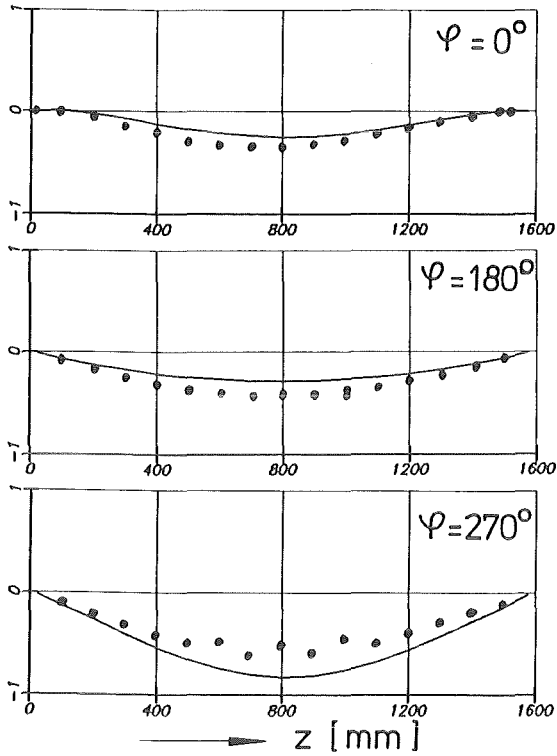
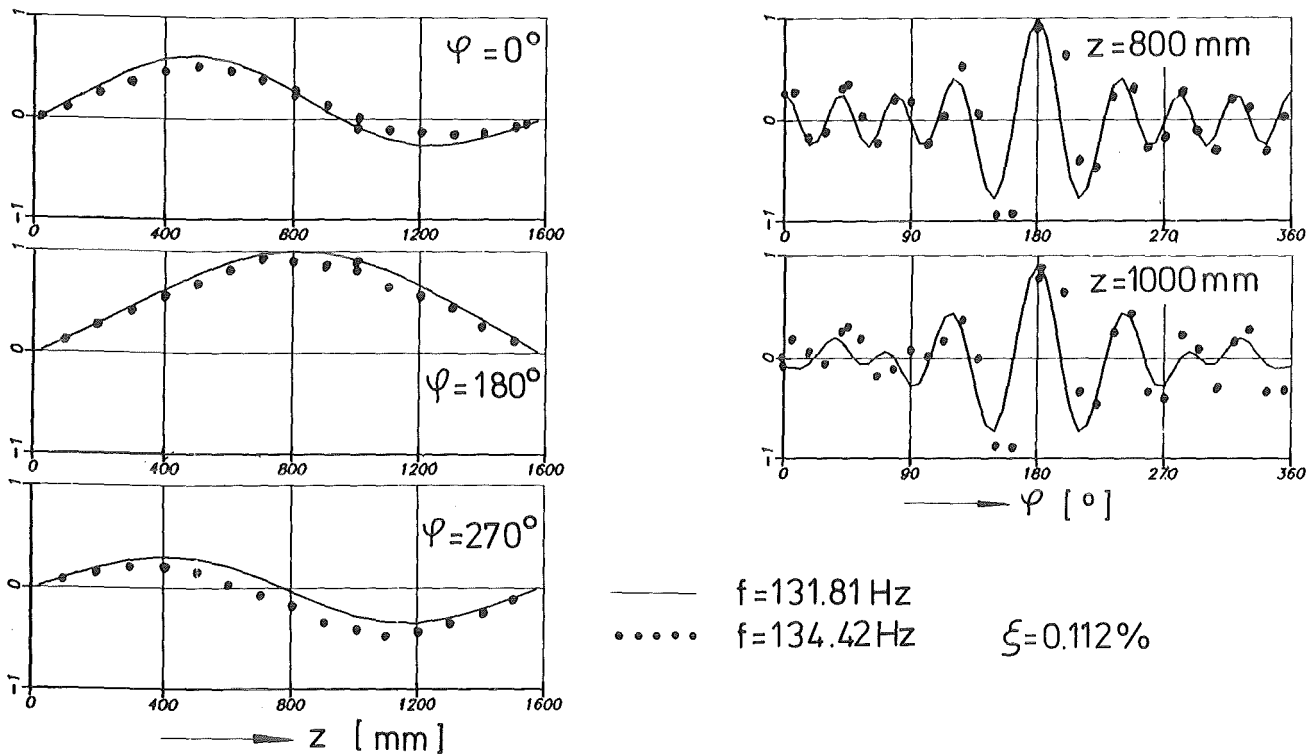Fig.39 :Mode shape of the 89.45Hz-eigenmode (test cylinder partly filled with water)
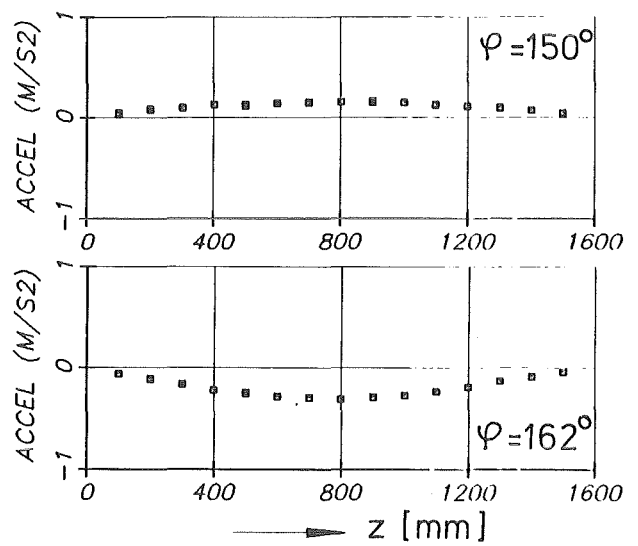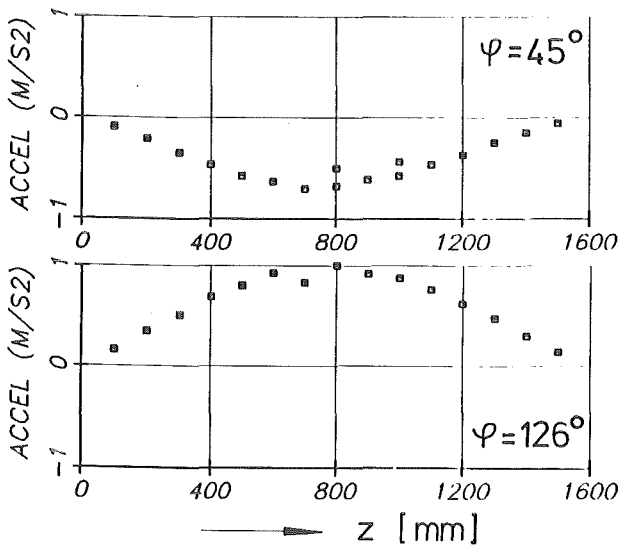
Fig.39a:Mode shape of the 89.45Hz-eigenmode (test cylinder partly filled with water)
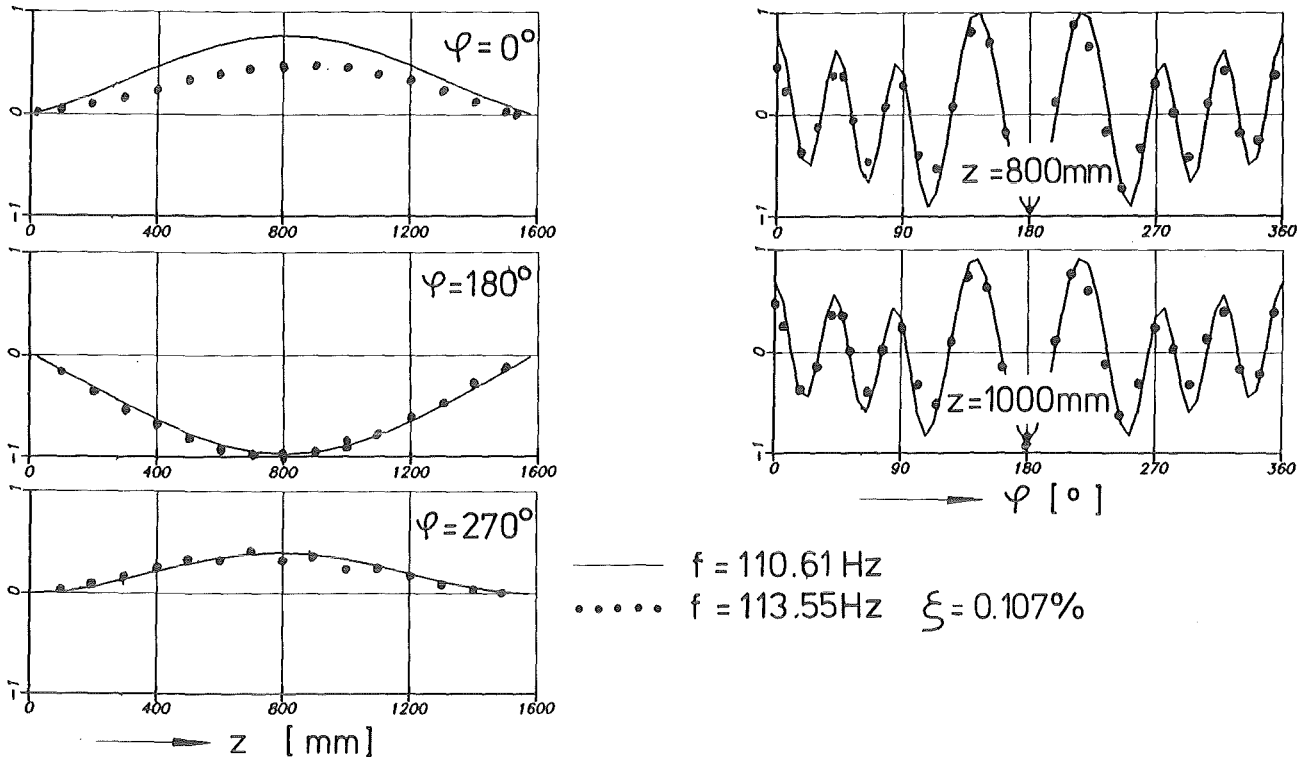
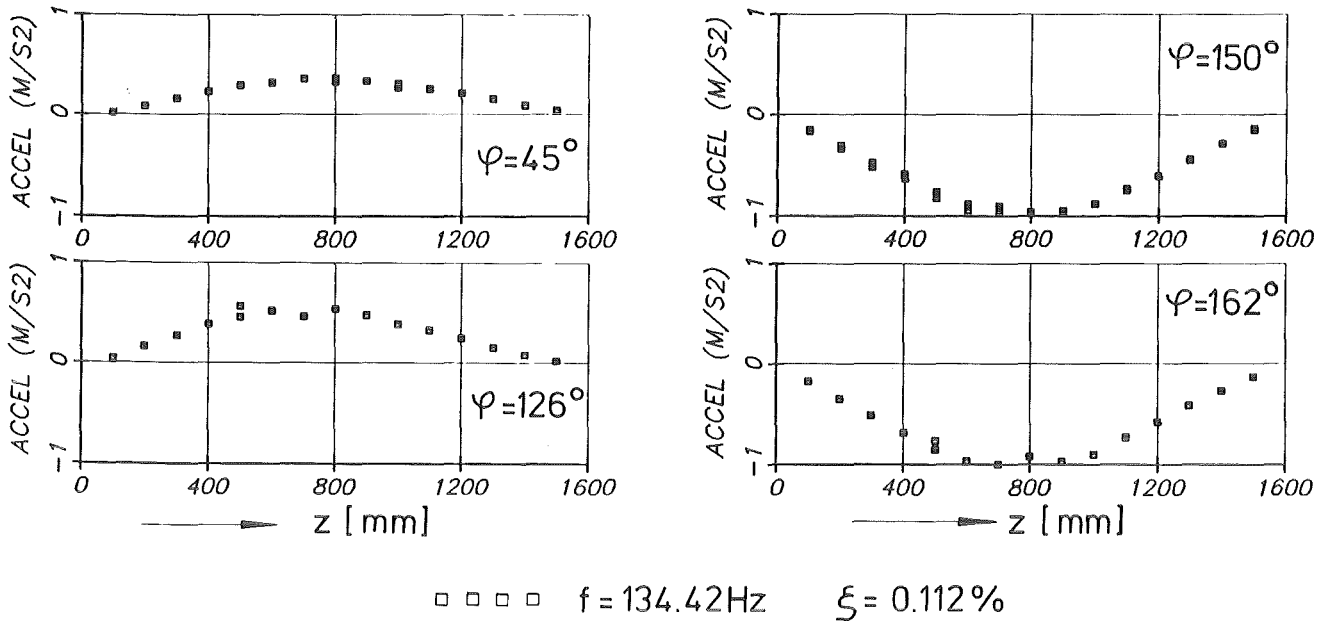Fig.40 :Mode shape of the 113.55 Hz-eigenmode (test cylinder partly filled with water)
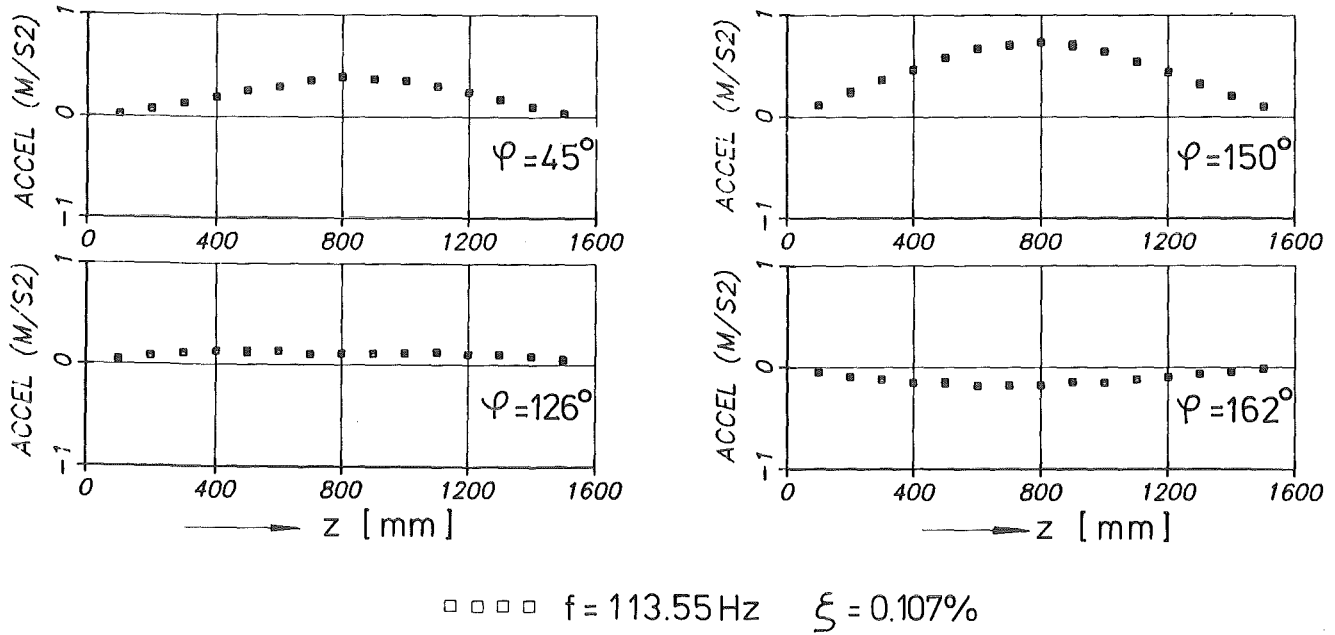
Fig.40a:Mode shape of the 113.55Hz-eigenmode (test cylinder partly filled with water)
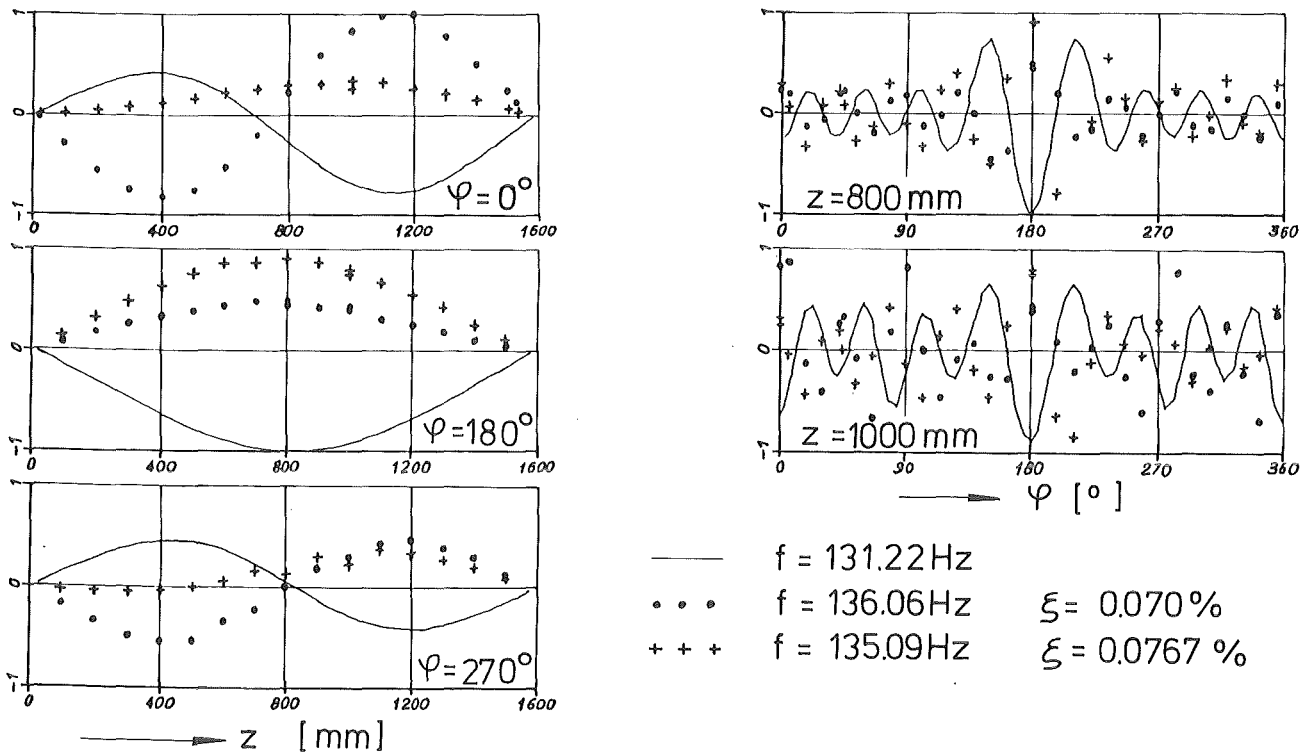
Fig.41 :Mode shape of the 135.09Hz-eigenmode (test cylinder partly filled with water)

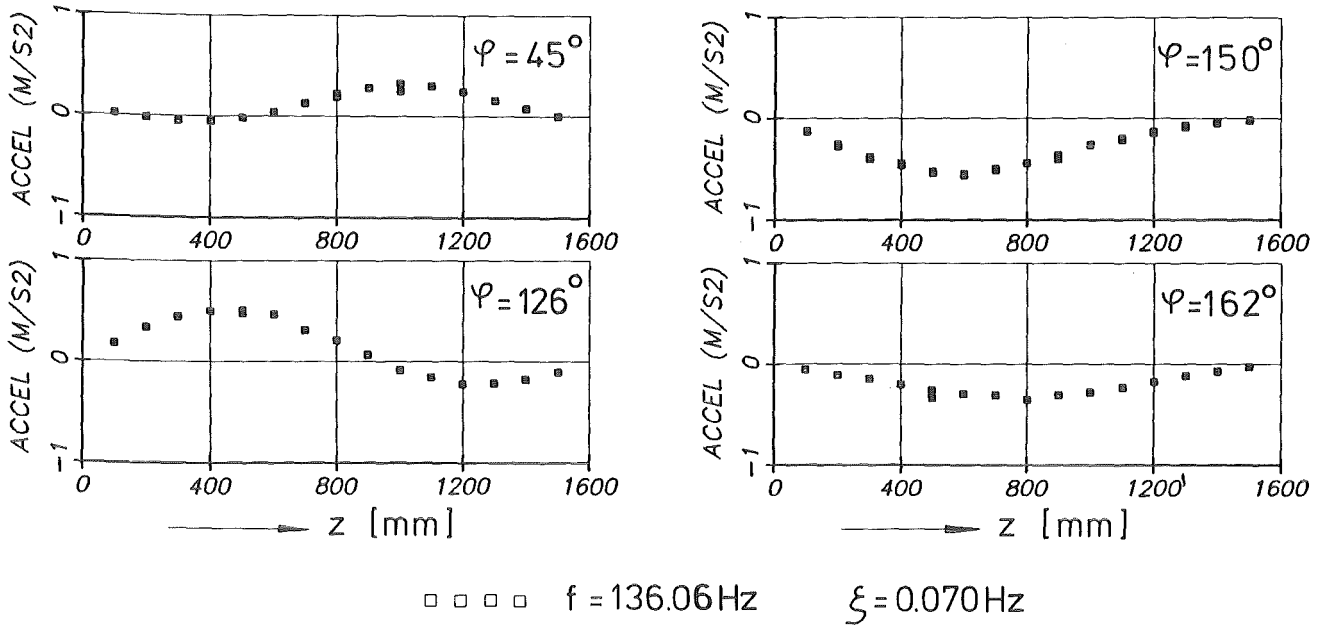Fig.41a:Mode shape of the 135.09Hz-eigenmode (test cylinder partly filled with water)

f=89,45 Hz

f =136,06 Hz
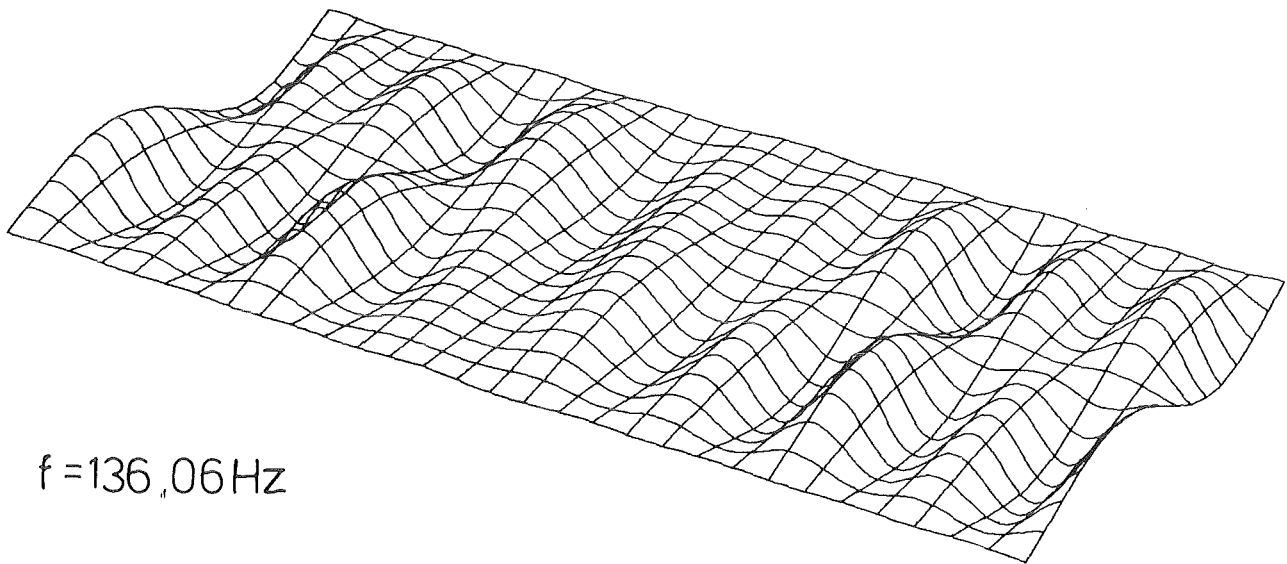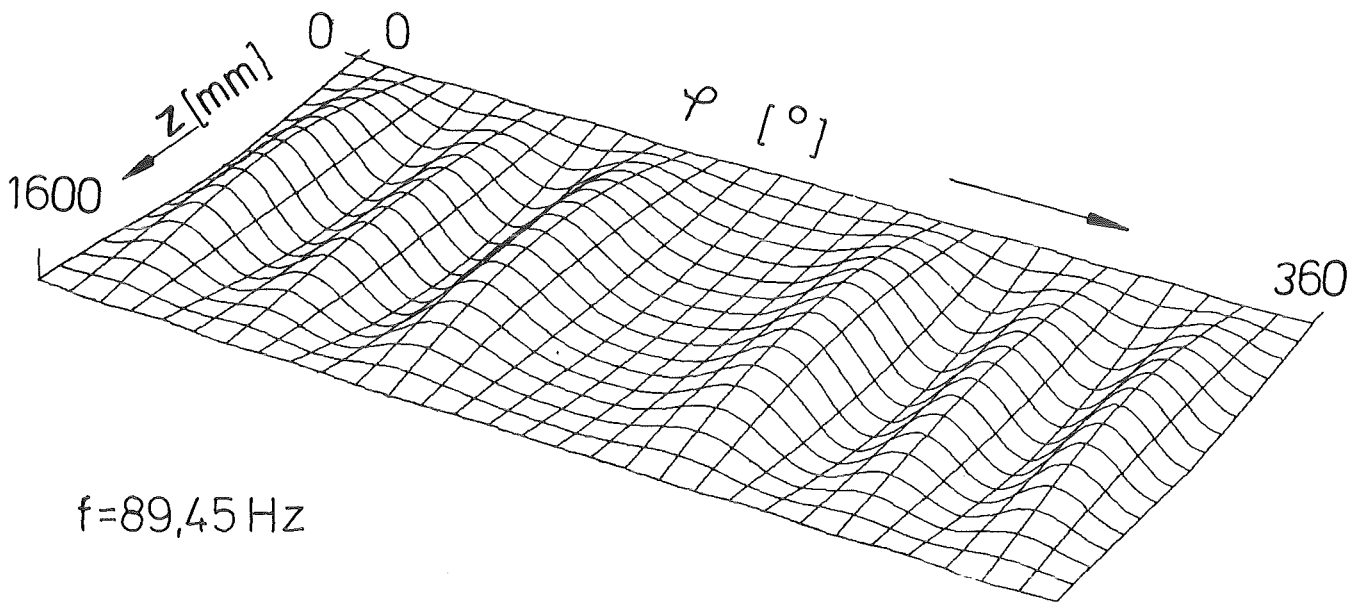
Fig.42:Relief plots of typical mode shapes extracted
(test cylinder filled)
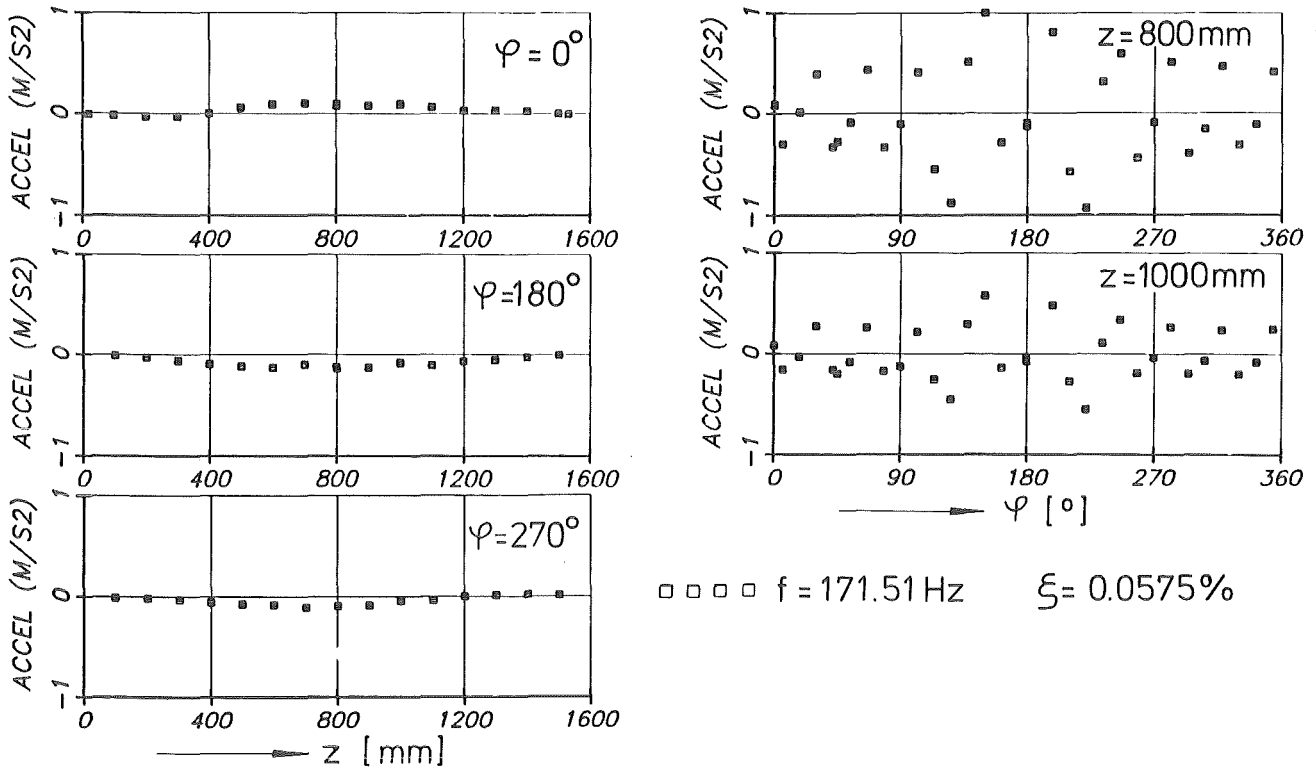
Fig.43 :Mode shape of the 171.51Hz-eigenmode (test cylinder partly filled with water)
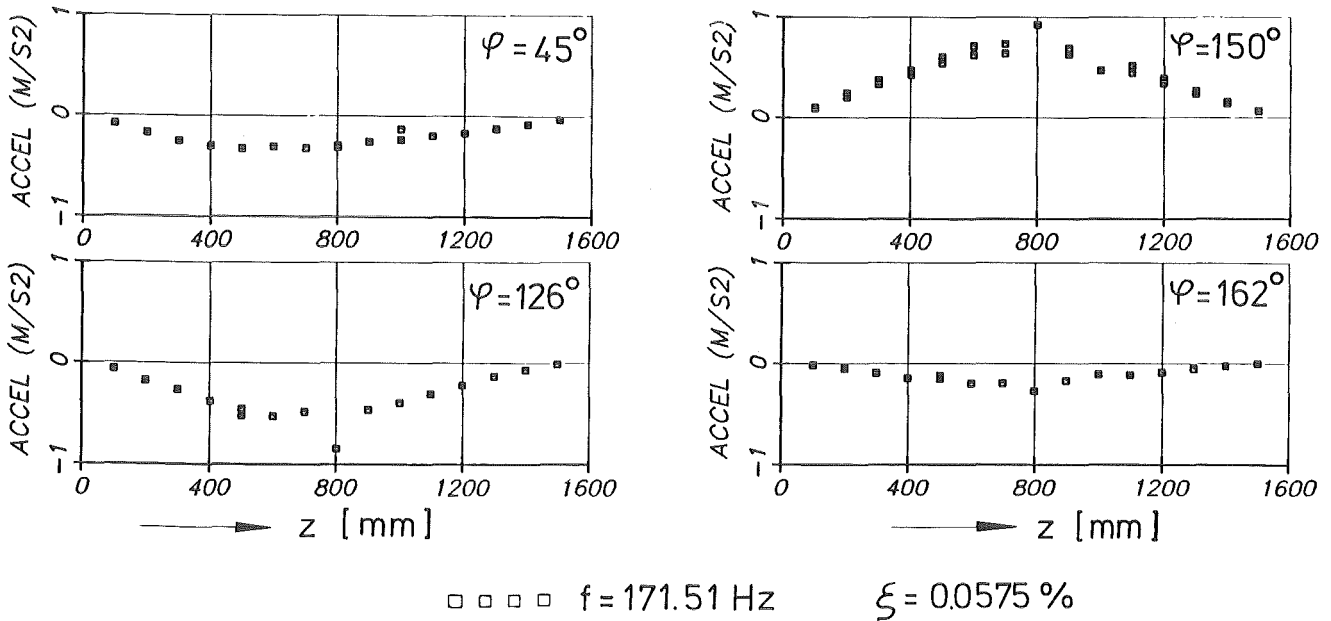
Fig.43a:Mode shape of the 171.51Hz-eigenmode (test cylinder partly filled with water)

Fig.44 : Mode shape of the 172.27 Hz-eigenmode (test cylinder partly filled with water)
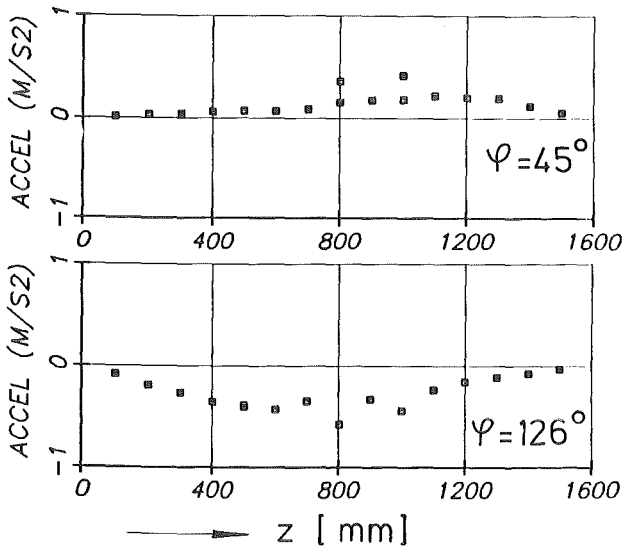
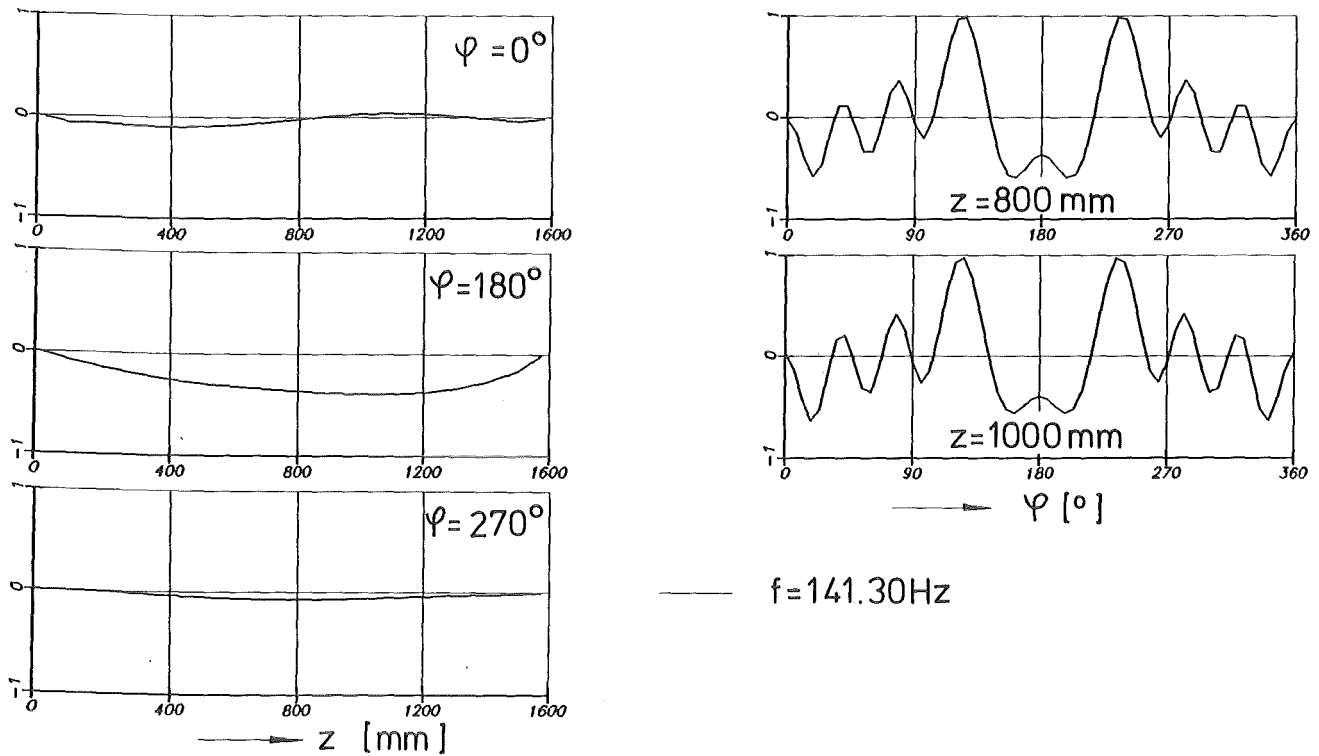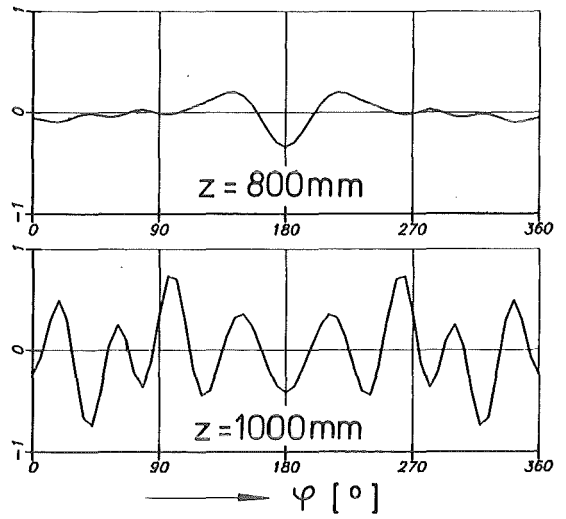Fig.44a: Mode shape of the 172.27Hz-eigenmode (test cylinder partly filled with water)

Fig.45 :Mode shape of the 111.69Hz-eigenmode (test cylinder partly filled with water)

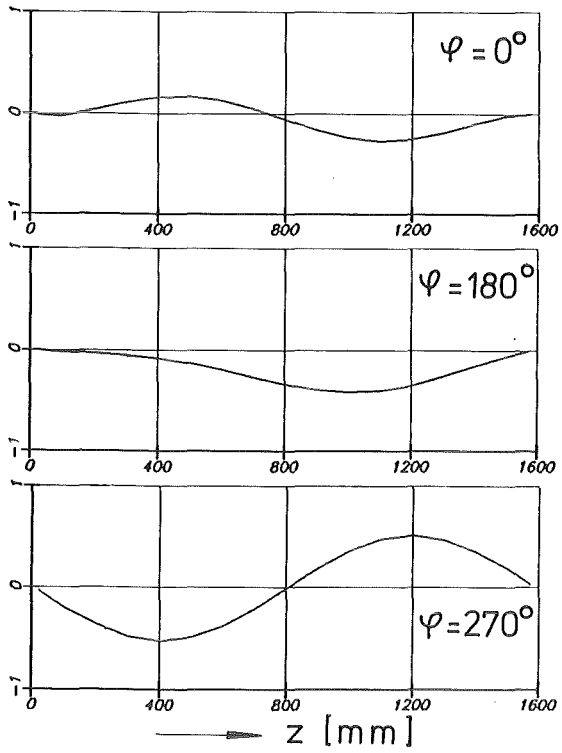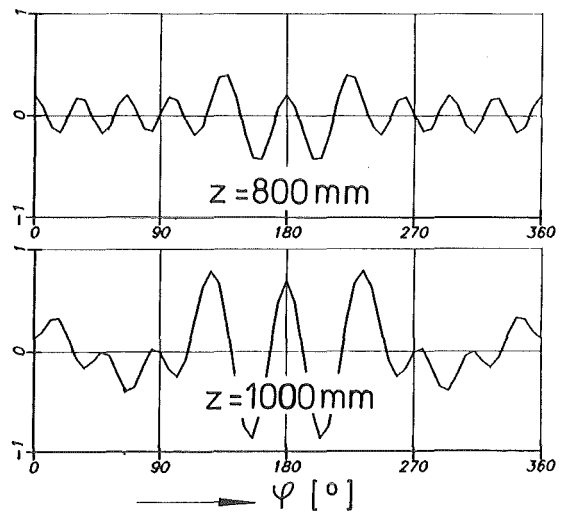Fig.45a:Mode shape of the 111.69Hz-eigenmode (test cylinder partly filled with water)
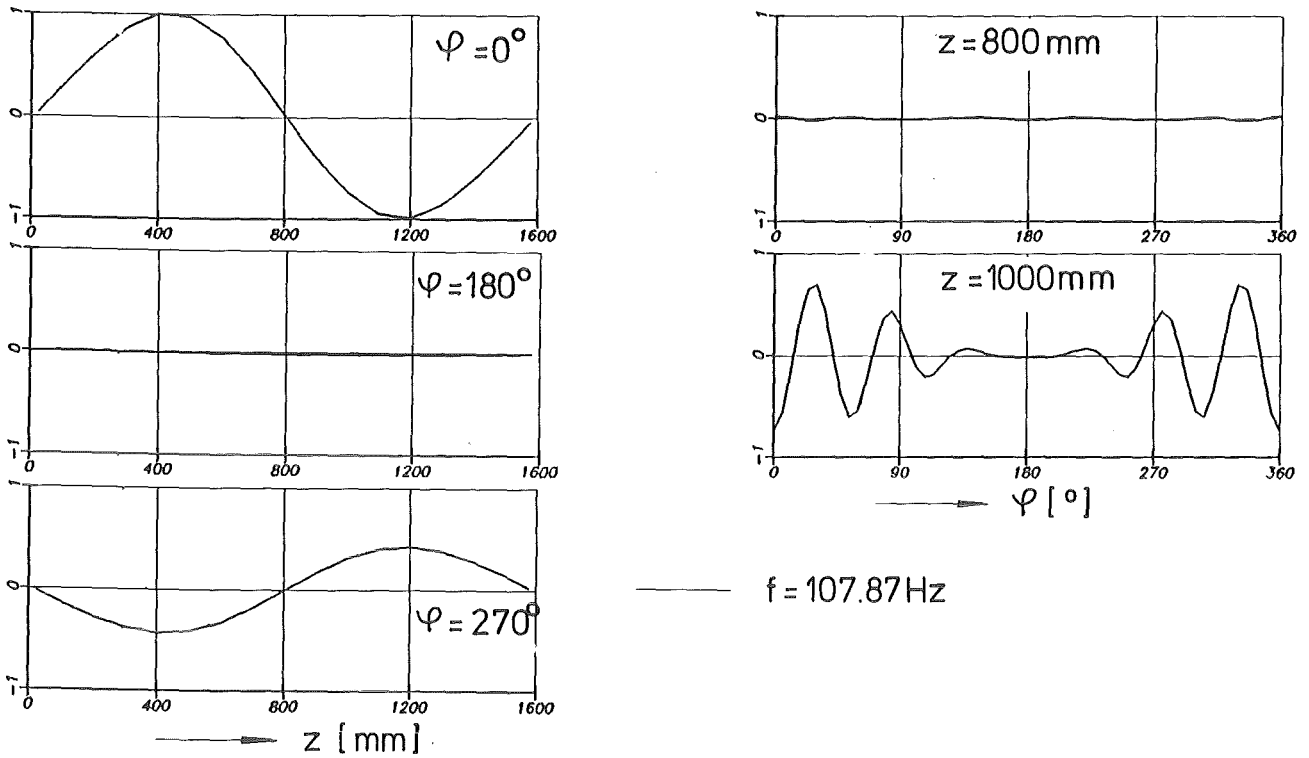
Fig. 46 : Mode shape of the 158.04Hz-eigenmode (test cylinder partly filled with water)

Fig. 47 : Mode shape of the 134.42Hz-eigenmode (test cylinder partly filled with water)

Fig.47a: Mode shape of the 134.42Hz-eigenmode (test cylinder partly filled with water)

Fig.48: Mode shape of the 136.06 and 135.09Hz-eigenmodes (test cylinder partly filled with water)

Fig.48a: Mode shape of the 136.06Hz-eigenmode (test cylinder partly filled with water)

Fig. 49 : Mode shape of the 141.30Hz-eigenmode (test cylinder partly filled with water)

Fig. 50 : Mode shape of the 148.53 Hz -eigenmode (test cylinder partly filled with water)

Fig. 51 : Mode shape of the 204.24Hz -eigenmode (test cylinder partly filled with water)

Fig. 52 : Mode shape of the 107.87 Hz-eigenmode (test cylinder partly filled with water)
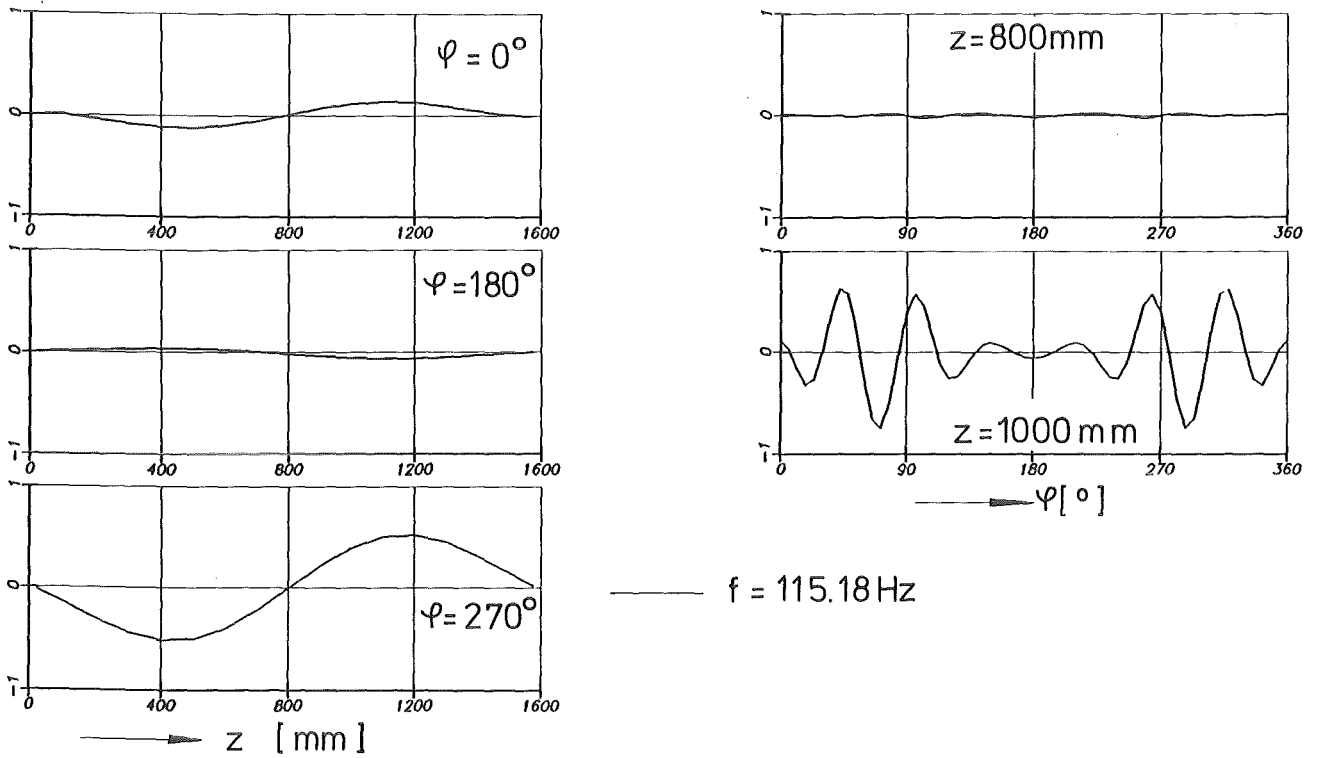

Fig. 53: Mode shape of the 115.18 Hz-eigenmode (test cylinder partly filled with water)
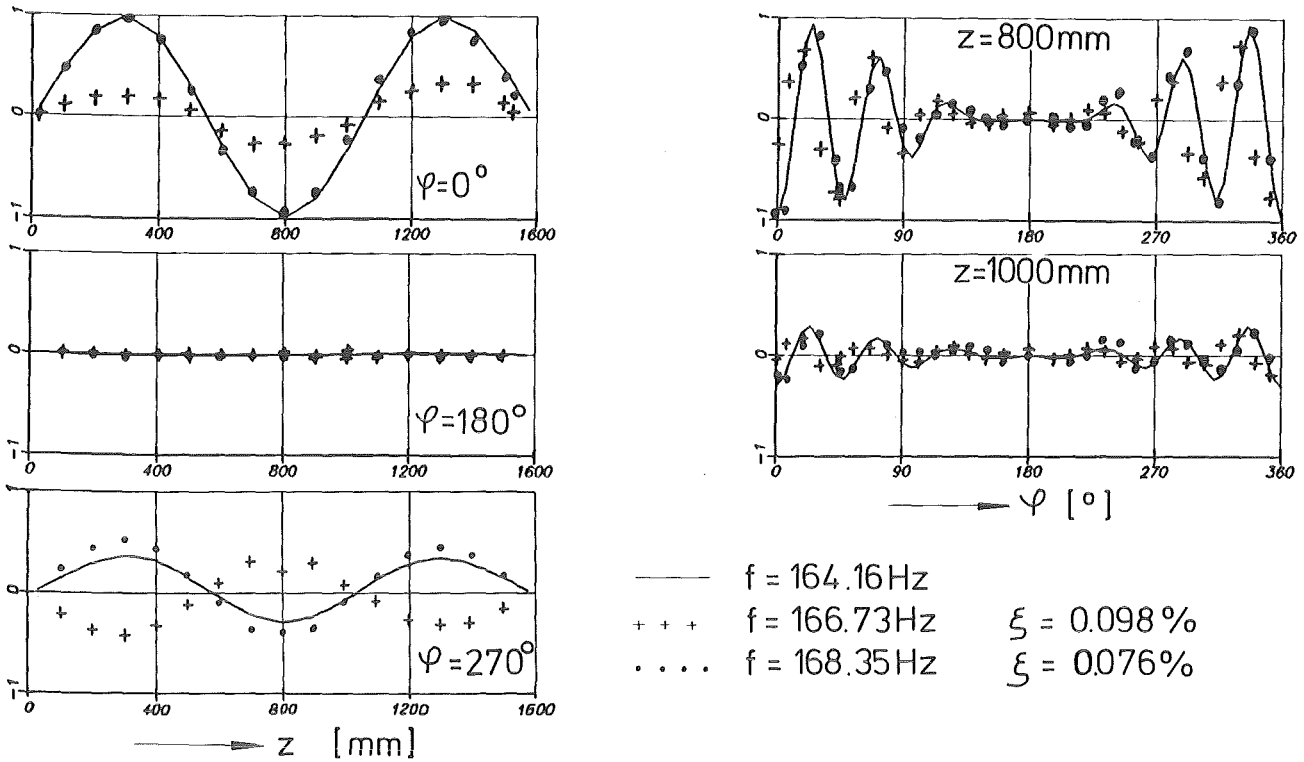
Fig.54 : Mode shape of the 185.40Hz-eigenmode (test cylinder partly filled with water)

Fig.54a: Mode shape of the 185.40Hz-eigenmode (test cylinder partly filled with water)

Fig. 55: Mode shape of the 166.73 and 168.35 Hz-eigenmodes (test cylinder partly filled with water)
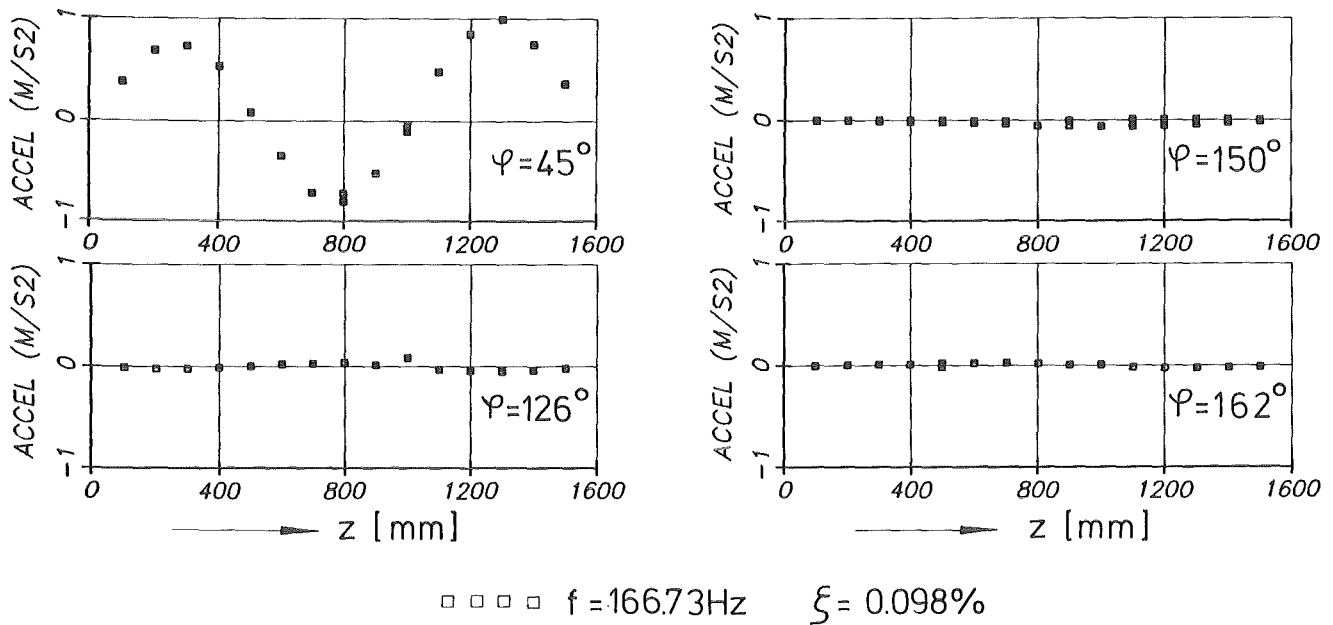

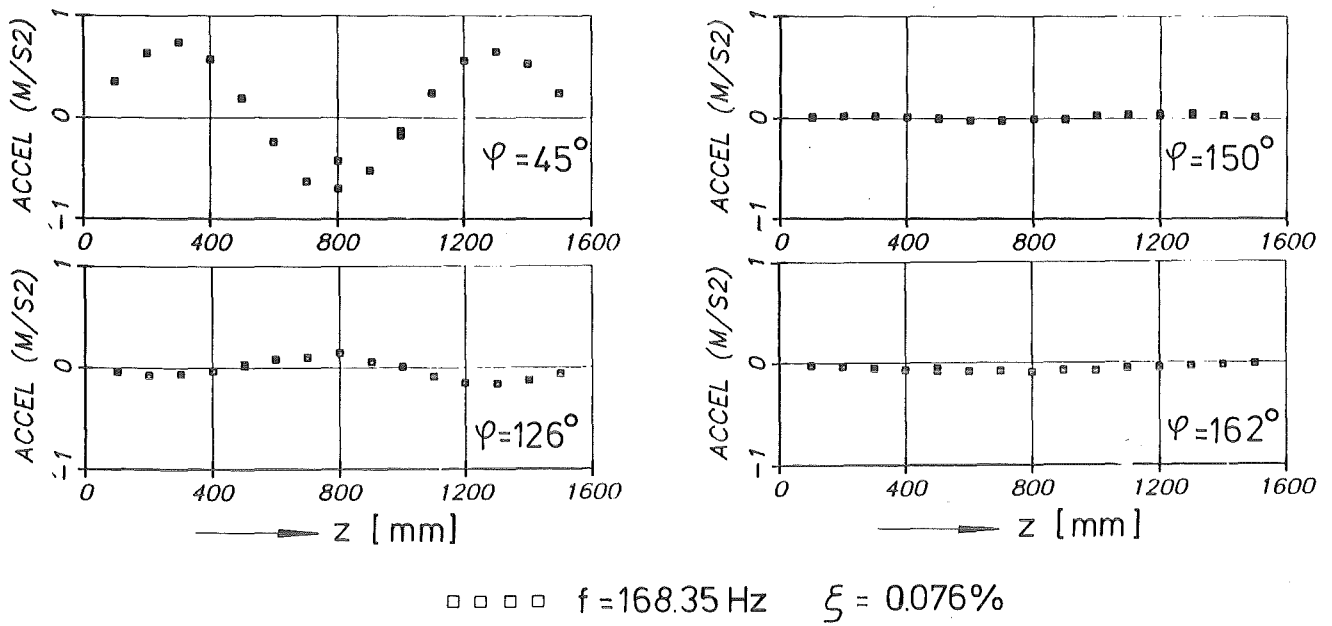Fig.55a: Mode shape of the 166.73Hz-eigenmode (test cylinder partly filled with water)

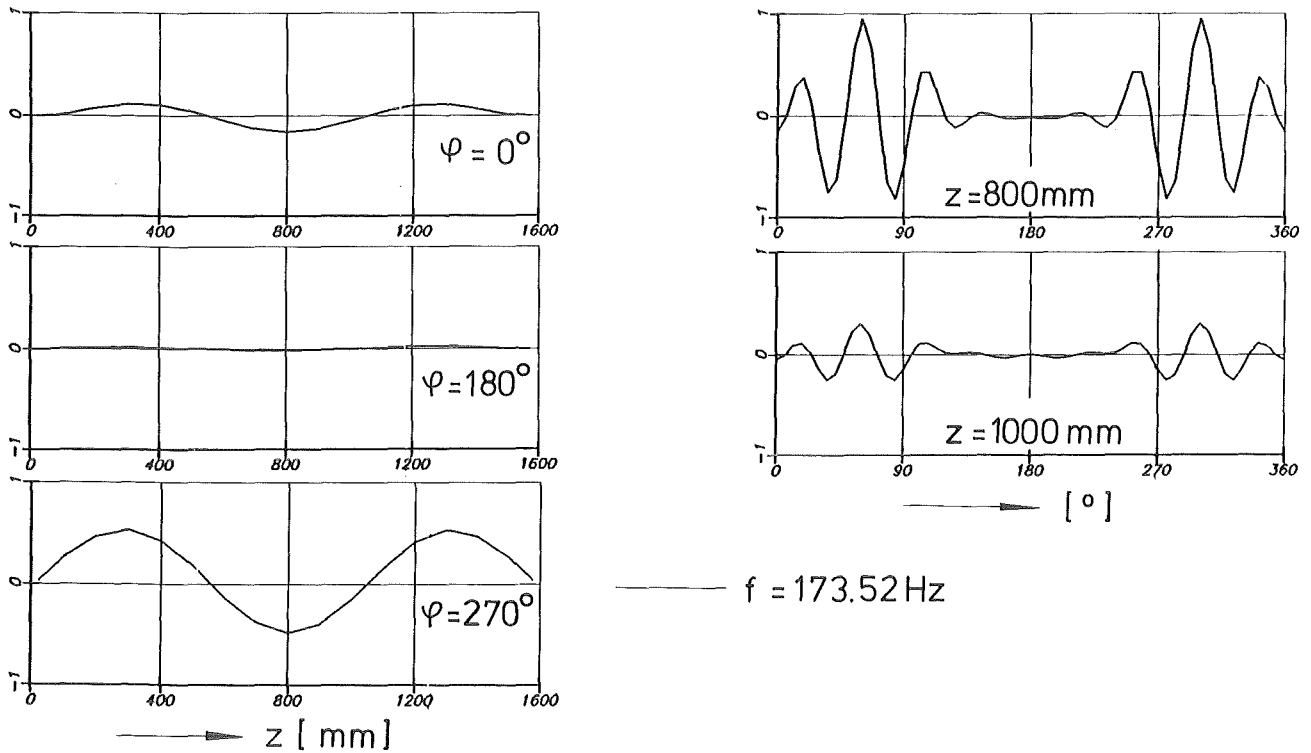Fig.55b:Mode shape of the 168.35Hz-eigenmode (test cylinder partly filled with water)

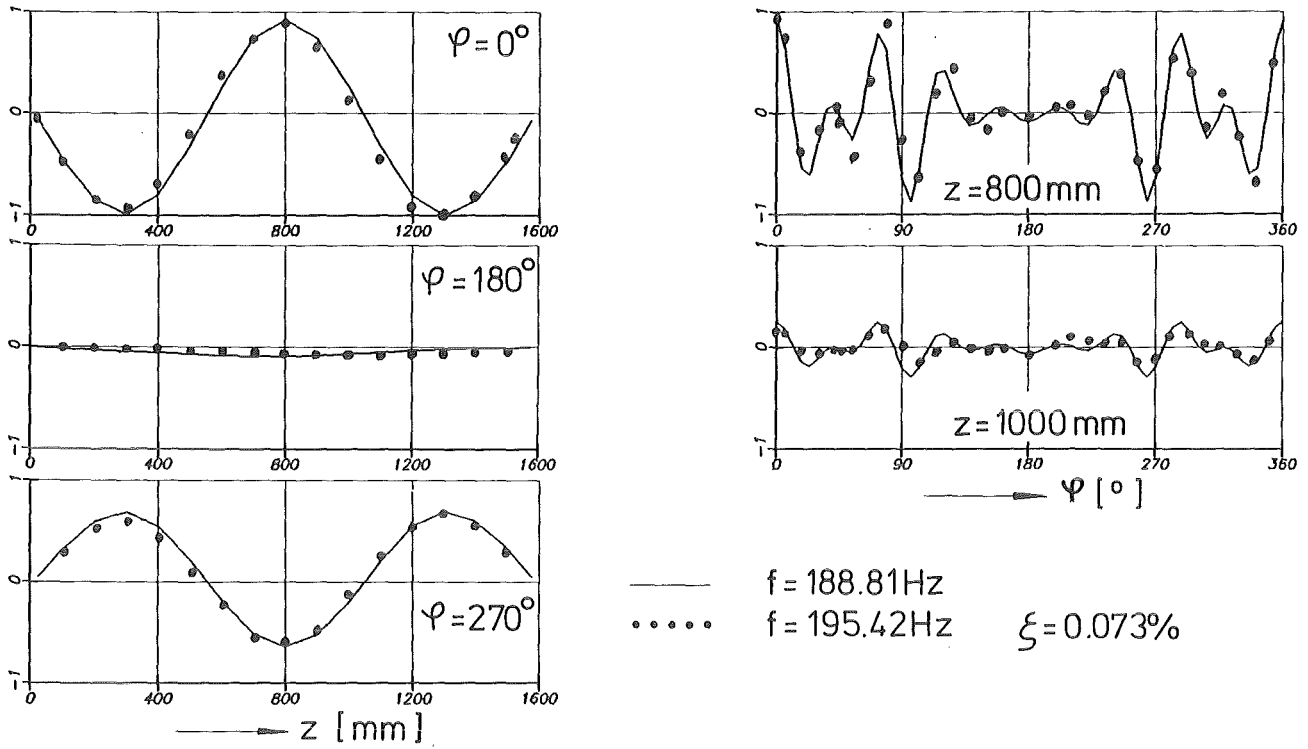Fig. 56:Mode shape of the 173.52Hz-eigenmode (test cylinder partly filled with water)

Fig. 57 : Mode shape of the 195.42Hz-eigenmode (test cylinder partly filled
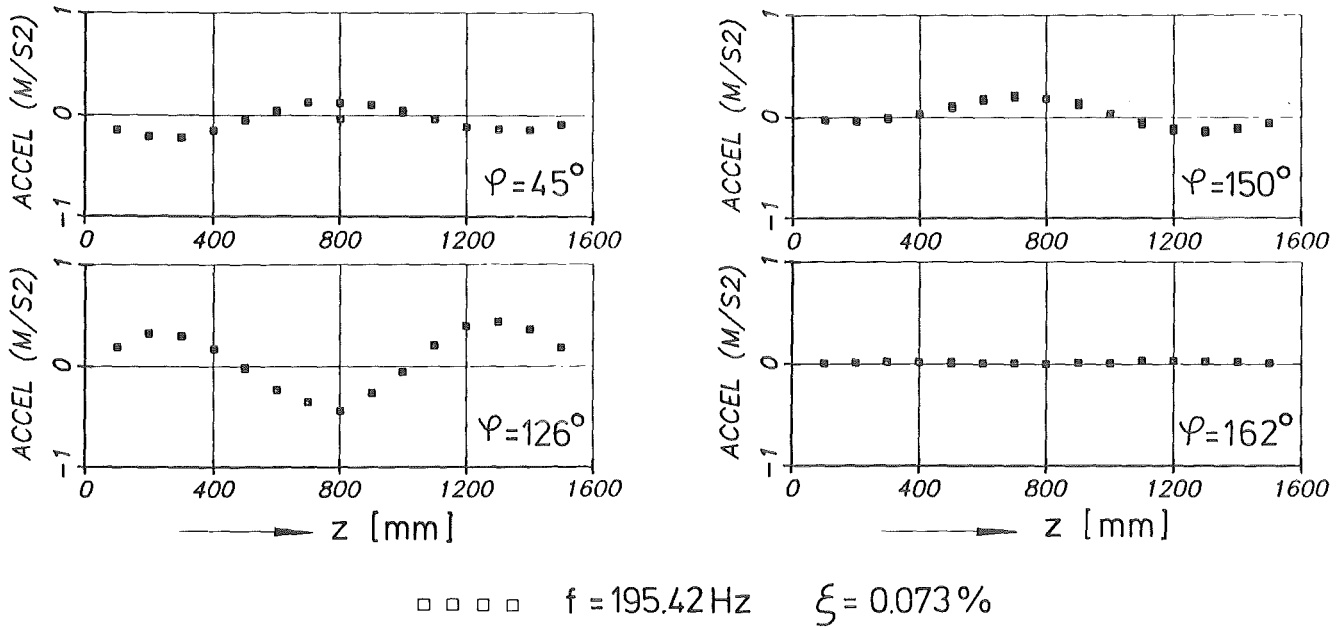with water)

Fig.57a: Mode shape of the 195.42Hz-eigenmode (test cylinder partly filled
with water)